Sensitivity Analyses of Surface Boundary Conditions During Long-Term Climate Change

NWMO-TR-2016-19 October 2016

Gordan Stuhne and W. R. Peltier

University of Toronto, Department of Physics

nwmo

NUCLEAR WASTE MANAGEMENT ORGANIZATION

SOCIÉTÉ DE GESTION DES DÉCHETS NUCLÉAIRES

Nuclear Waste Management Organization
22 St. Clair Avenue East, 6th Floor
Toronto, Ontario
M4T 2S3
Canada

Tel: 416-934-9814
Web: www.nwmo.ca

Sensitivity Analyses of Surface Boundary Conditions During Long-Term Climate Change

NWMO-TR-2016-19

October 2016

Gordan Stuhne and W. Richard Peltier
University of Toronto, Department of Physics

Document History

Title:	Sensitivity Analyses of Surface Boundary Conditions During Long-Term Climate Change		
Report Number:	NWMO-TR-2016-19		
Revision:	R000	Date:	October 2016
University of Toronto, Department of Physics			
Authored by:	Gordan Stuhne and W. Richard Peltier		
Verified by:	W. Richard Peltier		
Approved by:	W. Richard Peltier		
Nuclear Waste Management Organization			
Verified by:	Eric Sykes		
Reviewed by:	Eric Sykes		
Accepted by:	Mark Jensen		

ABSTRACT

Title: **Sensitivity Analyses of Surface Boundary Conditions During Long-Term Climate Change**
Report No.: **NWMO-TR-2016-19**
Author(s): Gordan Stuhne and W. Richard Peltier
Company: University of Toronto, Department of Physics
Date: October 2016

Abstract

A set of 107 numerical simulations of the evolution of surface boundary conditions over a 122.5 kyr glacial cycle is analyzed in order to estimate the sensitivity of predictions to variations in key parameters of the University of Toronto Glacial Systems Model (UofTGSM). As described in a previous Report (TR-2015-16) that introduced reference surface boundary condition datasets deriving from a typical parameter regime (i.e., from the SeaRISE protocols for modern Greenland and Antarctic climate change studies), individual simulations are globally constrained by a data assimilation procedure that nudges simulated North American ice thickness histories towards the observationally well-validated ICE-6G_C reconstruction. The incorporation of nudging distinguishes sensitivity to ice model parameters from sensitivity to paleoclimate conditions that are very poorly constrained over the portion of the glacial cycle preceding Last Glacial Maximum (LGM). In earlier sensitivity analyses that referred to a smaller number of simulations deriving from a previous version of the UofTGSM (the GSM model of Tarasov and Peltier, 1999, 2002, 2003, 2004), Peltier (2006, 2011) showed differences between realizations to be dominated by pre-LGM paleoclimate-dependent fluctuations that were inconsistent with the eustatic sea-level record. Beyond considering a larger number of realizations deriving from a state-of-the-art version of the UofTGSM, the new sensitivity analyses described herein focus upon the bounds in surface boundary conditions associated with specific structures (e.g., glacial margins and ice domes) within the possible, observationally consistent ICE-6G_C ice thickness reconstruction. The parameter-sensitivities of ice thickness, permafrost thickness, basal temperature, meltwater production, lake depth, basal velocity, and basal shear stress are of the same order of magnitude as the amplitudes of predictions in Peltier (2006, 2011) and TR-2015-16 across a variety of simulation ensembles and nudging time scales.

TABLE OF CONTENTS

LIST OF TABLES

LIST OF FIGURES

1. INTRODUCTION

In a previous report (Stuhne and Peltier, 2015; hereafter SP15), a set of surface boundary conditions (BCs) deriving from simulations of the evolution of Canadian ice-sheets over the last glacial cycle ($\sim$100 kyr BP to present) were discussed. These simulations employed the latest version of the University of Toronto Glacial Systems Model (UofTGSM), and were designed to hindcast past variations in BC fields in a manner that enforced consistency not only with the ice-sheet dynamics of this model, but also with all available observational constraints upon North American and global glaciation. On the reasonable assumption that surface BC variations are approximately repetitive over successive ice age cycles, the results of SP15 predict the local variations of ice thickness, ice velocity, normal stress, basal temperature, basal meltwater production, and proglacial lake depth that future glaciation would impose upon a Deep Geologic Repository located in Canada. These results built upon earlier work addressing the same problem (Peltier 2006; 2008; 2011; hereafter P*yy*), but started from more realistic modeling assumptions that included both the state-of-the-art physics approximations of the new UofTGSM and an expanded set of observational constraints that were introduced through nudging towards the ICE-6G_C (VM5a) reconstruction of historical ice sheet thickness (Argus et al., 2014; Peltier et al., 2015). Predictions of surface BC field bounding values and other aspects of long-term ice-sheet evolution were broadly consistent with those of P*yy*, but the new work of SP15 also highlighted sources of uncertainty that had not previously been addressed. These uncertainties pertain primarily to glacial evolution preceding the Last Glacial Maximum (LGM, $\sim$25 kyr BP), at which point the most recent expansion of continental ice-sheets largely erased most of the detailed proxy evidence constraining ice-sheet dynamics over the earlier part of the last 100 kyr glacial cycle. The assumptions that P*yy* made about pre-LGM surface BCs with more limited observational constraints resulted in a more rapid succession of glacial advances and retreats than what was predicted by the strategy employed by SP. P*yy* had attempted to quantify the uncertainties in their results by applying a Bayesian-type methodology to the parameter space of the earlier UofTGSM model. The analyses described in this report will build upon the results of SP to further quantify the uncertainties associated with ensembles of ice-sheet dynamical simulations, including uncertainties associated with pre-LGM time-dependence of glacial BCs.

The general approach adopted in SP15 has been extensively analyzed and justified for Antarctic and Greenland ice-sheet test cases in Stuhne and Peltier (2015) and for the Laurentide and Fennoscandian ice-sheets in a newly submitted follow-up publication (Stuhne and Peltier, 2016). The work of P*yy* was also extensively grounded in the journal literature (see Tarasov and Peltier, 1997, 1999, 2000, 2002, 2003, 2004, 2007) (hereafter TP*yy*), and TP04 in particular discussed the aforementioned issues arising from a dearth of constraints upon pre-LGM ice-sheet

dynamics. In Section 2 of what follows, the improvements that distinguish the new sensitivity analyzes from the previous work of P*yy* will be discussed with reference to relevant points from the literature. Results will be presented in Section 3 and discussed in Section 4 and concluding remarks will appear in Section 5.

2. THEORY

2.1 Background

The observational constraints that apply to ice-sheet dynamics on paleoclimate time-scales consist mainly of proxies for local relative sea-level change (RSL change) since LGM and of direct GPS-based measurements quantifying the modern viscoelastic response of the solid Earth surface to ice loss during this time interval. Pre-LGM glaciation is, as noted above, much more weakly constrained, and observations applying to the entire glacial cycle consist mainly of marine sediment-based proxies for global (eustatic) sea-level variation and of local ice-core based proxies for atmospheric temperature. The former constrain variations in total ice mass (which clearly complements sea-level by mass conservation), while the latter constrain surface paleoclimate change at discrete locations on the persistent Greenland and Antarctic ice sheets. Apart from the ice-core based temperature proxies (which are considered in more detail below), all of the observational constraints on post- and pre-LGM glacial evolution apply directly to the ice-sheet thickness history, $I(\Omega, t)$, independently of complex ice-sheet dynamical approximations about the dynamical time evolution of glaciation. This means, specifically, that the effects of any hypothetical surface I distribution upon glacial isostatic adjustment (GIA) and local sea-level change can, subject *only* to a modest further assumption about the viscous structure of the Earth's interior, be predicted with the aid of a well-established body of theory (Peltier, 1974, 1976a,b; Peltier and Andrews, 1976; Farrell and Clark, 1976; Clark et al., 1978; Peltier et al., 1978; Peltier, 1998, 2007; Peltier et al., 2015). Although pure GIA-based methods technically cannot be inverted to deduce a unique I and associated error estimate from observations, empirical techniques along these lines have yielded reconstructions of post-LGM ice thickness history consistently with the entire wide array of relevant evidence. Even in the pre-LGM limit for which there are few observational constraints, such methods effectively default to the prediction of eustatic sea-level change from the global integral of I. In tandem with the associated VM5a reconstruction of radial mantle viscosity variation, the ICE-6G_C ice-sheet thickness history ($I_{i6g}(t)$) invoked in SP15 reflects the state-of-the-art in GIA-based reconstruction.

As implied above, ice-core based proxies for surface temperature variation are the only observational evidence that constrains ice-sheet *dynamics* in a way that does not relate directly

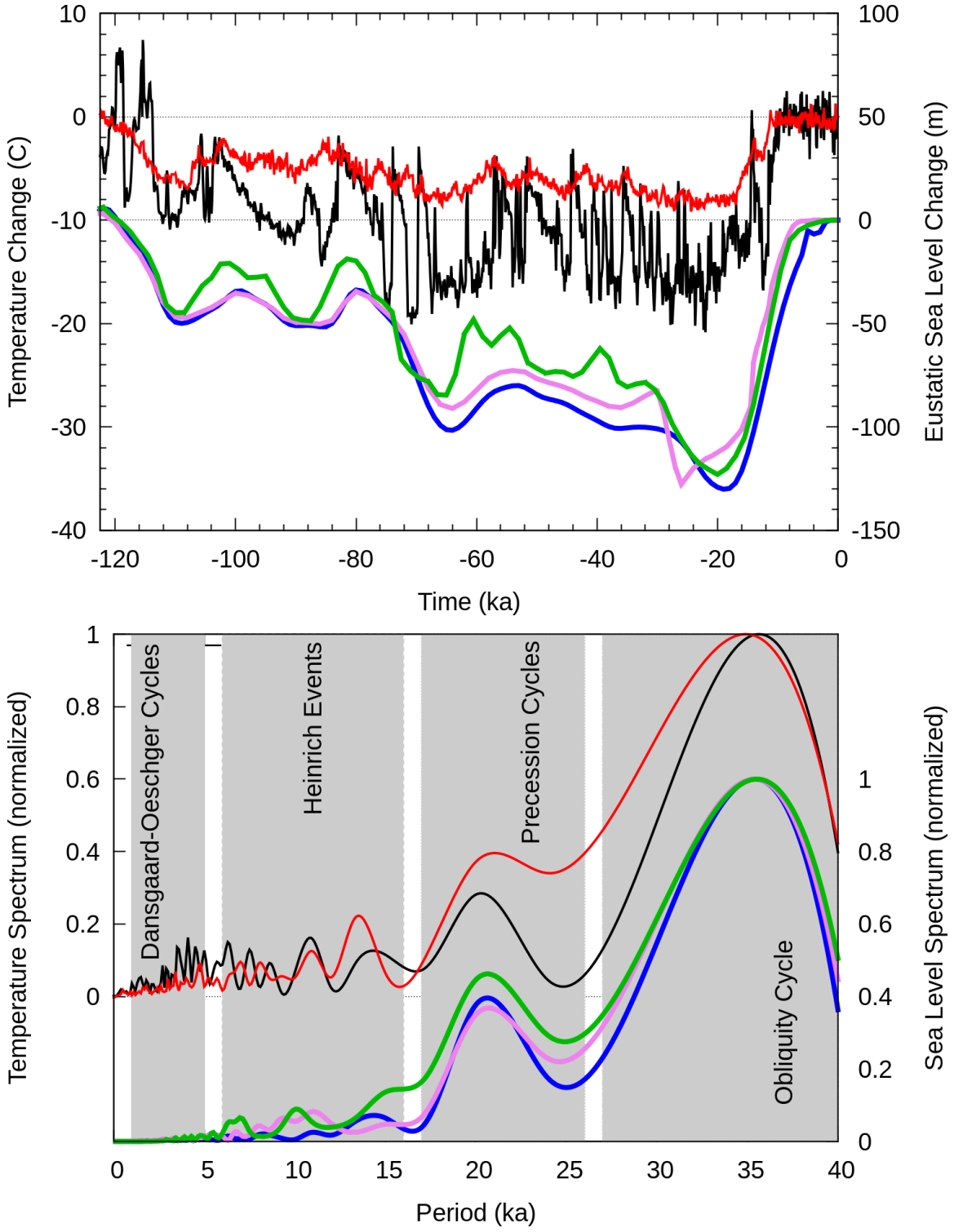

Figure 1: Time series of climatological temperature adjustment, $\Delta T(t)$, inferred from the Greenland GRIP ice core (black) and the Antarctic Vostok ice core (red). The SPECMAP time series of eustatic sea-level change is shown (in blue) along with a version corrected for ocean temperature (green) and an estimate based on eustatic sea-level equivalent I6G ice volume change (in violet). The y-scale for sea levels is shown on the right axis, and the smoothed and interpolated amplitude spectra of all time series are shown on the bottom frame.

to ice-sheet thickness, I. It is easy to formulate the BCs of any thermomechanical ice-sheet dynamical model consistently with any surface temperature distribution, and models generically propagate surface temperature and related constraints to ice-sheet thickness by prescribing the local mass balance, $G\left(\Omega, t; \Pi_1, \ldots, \Pi_n\right)$, and the corresponding horizontal ice flux, $\mathbf{Q}\left(\Omega, t; \Pi_1, \ldots, \Pi_n\right)$, in the two-dimensional ice conservation law:

$$\frac{\partial I}{\partial t} + \nabla_h \cdot \mathbf{Q}\left(\Omega, t; \Pi_1, \ldots, \Pi_n\right) = G\left(\Omega, t; \Pi_1, \ldots, \Pi_n\right) \quad (1)$$

in which $\Pi_1, \ldots, \Pi_n$ denote the discrete parameters of a model of arbitrary complexity. The mechanisms by which three-dimensional ice-sheet dynamical models determine ice thickness fluxes and sources are very complex in general, but simplified conclusions can be drawn about the constraints imposed by a known surface temperature time series, $T_s\left(\Omega_i, t\right)$ at an ice core site Ω_i. Sufficiently high local temperature promotes local ice loss through melting ($G\left(\Omega_i, t\right) < 0$) while sufficiently low local temperature promotes local ice accumulation through freezing ($G\left(\Omega_i, t\right) > 0$). The long-term time dependence of local temperature and associated mass balance should be expected to correlate to some extent with that of eustatic sea-level, but the limits of such correlation are manifest when these two proxies for long-term paleoclimate change are are directly compared. Showing both time series (top frame) and their smoothed spectral equivalents in amplitude-period space (bottom frame), Figure 1 compares local temperature changes (thin curves) with different reconstructions of global sea-level change (thick curves). Temperature information pertains to the GRIP ice core site in Greenland (Johnsen et al., 1997) (black curve) and the Vostok ice core site in Antarctica (Petit et al., 2001) (thin red curve), while sea-level information pertains to equivalent ice-volume variation from the I6G model (the violet curves) and from two proxy time-series that influenced this reconstruction: specifically, the SPECMAP eustatic sea-level time-series (Imbrie and McIntyre, 2006, blue curve); and, a refinement correcting for ocean temperature (Waelbroeck et al., 2002). The amplitude spectra of the various paleoclimate time-series are consistent over the long periods of insolation change due to obliquity and precession, but temperature and sea-level spectra differ at shorter periods. The signatures of the repetitive Heinrich Events are evident in the appropriate $5 - 15$ kyr range of the temperature spectra, but their manifestations in the sea-level time-series are debatable (Hemming, 2004). For periods below 5 kyr, the discrepancy becomes more pronounced as temperature spectra exhibit a millennial scale Dansgaard-Oeschger (DO) oscillation that entirely fails to appear in the sea-level spectra. Such results suggest that the high-frequency surface temperature variation recorded at high-latitude Greenland and Antarctic ice-core sites was not a feature of global paleoclimate change - at least, not to the degree that would be required to result in continental-scale ice sheet advances and retreats on a millenial time-scale.

Beyond making a wide variety of observationally unconstrained assumptions about $\mathbf{Q}$ and G in

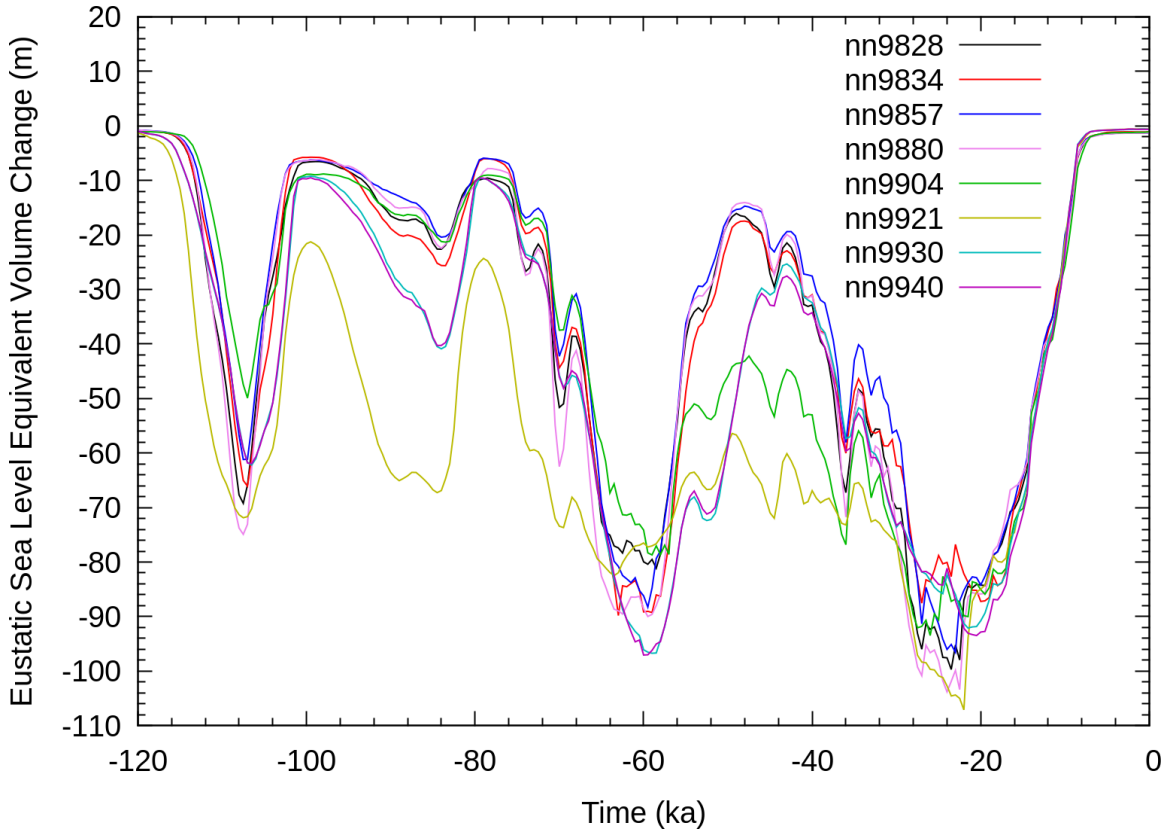

Figure 2: Time series of eustatic sea-level equivalent ice volume change from nnxxxx simulations from Peltier (2008).

Eq. (1) in order to enable simulations over paleoclimate time-scales, ice-sheet dynamical models adapt to the absence of high-frequency signal in the sea-level record by using ice-core data to prescribe surface temperature time-dependence on continental and global scales. Considering that fluctuations in the North American ice-sheet complex accounted for the bulk of eustatic sea-level change, such an approach should be suspected from the outset to conflict with the preceding discussion of climate change over a complete glacial cycle. Figure 2 confirms pre-LGM inconsistency with the marine sediment-based sea-level record by plotting North American ice-volume variations from the nn*xxxx* simulation ensemble of P*yy* as equivalent eustatic sea-level changes. Although the outlying nn9921 simulation appears reasonable in that it predicts persistent pre-LGM land ice cover of at least a quarter of the total LGM volume, it exhibits increased variability at various short time scales up to ~ 40 yr. The same variability also appears in the other nn*xxxx* simulations. The objective of this study is to make reasonable parameter variations in a representative ensemble of simulations to provide predictions that are consistent with observational constraints, with variability between simulations reflecting the uncertainties in these constraints.

In contrast to the preceding pre-LGM ice volume variations, the post-LGM ice volume variations plotted in Figure 2 do suggest representative variations about a “mean” that is approximately consistent with all individual simulations and with the eustatic sea-level record. This consistency was achieved through the introduction of explicit “margin forcing” that adjusted ice-sheet dynamics to fit glacial reconstructions like the Laurentide ice-margin chronologies of Dyke (2004). Although post-LGM ice thickness histories are consistent with the eustatic sea-level record, the predicted ice-thickness histories do not fit observations as well as pure GIA-based reconstructions. SP15 addressed these problems with the work of P*yy* by consolidating all artificial dynamical constraints upon ice thickness into a coherent mechanism for nudging I towards the pure GIA-based reconstruction, I_{i6g} (which naturally entrains all observational constraints except for surface temperatures at ice core sites). Nudging is a simple, well-known data assimilation procedure that modifies Eq. (1) by introducing an anomalous mass balance, ΔG, to exponentially relax ice thickness towards I_{i6g} at exponential time-scale τ_f: i.e.,

$$\begin{aligned} \frac{\partial I}{\partial t} + \nabla_h \cdot \mathbf{Q} &= G + \Delta G \\ \Delta G &= -\frac{I - I_{i6g}}{\tau_f}. \end{aligned} \tag{2}$$

Since the time dependence of the GIA-based reconstruction is based upon eustatic sea-level variation throughout the glacial cycle, nudging should constrain unrepresentative variability of the kind seen pre-LGM in Figure 2 to a degree that should increase as τ_f decreases towards 0. SP15 investigated the consistency of simulations with a range of nudging time scales, τ_f, by studying

how ice-sheet dynamical "smoothing" affected the quality of the baseline ICE-6G_C fit to observations and by considering whether the associated mass balance adjustments, ΔG, could be physically interpreted. With other parameters specified according to the widely cited SeaRISE protocols (Bindschadler et al., 2013; Nowicki et al., 2013a,b), consistency between nudged ice-sheet dynamics and the GIA-based reconstruction was established in all these respects for sub-millennial τ_f. A reference value of $\tau_f = 100$ yr was selected for the dataset, and a corresponding "error estimate" was deduced by analyzing the range of model predictions for consistent τ_f.

2.2 P*yy* and TP*yy* Ensemble Parameters and Surface Climate

The parameter variations that P*yy* employed to specify ensembles of simulations are not directly applicable in the new UofTGSM framework because the updated model incorporates much more sophisticated physics approximations along with the previously discussed philosophy for representing climatological forcing. We can nevertheless discuss the general physical nature of the parameter space that was explored in the earlier studies as a starting point for our more sophisticated extension of this work. Table 1 in TP04 summarizes 20 ensemble parameters of the old UofTGSM, and we can categorize these into three basic types based on the physics that is being parameterized: i.e.,

- *Basal sliding (1 parameter)*: Ice-sheet dynamics depends critically upon friction and sliding at the base, and the parameterization assumed in TP*yy* simplified this complex phenomenology such that variations could be expressed in terms of a single parameter - a till viscosity.
- *Calving (3 parameters)*: As is evident in relation to the modern West Antarctic Ice Sheet, the buttressing of grounded ice by floating ice shelves and the calving of icebergs from the latter play a crucial role in determining the stability of major ice sheets. Such phenomenology is certain to have been important at critical junctures in the history of the North American ice sheets, and TP04 parameterized it in terms of a model with three ensemble parameters. Two of these are global in scope (a critical temperature and calving front velocity), while a third regionally adjusts calving rates in the northwestern zone.
- *Paleoclimate (16 parameters)*: TP04 did to some extent recognize, and attempt to address, the previously discussed problems inherent in the determination of continental-scale paleoclimate BCs from isolated local ice-core records. The variability seen in Figure 2 was generated by means of an elaborate phenomenological model in which each of the 16 parameters effectively adjusts surface mass balance either globally or in a manner that is

Parameter	Description (units)	Range	SP15 value
τ_f	Nudging time constant (years)	20 - 1000	100
A_{SIA}	SIA ice hardness factor	1.5 - 7.0	5.6
A_{SSA}	SIA ice hardness factor	0.5 - 6.0	1.0
I_{crit}	Critical ice thickness for calving (m)	150 - 350	250
U_{ref}	Velocity parameter in sliding law (m/s)	25.0 - 300.0	100
ϕ_{min}	Till geometry minimum angle (degrees)	5.0 - 25.0	5
ϕ_{max}	Till geometry maximum angle (degrees)	27.0 - 42.0	40
B_{min}	Till geometry elevation minimum (m)	-400 - -10	-300
B_{max}	Till geometry elevation maximum (m)	0 - 800	700

Table 1: Ensemble parameters varied in the sensitivity analyses, with descriptions, units, ranges, and SP15 values.

localized by position or time.

The above-described ensemble structure is clearly limiting in the sense that 4 of the 20 parameters pertain to ice physics approximations while the other 16 explore surface BC regimes that can be seen to deviate from the sea-level record. From the perspective of pure ice-sheet dynamical methodology, the inclusion of parameters for the arbitrary local modification of physics and associated BCs is an unsatisfying compromise that respects neither observational fidelity nor logically coherent dynamical systems analysis. Beyond applying more sophisticated, but nevertheless global, physical approximations that expand the UofTGSM parameter space, the new approach adopted in the present work logically restricts local tuning to the pure GIA-based adjustment of reconstructed ice sheet thickness, I_{i6g}, to enforce leading-order consistency with the observations.

2.3 New Model Parameter Space

Even though the mass balance adjustment, ΔG, in Eq. 2 is designed to enforce consistency with pure GIA-based reconstructions, it can be regarded as a "pseudo-random" perturbation of any globally and externally parameterized surface mass balance, G. The hypothesis that misfits between GIA-based and dynamically simulated ice-sheet thicknesses are, in fact, "random errors" is consistent for a given global nudging time scale, τ_f, if ΔG respects the (not necessarily small) uncertainties in G. Since the ice-sheet structure is known to be strongly and unpredictably affected, for instance, by the aforementioned basal sliding and calving phenomenology as well as by surface accumulation and ablation, simulations with small τ_f and correspondingly large ΔG

are consistently interpretable even though there would be no plausibly large external ice sources or sinks if the model actually had predictive skill. After adopting the Parallel Ice Sheet Model (PISM) as a typical physical approximation of ice dynamics and specifying other model parameters based based upon the SeaRISE protocol (Winkelmann et al., 2011; Bindschadler et al., 2013; Nowicki et al., 2013a,b), SP15 applied this reasoning to extract ice-sheet dynamical information from Greenland, Antarctic, and Laurentide ice-sheet simulations that were nudged towards ICE-6G_C at time-scales of $\tau_f = 20$, 100, 200, and 1000 years. "Undersmoothed" simulations with 20 yr simulations occasionally exhibited markedly unrealistic surface BCs in order to enforce consistency with the GIA-based reconstruction, while "oversmoothed" simulations with 1000 yr occasionally exhibited the complementary failure mode by diverging from observational consistency in order to limit ΔG to the same order of magnitude (~ 1 m/yr) as simple surface accumulation and ablation. A $\tau_f = 100$ yr nudging time-scale was selected for the reference data set, and some preliminary attempt was made to characterize the uncertainty in surface BC fields in terms of variability over the set of all four τ_f values.

SP15 and Stuhne and Peltier (2015, 2016) demonstrated the generic applicability of their approach by simulating all major ice sheets using generic SeaRISE-based values for ice dynamical parameters other than τ_f, but this work did not address the variability associated with the global parameter space. The variability will be addressed in the present work, which describes sensitivity analyses based on an overall set of 107 North American ice sheet simulations obtained by variation of 9 global physical parameters. Table 1 summarizes information about the symbols, value ranges, and interpretations of τ_f and 8 other parameters. Analogously to the 4 non-climate ensemble parameters considered by TP04, these relate mostly to the critical and uncertain dynamical approximations of calving and basal sliding. Unlike the earlier version of the UofTGSM considered by TP04, however, the new version more accurately represents basal and ice-shelf physics as aspects of a tightly coupled dynamical evolution of buttressed continental sheets having both grounded and marine components. The mathematical details of the PISM-based dynamical system are most fully addressed in our work in the Appendix of Stuhne and Peltier (2015), which includes references the broader literature on this important and ongoing research topic. The evolution of thick grounded ice cover continues to be represented (as in Pyy, TPyy and related work) by a three-dimensional shallow-ice approximation-based (SIA-based) thermomechanical equation system, but newer methods employ secondary, two-dimensional shelfy-stream-based (SSA-based) dynamics to represent both ice shelves and the basal BCs of the grounded ice model. Both the SIA and the SSA components of the problem entail the solution of nonlinear elliptic Stokes-types equations, and both components independently introduce arbitrary factors (denoted A_{SIA} and A_{SSA} in Table 1) into their respective parameterizations of ice viscosity. Iceberg calving at the boundaries of

SSA-based floating ice shelf models is approximated, as in earlier work, by a variety of phenomenological techniques, and the simulation ensembles discussed in this Report vary the critical ice thickness (H_{crit} in Table 1) below which ice sheets break down.

In regions with grounded ice, the 2-D SSA "ice shelf" approximation is naturally interpretable as a till model governing the relations between shear stress, friction, and sliding at the base of the SIA-approximated ice sheet. In Table 1, the sliding law velocity parameter U_{ref} is analogous to the till viscosity of TP04 in the sense that it controls the parameterized relationship between sliding and stress. Local transitions between the "ice shelf interpretation" and the "till interpretation" of SSA dynamics are governed by a "till fraction angle" that depends upon the elevation of bedrock relative to sea level in a manner parameterized by the final four parameters in Table 1 (ϕ_{min}, ϕ_{max}, B_{min}, B_{max}).

3. RESULTS

3.1 Simulations and Ensembles

The 107 simulations considered in this Report are summarized in Tables 3-8, which appear at the end to facilitate readability. Individual simulations are assigned tags that loosely suggest the parameter changes differentiating the corresponding dataset from the reference datasets discussed in SP15. As the nomenclature evolved, these original datasets ended up with the respective labels f0500c0ssa0, f0100c0ssa0, f0050c0ssa0, and f0010c0ssa0 for the nudging time constants $\tau_f = 20$ yr, 100 yr, 200 yr, and 1000 yr. The sensitivity analyses that follow will consider the variability of the key results (ice thickness, permafrost thickness, basal temperature, basal melting rate, velocity, shear stress, and lake depth) over simulation ensembles consisting of subsets of the overall set of simulations in Tables 3-8. Table 2 summarizes the ensembles that will be considered in this Report by assigning each an ensemble tag and listing the individual constituent simulations (using an asterisk to denote the SP15 case that serves as the reference solution for that ensemble). Since the sensitivity of individual simulations to the nudging time scale τ_f was extensively discussed in previous works and since sensitivity to other model parameters is of a different logical character, each ensemble consists of simulations with a definite τ_f value encoded by the first 5 characters of its tag (f0500 for 20 yr, f0100 for 100 yr, f0050 for 200 yr, and f0010 for 1000 yr). The remaining characters suggest the nature of the assumed variations in other parameters within the ensemble. For instance, c0ssax denotes a set of simulations in which the assumed SSA scaling factor A_{SSA} varies for constant τ_f; c0siax is the analogue referring to the SIA scaling factor A_{SSA}. Ensembles ending with c0ttpx entrain variability with respect to the 4 closely related till geometry parameters, while ensembles ending

Index	Ensemble tag	Constituent solutions
1	f0010c0ssax	f0010c0ssa0* f0010c0ssa1 f0010c0ssa2 f0010c0ssa3
2	f0050c0ssax	f0050c0ssa0* f0050c0ssa1 f0050c0ssa2 f0050c0ssa3
3	f0100c0ssax	f0100c0ssa0* f0100c0ssa1 f0100c0ssa2 f0100c0ssa3
4	f0500c0ssax	f0500c0ssa0* f0500c0ssa1 f0500c0ssa2 f0500c0ssa3
5	f0010rnxxx	f0010c0ssa0* f0010rn001 f0010rn002 f0010rn003 f0010rn004 f0010rn005 f0010rn006 f0010rn007 f0010rn008 f0010rn009 f0010rn010 f0010rn011 f0010rn012 f0010rn013 f0010rn014 f0010rn015 f0010rn016 f0010rn017 f0010rn018 f0010rn019 f0010rn020
6	f0050rnxxx	f0050c0ssa0* f0050rn001 f0050rn002 f0050rn003 f0050rn004 f0050rn005 f0050rn006 f0050rn007 f0050rn008 f0050rn009 f0050rn010 f0050rn011 f0050rn012 f0050rn013 f0050rn014 f0050rn015 f0050rn016 f0050rn017 f0050rn018 f0050rn019 f0050rn020
7	f0100rnxxx	f0100c0ssa0* f0100rn001 f0100rn002 f0100rn003 f0100rn005 f0100rn006 f0100rn007 f0100rn008 f0100rn009 f0100rn010 f0100rn011 f0100rn012 f0100rn013 f0100rn014 f0100rn015 f0100rn016 f0100rn017 f0100rn018 f0100rn019 f0100rn020
8	f0500rnxxx	f0500c0ssa0* f0500rn001 f0500rn002 f0500rn003 f0500rn004 f0500rn005 f0500rn006 f0500rn007 f0500rn008 f0500rn009 f0500rn010 f0500rn011 f0500rn012 f0500rn013 f0500rn014 f0500rn015 f0500rn016 f0500rn017 f0500rn018 f0500rn019 f0500rn020
9	f0010c0ttpx	f0010c0ssa0* f0010c0ttp1 f0010c0ttp2
10	f0050c0ttpx	f0050c0ssa0* f0050c0ttp1 f0050c0ttp2
11	f0100c0ttpx	f0100c0ssa0* f0100c0ttp1 f0100c0ttp2
12	f0500c0ttpx	f0500c0ssa0* f0500c0ttp1 f0500c0ttp2
13	f0010c0siax	f0010c0ssa0* f0010c0sia1
14	f0050c0siax	f0050c0ssa0* f0050c0sia1
15	f0100c0siax	f0100c0ssa0* f0100c0sia1
16	f0500c0siax	f0500c0ssa0* f0500c0sia1
17	f0100rn01x	f0100c0ssa0* f0100rn010 f0100rn011 f0100rn012 f0100rn013 f0100rn014 f0100rn015 f0100rn016 f0100rn017 f0100rn018 f0100rn019

Table 2: Record of all ensembles considered, with tags assigned to subsets of the simulations in Tables 3 through 8 and asterisks denoting the reference solution within each ensemble.

with rnxxx entrain “generic” variability through the selection of random values for all parameters (other than τ_f) within the ranges listed in Table 1. For the particular nudging time constant ($\tau_f = 100$ yr) used for the canonical SP15 surface BC dataset, a f0100rn01x ensemble consisting of a 10-member subset of the full f0100rnxxx ensemble is also considered.

3.2 Measure of Sensitivity in Surface BCs

SP15 considered a limited simulation ensemble in which only the nudging time constant was varied, and devised a measure for characterizing the sensitivity of the reference dataset based on the f0100c0ssa0 simulation to variations in τ_f. This measure is not well suited to the more extensive sensitivity analyses described in this Report, in which the sensitivity of predictions to other model variables while τ_f is held constant within ensembles is considered. Considering that ensemble sizes are still relatively small and that results are highly correlated, it would also not be particularly informative to discuss standard quantities like the means and standard deviations of predicted surface BCs at potential DGR sites. The most relevant statistical information in a particular ensemble inheres, rather, in the largest deviations of predictions from the ensemble reference solution. Recognizing that it must preserve the signs of maximum-amplitude deviations, this sensitivity metric is computable for a given field, Ξ, as follows: i.e.,

$$\Xi_{\text{err}} = \begin{cases} \Xi_{\text{max}} - \Xi_{\text{ref}} & \text{if } \Xi_{\text{max}} - \Xi_{\text{ref}} > \Xi_{\text{ref}} - \Xi_{\text{min}} \\ \Xi_{\text{min}} - \Xi_{\text{ref}} & \text{otherwise,} \end{cases} \tag{3}$$

in which Ξ_{ref}, Ξ_{min}, and Ξ_{max} determine Ξ_{err} as a function of position and time for a given ensemble of simulations.

With regards to the earlier discussion, the application of the local sensitivity measure defined by Eq. (3) to nudged simulations treats uncertainties in the ice dynamics associated with a given GIA-based ice thickness reconstruction in an appropriately different manner than uncertainties in the reconstruction itself. Extensive analyses of the latter sources of uncertainty would require that the ICE-6G_C ice sheet thickness reconstruction be modified so as to nudge ice dynamics towards globally different land-ice evolution scenarios (for instance, scenarios in which pre-LGM ice margins advance and retreat with increased frequency as in TP*yy* and P*yy*). Considering that there is no doubt about the fact that all potential DGR sites are subject to repeated glaciation and deglaciation, the precise temporal and geographical patterns of such events are far less crucial than the local surface BC variability triggered by particular events (e.g., when ice cover is deepest at a site, when the ice margin crosses a site, etc.). Whereas the P*yy* analyses combined all the various sources of uncertainty in all of their simulation ensembles, the present sensitivity analyses will carefully consider the local sensitivity of surface BCs under conditions in which

uncertainties in ice sheet thickness are explicitly constrained by the nudging time constant, τ_f. Although unconstrained ice sheet dynamics (or, dynamics with very large τ_f) may admit observationally consistent glaciation scenarios with different spatio-temporal structures, the limiting amplitudes of local surface BC variations in these scenarios should not differ significantly from the results of the following sensitivity analyses.

3.3 General Considerations and Ice Thickness

Since the aim of this report is to analyze the sensitivity of a number of surface BC predictions to parameter variations determining a number of different ensembles, a relatively large number of combinations arise. To facilitate readability, the Figures referred to in this Section appear at the end of the Report in a systematic sequence that addresses ice thickness, permafrost depth, basal temperature, basal meltwater production, basal velocity, basal shear stress, and proglacial lake depth in the same order as they they were considered in SP15. As discussed in the preceding, ice thickness predictions are considered first because they have a special logical significance in the interpretation of nudged ice sheet simulations. Three frames at top and left of Figure 5 depict the ice thickness field from the f0100c0ssa0 reference solution of SP15 at three times that will be used for illustrative purposes in what follows. ~ 26 kyr BP represents conditions around LGM; 8.2 kyr BP represents conditions around the time Hudson's Bay opened to the ocean due to complex grounded and marine ice dynamics; and, 12.5 kyr BP represents intermediate conditions during the last deglaciation. The remaining 5 frames of the Figure illustrate ice thickness sensitivity at 12.5 kyr BP for five ensembles with the same constant nudging time constant ($\tau_f = 100$ yr). As should be expected, ensemble sensitivities tend to be concentrated near the edges of the ice sheet structure that was assimilated into all constituent simulations through the nudging. Ice sheet sensitivities have relatively consistent and significant (order 1000 m) bounds over all ensembles, but their extents and specific locations are highly ensemble dependent. Sensitivities to the SIA and SSA stiffness factors, A_{SIA} and A_{SSA}, are concentrated in a northeastern coastal zone where Baffin Bay ice shelf buttressing and calving are presumably coming into play, while sensitivity to till geometry parameterization is more broadly distributed along the ice sheet margins. The random f0100rnxxx ensemble exhibits the sensitivities of all parameter-focused ensembles simultaneously and in moderately amplified form. The f0100rn01x subset of the this ensemble exhibits almost exactly the same sensitivities, which consequently appear to be accounted for by a limited number of "outlying" ensemble constituents.

Focusing upon the 26 kyr BP and 8.2 kyr BP time levels, Figures 6 through 9 illustrate the effects of nudging time constant upon the sensitivity of ice thickness for a succession of ensembles determined by A_{SIA} variations, till parameterization variations, A_{SIA} variations, and random

multi-parameter variations, respectively. The 8.2 kyr BP timeframe differs from the others considered in the sense that the Laurentide ice sheet has mostly retreated away from coastlines other than that of Hudson's Bay, whose contemporary emergence constituted a kind of paleogeographical "tipping point." Under such sensitive conditions, simulations that are only weakly nudged towards ICE-6G_C clearly exhibit greater local sensitivity to other parameters than strongly nudged simulations. The maximally extended LGM ice sheet exhibits consistently strong thickness sensitivities at its margins, although the extent of sensitive regions increases as nudging weakens (i.e., as τ_f increases). Since potential repository sites lie well within glaciated regions at the times when ice cover reaches its maximal extent, predictions of surface BCs under these limiting conditions should not be affected by strong parameter-sensitivity at the glacial margins.

3.4 Permafrost Thickness

Figures 10 through 14 depict the same sensitivity information for permafrost thickness as the corresponding Figures 5 through 9 depict for ice thickness. The preceding discussion about local sensitivities in the various simulation ensembles mostly extends to this surface BC prediction as well, but there are two clear distinctions to be drawn. Most obviously, the consistent absence of 8.2 kyr BP permafrost thickness sensitivity near Hudson's Bay indicates that this surface BC was not affected by the aforementioned "tipping point" dynamics. The other, somewhat more subtle, deviations from the ice sheet thickness sensitivity analyses relate to sensitivity in marginal regions, which have considerably narrower extents that consistently *decrease* as τ_f increases.

3.5 Basal Temperature

Since the physics of basal temperature are closely coupled to permafrost thickness, it is not surprising that Figures 15 through 19 exhibit very similar sensitivity behavior as their analogues for permafrost thickness. The Hudson's Bay "tipping point" is once again absent, and there is, once again, a subtle but consistent decrease in marginal sensitivity with increasing τ_f.

3.6 Basal Meltwater Production

Whereas the decreases in marginal sensitivity with increasing nudging time constant were somewhat subtle in the permafrost thickness and basal temperature sensitivity analyses, they become glaringly obvious in the basal meltwater production results depicted in Figures 20 through 24. At the same time, this surface BC field also exhibits some of the characteristics that

were seen in the ice thickness sensitivity analyses. There is, in particular, clear evidence of Hudson's Bay "tipping point" behavior at 8.2 kyr BP.

3.7 Basal Velocity, Shear Stress, and Lake Depth

The themes of the preceding four subsections continue to occur in relation to the basal velocity, basal shear stress, and proglacial lake depth fields, whose sensitivity analyses are presented in Figures 25 through 39 in the continuation of the preceding sequence. Vector plots are used to depict the values and sensitivities of the vector velocity and shear stress fields. The basal shear stress sensitivity analyses are consistent with those of ice thickness in the sense that decreased nudging tends to increase sensitivity. In contrast, basal velocity and proglacial lake depth exhibit a mixture of "forward sensitivity" that increases with τ_f and "reverse sensitivity" that decreases with τ_f. Lake depth sensitivity, for instance, appears to adhere to the former pattern in the 8.2 kyr BP climate state while adhering to the latter pattern in the LGM climate state (as seen in Figure 39). Basal velocity sensitivity is even more complex in the sense that its variation with respect to nudging intensity depends both upon the instantaneous ice sheet configuration and upon the ensemble under consideration. With regards to the sensitivity of basal velocity to till geometry, Figure 27 resembles the proglacial lake depth results in exhibiting reverse sensitivity at LGM and forward sensitivity at 8.2 kyr. The sensitivities of basal velocity to other parameters more closely resemble the consistently forward sensitivities seen in the ice thickness and basal shear stress results. The special significance of till geometry parameters can in this context be understood in terms of their role in the physical coupling of basal velocity to basal meltwater production. In the absense of a sophisticated basal sliding parameterization, the shallow ice approximation would determine horizontal velocity in terms of ice thickness and basal shear stress (and thereby propagate the simple forward sensitivities of these fields to the velocity field). The dynamical complexities of the basal sliding parameterization also affect the aforementioned proglacial lake depth field, which SP15 diagnosed from other ice dynamical fields using a simplified approximation of surface hydrology. The improvement of the surface hydrological model and the corresponding refinement of sensitivity analyses are the objectives of ongoing work.

4. DISCUSSION

In discussing the results of the previous Section and assessing their implications for the surface BC analyses of SP15, it is important to continue expanding upon the previously discussed distinction between the sensitivity of predictions to (GIA-reconstructed) ice thickness and their sensitivity to ice sheet dynamical model parameters. The sensitivity analyses described herein

address the latter form of parameter sensitivity subject to dynamics in which the critical structures of the ice thickness history (e.g., ice margins and ice domes) are constrained by nudging towards the assumed ICE-6G_C reconstruction. It was shown that the sensitivities of the surface BC predictions of SP15 to ice dynamical parameters other than τ_f were mostly localized around the imposed ice sheet margins (especially the coastal margins). The detailed spatial patterns of this localization depended upon the nature of parameter variations within an ensemble, with the most extensive and highest amplitude sensitivities occurring in ensembles where multiple parameters vary randomly. The extents of sensitive marginal regions also tended to vary systematically with the nudging time scale, τ_f, but *not* necessarily in the sense of simple forward sensitivity that increased as nudging towards the reference solution becomes weaker (i.e., as τ_f increases). Ice thickness and basal shear stress did consistently exhibit forward sensitivity, but permafrost thickness, basal temperature, and (especially) basal meltwater production just as consistently exhibited reverse sensitivity that *decreased* as τ_f increased. Basal velocity and lake depth exhibited aspects of both behavior.

If the assimilation of GIA-based ice thickness information through nudging is regarded as a mechanism for forcing ice dynamics towards a fixed "reference solution," then it may seem very unusual that certain ice dynamical predictions exhibit sensitivity that increases with nudging intensity. This reverse sensitivity is, however, explainable in terms of the fact that ice dynamics flushes the "anomalous" mass balances arising from ΔG through the mass-conserving system. It makes sense that ice sources and sinks arising from strong nudging can counteract decreased sensitivity in ice thickness by triggering strong, parameter-dependent fluctuations in fields like basal meltwater production. SP15 treated nudging at time scale $\tau_f = 20$ yr as suspect because it gave rise to high amplitude anomalous mass balances with unusual spatial signatures, and the sensitivity analysis results for basal meltwater production (especially in the top left frame of Figure 20) appear to justify this caution. At the other end of the nudging time scale spectrum ($\tau_f = 1000$ yr), the previous results of SP15 and Stuhne and Peltier (2015, 2016) imply that dynamical ice thickness is sufficiently sensitive to ice model parameters to disrupt the observational consistency of the ICE-6G_C reconstruction. The results of the sensitivity analyses further clarify how the selection of the $\tau_f = 100$ yr solution as the reference solution for the SP15 dataset avoided the potential problems at very small and very large nudging time scales.

Even when ensembles at the minimum and maximum of the nudging time-scale spectrum are admitted as legitimate results, the absolute amplitudes of surface BC sensitivities appear to be reasonably consistent between ensembles. It can be seen upon examination of the Figures and Figure legends that field sensitivities, Φ_{err}, are much smaller in the ice sheet interior than at margins, where they saturate at amplitudes comparable to those of the corresponding reference solutions, Φ_{ref}. Since the globally maximal ice thickness at LGM occurs in the ice sheet interior,

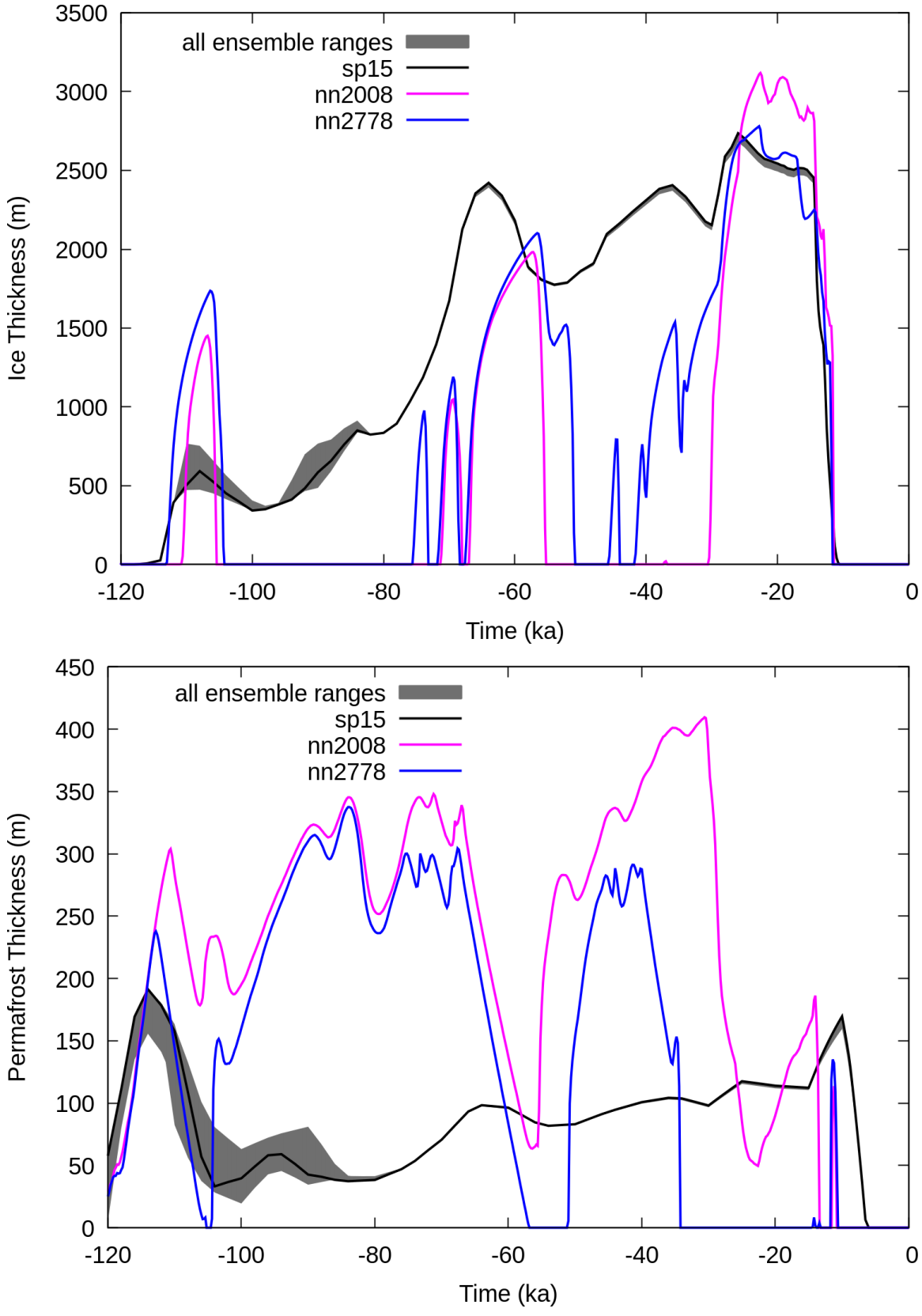

Figure 3: Ice and permafrost thickness time series illustrate the reference solution at the 4CS site, compared to nn2008 and nn2778 solutions (with the shaded area indicating total variability over all ensembles with $\tau_f = 100$ yr).

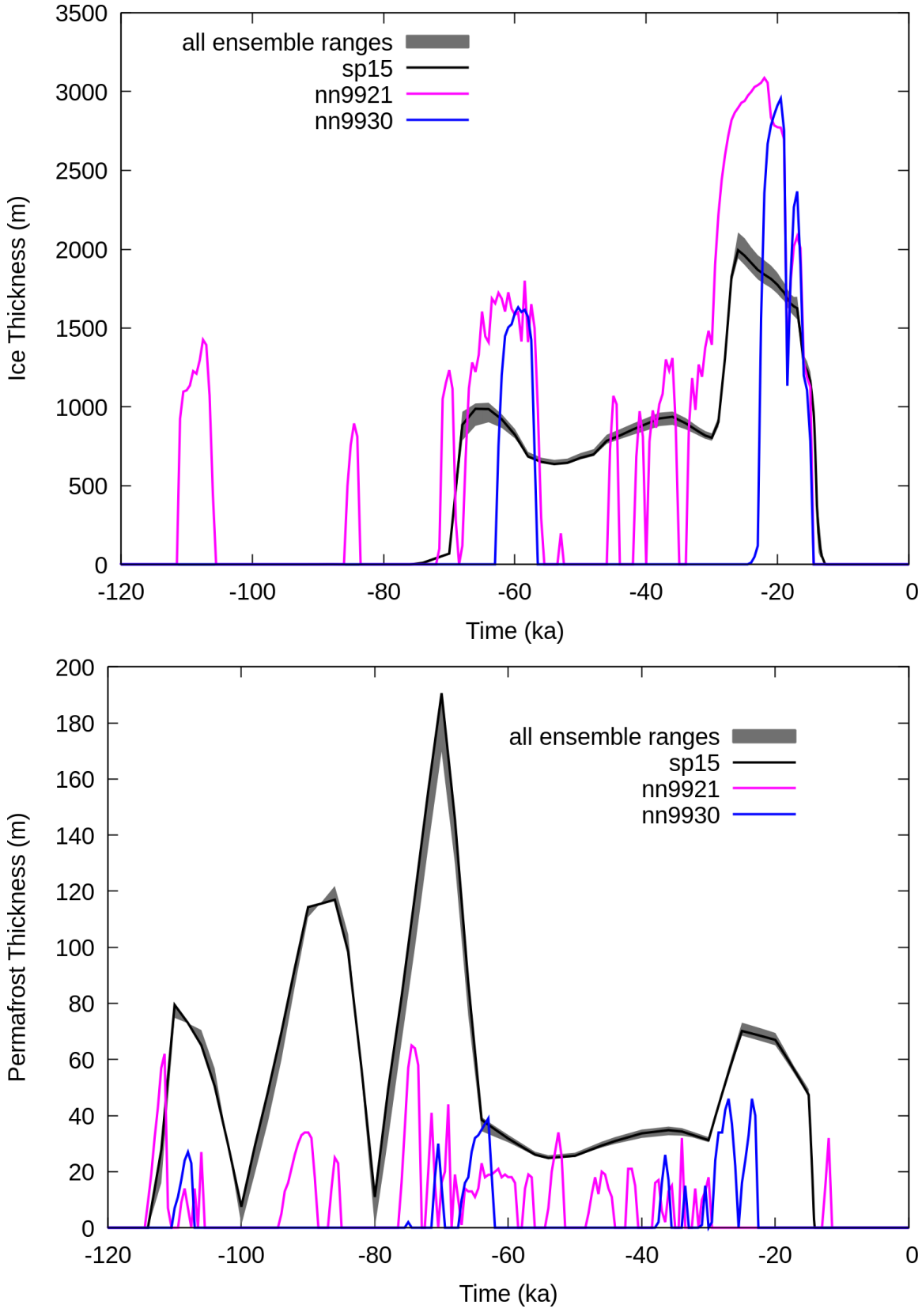

Figure 4: Analogue of Figure 3 at the 5CS site, with comparisons to nn9921 and nn9930 solutions.

this aspect of the solutions is very well constrained by GIA observations. The new sensitivity results are consistent with SP15, where examination of surface BC time series at hypothetical repository sites confirmed that the reference solution agreed with the earlier solutions of P*yy* to within approximately a factor of two. In order to further illustrate the local time variations of model sensitivities, Figures 3 and 4 plot the evolution of ice thickness and permafrost thickness at the sites considered in SP15 (4CS and 5CS, respectively, with the appropriate local nn*xxxx* solutions overlaid for comparison). Black lines indicate the SP15 reference solution curves, while the gray areas are delimited by minimum and maximum values over all of the $\tau_f = 100$ yr ensembles considered in the present report. SP15 employed a simple approximation to estimate ice dynamical uncertainty based solely upon sensitivity to τ_f, and comparisons with the results of this report confirm that the ranges of variations in predicted fields are relatively narrow when τ_f is fixed at the 100 yr value employed to compute the reference solution.

As exemplified in Figures 3 and 4, the detailed time variations of ice thickness and other fields at a given site are highly dependent upon complex ice dynamical parameterizations and surface climate BCs, and the assumptions made by SP15 and in the present sensitivity analyses give rise to slow glaciation-deglaciation cycles rather than to the highly intermittent cycles seen in TP*yy*. The methodology employed weights simulation ensembles in favour of solutions that are consistent with the sea-level record, but predictions of the local extreme values of fields are reproducible to within an order of magnitude between models and simulation ensembles regardless of which assumptions are made about long-term global climate change. Ongoing research aims to further tighten the constraints upon models of long-term global climate change. The sensitivity results discussed herein reinforce P*yy* in suggesting that the estabilished understanding of bounding glacialogical conditions is reasonably sound.

5. SUMMARY AND CONCLUSIONS

The key points of this paper and the advances in the described work can be summarized in terms of the following concluding remarks:

- With reference to 107 ice dynamical simulations and subject to a global constraint that nudges simulated ice thickness towards the GIA-based ICE-6G_C reconstruction at time scale τ_f, the sensitivity of the surface BCs of SP15 to a set of key ice model parameters was analyzed.
- As SP15 saw in the comparison of local surface BC time series with the earlier predictions of P*yy*, the amplitudes of parameter-dependent fluctuations are consistently within the same order of magnitude as the reference solution.

- Parameter-sensitive regions are localized near ice margins and coastal grounding lines to extents that depend upon nudging time constant, τ_f, and upon the nature of parameter variation within a particular ensemble (with the most extensive sensitivity being to random parameter selections).
- Ice thickness and basal shear stress exhibit forward sensitivity that increases in extent as τ_f increases (i.e., as nudging is weakened), while the effects of ΔG upon mass balance trigger reverse sensitivity in permafrost thickness, basal temperature, basal meltwater production.
- Other fields exhibit mixed behavior, and the overall results build confidence in the reasonable selection of $\tau_f = 100$ yr for the SP15 dataset.
- The assumed GIA-based ICE-6G_C reconstruction of ice thickness at, and subsequent to, LGM is well constrained by observations, and nudged ice dynamical simulations consistently show that variability arising from model parameter sensitivity is consistently low ($\pm \sim 50$ m) in the ice sheet interior.

REFERENCES

Argus, D. F., W. R. Peltier, R. Drummond, and S. Moore (2014), The antarctic component of glacial isostatic adjustment model ICE-6G_C (VM5a) based upon GPS measurements of vertical motion of the crust, exposure age dating of ice thickness variations and relative sea level histories, Geophys J. Int., 198, 537–563.

Bindschadler, R. A., S. Nowicki, A. Abe-Ouchi, A. Aschwanden, H. Choi, J. Fastook, G. Granzow, R. Greve, G. Gutowski, U. Herzfeld, et al. (2013), Ice-sheet model sensitivities to environmental forcing and their use in projecting future sea level (the SeaRISE project), Journal of Glaciology, 59(214), 195–224.

Clark, J. A., W. E. Farrell, and W. R. Peltier (1978), Global changes in postglacial sea level: a numerical calculation, Quaternary Research, 9(3), 265–287.

Dyke, A. S. (2004), An outline of North American deglaciation with emphasis on central and northern Canada, Developments in Quaternary Sciences, 2, 373–424.

Farrell, W., and J. A. Clark (1976), On postglacial sea level, Geophysical Journal International, 46(3), 647–667.

Hemming, S. R. (2004), Heinrich events: Massive late Pleistocene detritus layers of the North Atlantic and their global climate imprint, Reviews of Geophysics, 42(1).

Imbrie, J., and A. McIntyre (2006), SPECMAP time scale developed by Imbrie et al., 1984 based on normalized planktonic records (normalized O-18 vs. time, specmap. 017), Earth Syst Sci Data, 10.

Johnsen, S. J., H. B. Clausen, W. Dansgaard, N. S. Gundestrup, C. U. Hammer, U. Andersen, K. K. Andersen, C. S. Hvidberg, D. Dahl-Jensen, J. P. Steffensen, et al. (1997), The δ18O record along the Greenland Ice Core Project deep ice core and the problem of possible Eemian climatic instability, Journal of Geophysical Research: Oceans (1978–2012), 102(C12), 26,397–26,410.

Nowicki, S., R. A. Bindschadler, A. Abe-Ouchi, A. Aschwanden, E. Bueler, H. Choi, J. Fastook, G. Granzow, R. Greve, G. Gutowski, et al. (2013a), Insights into spatial sensitivities of ice mass response to environmental change from the SeaRISE ice sheet modeling project I: Antarctica, Journal of Geophysical Research: Earth Surface, 118(2), 1002–1024.

Nowicki, S., R. A. Bindschadler, A. Abe-Ouchi, A. Aschwanden, E. Bueler, H. Choi, J. Fastook, G. Granzow, R. Greve, G. Gutowski, et al. (2013b), Insights into spatial sensitivities of ice

mass response to environmental change from the SeaRISE ice sheet modeling project II: Greenland, Journal of Geophysical Research: Earth Surface, 118(2), 1025–1044.

Peltier, W. (1974), The impulse response of a Maxwell Earth, Reviews of Geophysics, 12(4), 649–669.

Peltier, W. (1976a), Glacial-Isostatic AdjustmentII. The Inverse Problem, Geophysical Journal of the Royal astronomical society, 46(3), 669–705.

Peltier, W. (1976b), Glacio-isostatic adjustment-III. The inverse problem, Geophysics Journal, 46, 669–706.

Peltier, W. (1998), Postglacial variations in the level of the sea: Implications for climate dynamics and solid-earth geophysics, Reviews of Geophysics, 36(4), 603–689.

Peltier, W. (2007), History of Earth rotation, vol. 9, pp. 243–293, Elsevier Oxford.

Peltier, W., and J. Andrews (1976), Glacial-Isostatic AdjustmentI. The Forward Problem, Geophysical Journal of the Royal Astronomical Society, 46(3), 605–646.

Peltier, W., W. Farrell, and J. Clark (1978), Glacial isostasy and relative sea level: a global finite element model, Tectonophysics, 50(2), 81–110.

Peltier, W. R. (2006), Boundary conditions data sets for spent fuel repository performance assessment, Tech. Rep. 06819-REP-01200-10154-R00, Department of Physics, University of Toronto, East Lansing, Michigan.

Peltier, W. R. (2008), Phase I Long Term Climate Change Study, Tech. Rep. OPG 00216-REP-01300-00004-R00, Ontario Power Generation, http://www.opg.com/generating-power/nuclear/nuclear-waste-management/ Deep-Geologic-Repository/Documents/HPD/4.3.33_PhaseILongTermClimateChangeStudy.pdf.

Peltier, W. R. (2011), Long-term climate change, Tech. Rep. NWMO DGR-TR-2011-14, Department of Physics, University of Toronto, Toronto, Ontario.

Peltier, W. R., D. F. Argus, and R. Drummond (2015), Space geodesy constrains ice age terminal deglaciation: The global ICE-6G_C (VM5a) model, Journal of Geophysical Research: Solid Earth, 119, 1–38.

Petit, J., D. Jouzel, D. Raynaud, N. Barkov, J. Barnola, I. Basile, M. Bender, J. Chappellaz, J. Davis, G. Delaygue, et al. (2001), Vostok Ice Core Data for 420,000 Years, IGBP PAGES/World Data Center for Paleoclimatology Data Contribution Series# 2001-076, NOAA/NGDC Paleoclimatology Program, Boulder CO, USA.

Stuhne, G., and W. Peltier (2015), Reconciling the ICE-6G_C reconstruction of glacial chronology with ice sheet dynamics: the cases of Greenland and Antarctica, Journal of Geophysical Research: Land Surface, 120, 1841–1865.

Stuhne, G., and W. Peltier (2016), Assimilating the ICE-6G_C reconstruction of the latest Quaternary ice-age cycle into numerical simulations of the Laurentide and Fennoscandian ice-sheets, Journal of Geophysical Research: Land Surface, submitted.

Tarasov, L., and W. Peltier (1997), Terminating the 100 kyr ice age cycle, Journal of Geophysical Research, 102(D18), 21,665–21.

Tarasov, L., and W. Peltier (1999), Impact of thermomechanical ice sheet coupling on a model of the 100 kyr ice age cycle, Journal of Geophysical Research. D. Atmospheres, 104, 9517–9545.

Tarasov, L., and W. Peltier (2000), Laurentide ice sheet aspect ratio in models based on Glen's flow law, Annals of Glaciology, 30(1), 177–186.

Tarasov, L., and W. Peltier (2002), Greenland glacial history and local geodynamic consequences, Geophys. J. Int, 150, 198–229.

Tarasov, L., and W. Peltier (2003), Greenland glacial history, borehole constraints, and Eemian extent, J. Geophys. Res, 108(2143), 10–1029.

Tarasov, L., and W. Peltier (2004), A geophysically constrained large ensemble analysis of the deglacial history of the North American ice-sheet complex, Quaternary Science Reviews, 23(3), 359–388.

Tarasov, L., and W. Peltier (2007), Coevolution of continental ice cover and permafrost extent over the last glacial-interglacial cycle in North America, Journal of geophysical research, 112(F2).

Waelbroeck, C., L. Labeyrie, E. Michel, J. C. Duplessy, J. McManus, K. Lambeck, E. Balbon, and M. Labracherie (2002), Sea-level and deep water temperature changes derived from benthic foraminifera isotopic records, Quaternary Science Reviews, 21(1), 295–305.

Winkelmann, R., M. Martin, M. Haseloff, T. Albrecht, E. Bueler, C. Khroulev, and A. Levermann (2011), The Potsdam parallel ice sheet model (PISM-PIK)–Part 1: Model description, The Cryosphere, 5(3), 715–726.

APPENDIX A: TABLES AND FIGURES

The following Tables and Figures were omitted from the main body of the text in order to facilitate readability.

Index	Solution tag	Parameter changes
1	f0010c0ssa0	$\tau_f = 1000$ $I_{\text{crit}} = 250$ $A_{\text{SSA}} = 1.0$
2	f0010c0ssa1	$\tau_f = 1000$ $I_{\text{crit}} = 250$ $A_{\text{SSA}} = 2.0$
3	f0010c0ssa2	$\tau_f = 1000$ $I_{\text{crit}} = 250$ $A_{\text{SSA}} = 4.0$
4	f0010c0ssa3	$\tau_f = 1000$ $I_{\text{crit}} = 250$ $A_{\text{SSA}} = 0.5$
5	f0050c0ssa0	$\tau_f = 200$ $I_{\text{crit}} = 250$ $A_{\text{SSA}} = 1.0$
6	f0050c0ssa1	$\tau_f = 200$ $I_{\text{crit}} = 250$ $A_{\text{SSA}} = 2.0$
7	f0050c0ssa2	$\tau_f = 200$ $I_{\text{crit}} = 250$ $A_{\text{SSA}} = 4.0$
8	f0050c0ssa3	$\tau_f = 200$ $I_{\text{crit}} = 250$ $A_{\text{SSA}} = 0.5$
9	f0100c0ssa0	$\tau_f = 100$ $I_{\text{crit}} = 250$ $A_{\text{SSA}} = 1.0$
10	f0100c0ssa1	$\tau_f = 100$ $I_{\text{crit}} = 250$ $A_{\text{SSA}} = 2.0$
11	f0100c0ssa2	$\tau_f = 100$ $I_{\text{crit}} = 250$ $A_{\text{SSA}} = 4.0$
12	f0100c0ssa3	$\tau_f = 100$ $I_{\text{crit}} = 250$ $A_{\text{SSA}} = 0.5$
13	f0500c0ssa0	$\tau_f = 20$ $I_{\text{crit}} = 250$ $A_{\text{SSA}} = 1.0$
14	f0500c0ssa1	$\tau_f = 20$ $I_{\text{crit}} = 250$ $A_{\text{SSA}} = 2.0$
15	f0500c0ssa2	$\tau_f = 20$ $I_{\text{crit}} = 250$ $A_{\text{SSA}} = 4.0$
16	f0500c0ssa3	$\tau_f = 20$ $I_{\text{crit}} = 250$ $A_{\text{SSA}} = 0.5$
17	f0010c0sia1	$\tau_f = 1000$ $I_{\text{crit}} = 250$ $A_{\text{SIA}} = 2.8$
18	f0050c0sia1	$\tau_f = 200$ $I_{\text{crit}} = 250$ $A_{\text{SIA}} = 2.8$
19	f0100c0sia1	$\tau_f = 100$ $I_{\text{crit}} = 250$ $A_{\text{SIA}} = 2.8$
20	f0500c0sia1	$\tau_f = 20$ $I_{\text{crit}} = 250$ $A_{\text{SIA}} = 2.8$
21	f0010c0ttp1	$\tau_f = 1000$ $I_{\text{crit}} = 250$ $(\phi_{\text{min}}, \phi\text{max}, B_{\text{min}}, B\text{max}) = (5.0, 40.0, -300.0, 700.0)$
22	f0010c0ttp2	$\tau_f = 1000$ $I_{\text{crit}} = 250$ $(\phi_{\text{min}}, \phi\text{max}, B_{\text{min}}, B\text{max}) = (5.0, 10.0, -300.0, 700.0)$
23	f0050c0ttp1	$\tau_f = 200$ $I_{\text{crit}} = 250$ $(\phi_{\text{min}}, \phi\text{max}, B_{\text{min}}, B\text{max}) = (5.0, 40.0, -300.0, 700.0)$
24	f0050c0ttp2	$\tau_f = 200$ $I_{\text{crit}} = 250$ $(\phi_{\text{min}}, \phi\text{max}, B_{\text{min}}, B\text{max}) = (5.0, 10.0, -300.0, 700.0)$
25	f0100c0ttp1	$\tau_f = 100$ $I_{\text{crit}} = 250$ $(\phi_{\text{min}}, \phi\text{max}, B_{\text{min}}, B\text{max}) = (5.0, 40.0, -300.0, 700.0)$
26	f0100c0ttp2	$\tau_f = 100$ $I_{\text{crit}} = 250$ $(\phi_{\text{min}}, \phi\text{max}, B_{\text{min}}, B\text{max}) = (5.0, 10.0, -300.0, 700.0)$
27	f0500c0ttp1	$\tau_f = 20$ $I_{\text{crit}} = 250$ $(\phi_{\text{min}}, \phi\text{max}, B_{\text{min}}, B\text{max}) = (5.0, 40.0, -300.0, 700.0)$

Table 3: Record of all solutions considered, with tags and parameter changes from the SP15 simulation (part 1).

Index	Solution tag	Parameter changes
28	f0500c0ttp2	$\tau_f = 20$ $I_{\text{crit}} = 250$ $(\phi_{\text{min}}, \phi\text{max}, B_{\text{min}}, B\text{max}) = (5.0, 10.0, -300.0, 700.0)$
29	f0010rn001	$\tau_f = 1000$ $I_{\text{crit}} = 345.544$ $A_{\text{SIA}} = 3.970$ $A_{\text{SSA}} = 5.153$ $U_{\text{ref}} = 180.372$ $(\phi_{\text{min}}, \phi\text{max}, B_{\text{min}}, B\text{max}) = (17.503, 40.812, -74.736, 497.574)$
30	f0010rn002	$\tau_f = 1000$ $I_{\text{crit}} = 291.643$ $A_{\text{SIA}} = 4.273$ $A_{\text{SSA}} = 3.300$ $U_{\text{ref}} = 243.577$ $(\phi_{\text{min}}, \phi\text{max}, B_{\text{min}}, B\text{max}) = (11.285, 37.667, -367.816, 756.078)$
31	f0010rn003	$\tau_f = 1000$ $I_{\text{crit}} = 280.076$ $A_{\text{SIA}} = 6.673$ $A_{\text{SSA}} = 4.279$ $U_{\text{ref}} = 53.014$ $(\phi_{\text{min}}, \phi\text{max}, B_{\text{min}}, B\text{max}) = (12.091, 35.405, -64.119, 59.890)$
32	f0010rn004	$\tau_f = 1000$ $I_{\text{crit}} = 194.502$ $A_{\text{SIA}} = 3.381$ $A_{\text{SSA}} = 2.439$ $U_{\text{ref}} = 95.833$ $(\phi_{\text{min}}, \phi\text{max}, B_{\text{min}}, B\text{max}) = (6.143, 30.123, -215.385, 271.029)$
33	f0010rn005	$\tau_f = 1000$ $I_{\text{crit}} = 202.785$ $A_{\text{SIA}} = 4.076$ $A_{\text{SSA}} = 3.692$ $U_{\text{ref}} = 242.301$ $(\phi_{\text{min}}, \phi\text{max}, B_{\text{min}}, B\text{max}) = (22.817, 32.251, -336.609, 113.260)$
34	f0010rn006	$\tau_f = 1000$ $I_{\text{crit}} = 279.704$ $A_{\text{SIA}} = 3.730$ $A_{\text{SSA}} = 4.927$ $U_{\text{ref}} = 101.440$ $(\phi_{\text{min}}, \phi\text{max}, B_{\text{min}}, B\text{max}) = (10.406, 38.769, -56.359, 416.858)$
35	f0010rn007	$\tau_f = 1000$ $I_{\text{crit}} = 215.139$ $A_{\text{SIA}} = 3.964$ $A_{\text{SSA}} = 1.969$ $U_{\text{ref}} = 237.349$ $(\phi_{\text{min}}, \phi\text{max}, B_{\text{min}}, B\text{max}) = (12.279, 31.583, -314.542, 667.647)$
36	f0010rn008	$\tau_f = 1000$ $I_{\text{crit}} = 293.425$ $A_{\text{SIA}} = 3.097$ $A_{\text{SSA}} = 4.083$ $U_{\text{ref}} = 134.859$ $(\phi_{\text{min}}, \phi\text{max}, B_{\text{min}}, B\text{max}) = (22.346, 39.726, -306.199, 646.211)$
37	f0010rn009	$\tau_f = 1000$ $I_{\text{crit}} = 181.086$ $A_{\text{SIA}} = 4.313$ $A_{\text{SSA}} = 0.705$ $U_{\text{ref}} = 139.307$ $(\phi_{\text{min}}, \phi\text{max}, B_{\text{min}}, B\text{max}) = (5.501, 34.600, -316.803, 277.816)$
38	f0010rn010	$\tau_f = 1000$ $I_{\text{crit}} = 324.450$ $A_{\text{SIA}} = 4.336$ $A_{\text{SSA}} = 5.055$ $U_{\text{ref}} = 95.976$ $(\phi_{\text{min}}, \phi\text{max}, B_{\text{min}}, B\text{max}) = (19.252, 39.156, -175.524, 334.898)$
39	f0010rn011	$\tau_f = 1000$ $I_{\text{crit}} = 181.758$ $A_{\text{SIA}} = 6.489$ $A_{\text{SSA}} = 0.951$ $U_{\text{ref}} = 141.640$ $(\phi_{\text{min}}, \phi\text{max}, B_{\text{min}}, B\text{max}) = (24.915, 30.183, -317.530, 84.915)$
40	f0010rn012	$\tau_f = 1000$ $I_{\text{crit}} = 185.701$ $A_{\text{SIA}} = 2.594$ $A_{\text{SSA}} = 2.072$ $U_{\text{ref}} = 216.653$ $(\phi_{\text{min}}, \phi\text{max}, B_{\text{min}}, B\text{max}) = (8.544, 41.917, -107.765, 293.515)$
41	f0010rn013	$\tau_f = 1000$ $I_{\text{crit}} = 180.317$ $A_{\text{SIA}} = 1.692$ $A_{\text{SSA}} = 4.556$ $U_{\text{ref}} = 100.567$ $(\phi_{\text{min}}, \phi\text{max}, B_{\text{min}}, B\text{max}) = (14.757, 32.077, -166.514, 11.035)$
42	f0010rn014	$\tau_f = 1000$ $I_{\text{crit}} = 194.313$ $A_{\text{SIA}} = 4.964$ $A_{\text{SSA}} = 1.599$ $U_{\text{ref}} = 289.022$ $(\phi_{\text{min}}, \phi\text{max}, B_{\text{min}}, B\text{max}) = (18.631, 33.769, -382.980, 333.287)$
43	f0010rn015	$\tau_f = 1000$ $I_{\text{crit}} = 335.290$ $A_{\text{SIA}} = 3.170$ $A_{\text{SSA}} = 1.652$ $U_{\text{ref}} = 262.300$ $(\phi_{\text{min}}, \phi\text{max}, B_{\text{min}}, B\text{max}) = (7.943, 38.688, -281.252, 781.542)$

Table 4: Record of all solutions considered, with tags and parameter changes from the SP15 simulation (part 2).

Index	Solution tag	Parameter changes
44	f0010rn016	$\tau_f = 1000$ $I_{\text{crit}} = 203.298$ $A_{\text{SIA}} = 6.489$ $A_{\text{SSA}} = 0.965$ $U_{\text{ref}} = 51.437$ $(\phi_{\text{min}}, \phi\text{max}, B_{\text{min}}, B\text{max}) = (20.389, 39.244, -390.323, 480.703)$
45	f0010rn017	$\tau_f = 1000$ $I_{\text{crit}} = 239.621$ $A_{\text{SIA}} = 4.241$ $A_{\text{SSA}} = 5.628$ $U_{\text{ref}} = 74.416$ $(\phi_{\text{min}}, \phi\text{max}, B_{\text{min}}, B\text{max}) = (5.710, 27.124, -206.006, 634.346)$
46	f0010rn018	$\tau_f = 1000$ $I_{\text{crit}} = 203.670$ $A_{\text{SIA}} = 4.161$ $A_{\text{SSA}} = 3.376$ $U_{\text{ref}} = 221.915$ $(\phi_{\text{min}}, \phi\text{max}, B_{\text{min}}, B\text{max}) = (24.973, 34.136, -361.008, 522.233)$
47	f0010rn019	$\tau_f = 1000$ $I_{\text{crit}} = 175.306$ $A_{\text{SIA}} = 4.223$ $A_{\text{SSA}} = 3.779$ $U_{\text{ref}} = 154.003$ $(\phi_{\text{min}}, \phi\text{max}, B_{\text{min}}, B\text{max}) = (22.616, 35.260, -117.656, 423.841)$
48	f0010rn020	$\tau_f = 1000$ $I_{\text{crit}} = 152.087$ $A_{\text{SIA}} = 1.616$ $A_{\text{SSA}} = 0.774$ $U_{\text{ref}} = 177.468$ $(\phi_{\text{min}}, \phi\text{max}, B_{\text{min}}, B\text{max}) = (7.799, 35.713, -356.247, 207.038)$
49	f0050rn001	$\tau_f = 200$ $I_{\text{crit}} = 345.544$ $A_{\text{SIA}} = 3.970$ $A_{\text{SSA}} = 5.153$ $U_{\text{ref}} = 180.372$ $(\phi_{\text{min}}, \phi\text{max}, B_{\text{min}}, B\text{max}) = (17.503, 40.812, -74.736, 497.574)$
50	f0050rn002	$\tau_f = 200$ $I_{\text{crit}} = 291.643$ $A_{\text{SIA}} = 4.273$ $A_{\text{SSA}} = 3.300$ $U_{\text{ref}} = 243.577$ $(\phi_{\text{min}}, \phi\text{max}, B_{\text{min}}, B\text{max}) = (11.285, 37.667, -367.816, 756.078)$
51	f0050rn003	$\tau_f = 200$ $I_{\text{crit}} = 280.076$ $A_{\text{SIA}} = 6.673$ $A_{\text{SSA}} = 4.279$ $U_{\text{ref}} = 53.014$ $(\phi_{\text{min}}, \phi\text{max}, B_{\text{min}}, B\text{max}) = (12.091, 35.405, -64.119, 59.890)$
52	f0050rn004	$\tau_f = 200$ $I_{\text{crit}} = 194.502$ $A_{\text{SIA}} = 3.381$ $A_{\text{SSA}} = 2.439$ $U_{\text{ref}} = 95.833$ $(\phi_{\text{min}}, \phi\text{max}, B_{\text{min}}, B\text{max}) = (6.143, 30.123, -215.385, 271.029)$
53	f0050rn005	$\tau_f = 200$ $I_{\text{crit}} = 202.785$ $A_{\text{SIA}} = 4.076$ $A_{\text{SSA}} = 3.692$ $U_{\text{ref}} = 242.301$ $(\phi_{\text{min}}, \phi\text{max}, B_{\text{min}}, B\text{max}) = (22.817, 32.251, -336.609, 113.260)$
54	f0050rn006	$\tau_f = 200$ $I_{\text{crit}} = 279.704$ $A_{\text{SIA}} = 3.730$ $A_{\text{SSA}} = 4.927$ $U_{\text{ref}} = 101.440$ $(\phi_{\text{min}}, \phi\text{max}, B_{\text{min}}, B\text{max}) = (10.406, 38.769, -56.359, 416.858)$
55	f0050rn007	$\tau_f = 200$ $I_{\text{crit}} = 215.139$ $A_{\text{SIA}} = 3.964$ $A_{\text{SSA}} = 1.969$ $U_{\text{ref}} = 237.349$ $(\phi_{\text{min}}, \phi\text{max}, B_{\text{min}}, B\text{max}) = (12.279, 31.583, -314.542, 667.647)$
56	f0050rn008	$\tau_f = 200$ $I_{\text{crit}} = 293.425$ $A_{\text{SIA}} = 3.097$ $A_{\text{SSA}} = 4.083$ $U_{\text{ref}} = 134.859$ $(\phi_{\text{min}}, \phi\text{max}, B_{\text{min}}, B\text{max}) = (22.346, 39.726, -306.199, 646.211)$
57	f0050rn009	$\tau_f = 200$ $I_{\text{crit}} = 181.086$ $A_{\text{SIA}} = 4.313$ $A_{\text{SSA}} = 0.705$ $U_{\text{ref}} = 139.307$ $(\phi_{\text{min}}, \phi\text{max}, B_{\text{min}}, B\text{max}) = (5.501, 34.600, -316.803, 277.816)$
58	f0050rn010	$\tau_f = 200$ $I_{\text{crit}} = 324.450$ $A_{\text{SIA}} = 4.336$ $A_{\text{SSA}} = 5.055$ $U_{\text{ref}} = 95.976$ $(\phi_{\text{min}}, \phi\text{max}, B_{\text{min}}, B\text{max}) = (19.252, 39.156, -175.524, 334.898)$
59	f0050rn011	$\tau_f = 200$ $I_{\text{crit}} = 181.758$ $A_{\text{SIA}} = 6.489$ $A_{\text{SSA}} = 0.951$ $U_{\text{ref}} = 141.640$ $(\phi_{\text{min}}, \phi\text{max}, B_{\text{min}}, B\text{max}) = (24.915, 30.183, -317.530, 84.915)$

Table 5: Record of all solutions considered, with tags and parameter changes from the SP15 simulation (part 3).

Index	Solution tag	Parameter changes
60	f0050rn012	$\tau_f = 200$ $I_{\text{crit}} = 185.701$ $A_{\text{SIA}} = 2.594$ $A_{\text{SSA}} = 2.072$ $U_{\text{ref}} = 216.653$ $(\phi_{\text{min}}, \phi\text{max}, B_{\text{min}}, B\text{max}) = (8.544, 41.917, -107.765, 293.515)$
61	f0050rn013	$\tau_f = 200$ $I_{\text{crit}} = 180.317$ $A_{\text{SIA}} = 1.692$ $A_{\text{SSA}} = 4.556$ $U_{\text{ref}} = 100.567$ $(\phi_{\text{min}}, \phi\text{max}, B_{\text{min}}, B\text{max}) = (14.757, 32.077, -166.514, 11.035)$
62	f0050rn014	$\tau_f = 200$ $I_{\text{crit}} = 194.313$ $A_{\text{SIA}} = 4.964$ $A_{\text{SSA}} = 1.599$ $U_{\text{ref}} = 289.022$ $(\phi_{\text{min}}, \phi\text{max}, B_{\text{min}}, B\text{max}) = (18.631, 33.769, -382.980, 333.287)$
63	f0050rn015	$\tau_f = 200$ $I_{\text{crit}} = 335.290$ $A_{\text{SIA}} = 3.170$ $A_{\text{SSA}} = 1.652$ $U_{\text{ref}} = 262.300$ $(\phi_{\text{min}}, \phi\text{max}, B_{\text{min}}, B\text{max}) = (7.943, 38.688, -281.252, 781.542)$
64	f0050rn016	$\tau_f = 200$ $I_{\text{crit}} = 203.298$ $A_{\text{SIA}} = 6.489$ $A_{\text{SSA}} = 0.965$ $U_{\text{ref}} = 51.437$ $(\phi_{\text{min}}, \phi\text{max}, B_{\text{min}}, B\text{max}) = (20.389, 39.244, -390.323, 480.703)$
65	f0050rn017	$\tau_f = 200$ $I_{\text{crit}} = 239.621$ $A_{\text{SIA}} = 4.241$ $A_{\text{SSA}} = 5.628$ $U_{\text{ref}} = 74.416$ $(\phi_{\text{min}}, \phi\text{max}, B_{\text{min}}, B\text{max}) = (5.710, 27.124, -206.006, 634.346)$
66	f0050rn018	$\tau_f = 200$ $I_{\text{crit}} = 203.670$ $A_{\text{SIA}} = 4.161$ $A_{\text{SSA}} = 3.376$ $U_{\text{ref}} = 221.915$ $(\phi_{\text{min}}, \phi\text{max}, B_{\text{min}}, B\text{max}) = (24.973, 34.136, -361.008, 522.233)$
67	f0050rn019	$\tau_f = 200$ $I_{\text{crit}} = 175.306$ $A_{\text{SIA}} = 4.223$ $A_{\text{SSA}} = 3.779$ $U_{\text{ref}} = 154.003$ $(\phi_{\text{min}}, \phi\text{max}, B_{\text{min}}, B\text{max}) = (22.616, 35.260, -117.656, 423.841)$
68	f0050rn020	$\tau_f = 200$ $I_{\text{crit}} = 152.087$ $A_{\text{SIA}} = 1.616$ $A_{\text{SSA}} = 0.774$ $U_{\text{ref}} = 177.468$ $(\phi_{\text{min}}, \phi\text{max}, B_{\text{min}}, B\text{max}) = (7.799, 35.713, -356.247, 207.038)$
69	f0100rn001	$\tau_f = 100$ $I_{\text{crit}} = 345.544$ $A_{\text{SIA}} = 3.970$ $A_{\text{SSA}} = 5.153$ $U_{\text{ref}} = 180.372$ $(\phi_{\text{min}}, \phi\text{max}, B_{\text{min}}, B\text{max}) = (17.503, 40.812, -74.736, 497.574)$
70	f0100rn002	$\tau_f = 100$ $I_{\text{crit}} = 291.643$ $A_{\text{SIA}} = 4.273$ $A_{\text{SSA}} = 3.300$ $U_{\text{ref}} = 243.577$ $(\phi_{\text{min}}, \phi\text{max}, B_{\text{min}}, B\text{max}) = (11.285, 37.667, -367.816, 756.078)$
71	f0100rn003	$\tau_f = 100$ $I_{\text{crit}} = 280.076$ $A_{\text{SIA}} = 6.673$ $A_{\text{SSA}} = 4.279$ $U_{\text{ref}} = 53.014$ $(\phi_{\text{min}}, \phi\text{max}, B_{\text{min}}, B\text{max}) = (12.091, 35.405, -64.119, 59.890)$
72	f0100rn005	$\tau_f = 100$ $I_{\text{crit}} = 202.785$ $A_{\text{SIA}} = 4.076$ $A_{\text{SSA}} = 3.692$ $U_{\text{ref}} = 242.301$ $(\phi_{\text{min}}, \phi\text{max}, B_{\text{min}}, B\text{max}) = (22.817, 32.251, -336.609, 113.260)$
73	f0100rn006	$\tau_f = 100$ $I_{\text{crit}} = 279.704$ $A_{\text{SIA}} = 3.730$ $A_{\text{SSA}} = 4.927$ $U_{\text{ref}} = 101.440$ $(\phi_{\text{min}}, \phi\text{max}, B_{\text{min}}, B\text{max}) = (10.406, 38.769, -56.359, 416.858)$
74	f0100rn007	$\tau_f = 100$ $I_{\text{crit}} = 215.139$ $A_{\text{SIA}} = 3.964$ $A_{\text{SSA}} = 1.969$ $U_{\text{ref}} = 237.349$ $(\phi_{\text{min}}, \phi\text{max}, B_{\text{min}}, B\text{max}) = (12.279, 31.583, -314.542, 667.647)$
75	f0100rn008	$\tau_f = 100$ $I_{\text{crit}} = 293.425$ $A_{\text{SIA}} = 3.097$ $A_{\text{SSA}} = 4.083$ $U_{\text{ref}} = 134.859$ $(\phi_{\text{min}}, \phi\text{max}, B_{\text{min}}, B\text{max}) = (22.346, 39.726, -306.199, 646.211)$

Table 6: Record of all solutions considered, with tags and parameter changes from the SP15 simulation (part 4).

Index	Solution tag	Parameter changes
76	f0100rn009	$\tau_f = 100$ $I_{\text{crit}} = 181.086$ $A_{\text{SIA}} = 4.313$ $A_{\text{SSA}} = 0.705$ $U_{\text{ref}} = 139.307$ $(\phi_{\text{min}}, \phi\text{max}, B_{\text{min}}, B\text{max}) = (5.501, 34.600, -316.803, 277.816)$
77	f0100rn010	$\tau_f = 100$ $I_{\text{crit}} = 324.450$ $A_{\text{SIA}} = 4.336$ $A_{\text{SSA}} = 5.055$ $U_{\text{ref}} = 95.976$ $(\phi_{\text{min}}, \phi\text{max}, B_{\text{min}}, B\text{max}) = (19.252, 39.156, -175.524, 334.898)$
78	f0100rn011	$\tau_f = 100$ $I_{\text{crit}} = 181.758$ $A_{\text{SIA}} = 6.489$ $A_{\text{SSA}} = 0.951$ $U_{\text{ref}} = 141.640$ $(\phi_{\text{min}}, \phi\text{max}, B_{\text{min}}, B\text{max}) = (24.915, 30.183, -317.530, 84.915)$
79	f0100rn012	$\tau_f = 100$ $I_{\text{crit}} = 185.701$ $A_{\text{SIA}} = 2.594$ $A_{\text{SSA}} = 2.072$ $U_{\text{ref}} = 216.653$ $(\phi_{\text{min}}, \phi\text{max}, B_{\text{min}}, B\text{max}) = (8.544, 41.917, -107.765, 293.515)$
80	f0100rn013	$\tau_f = 100$ $I_{\text{crit}} = 180.317$ $A_{\text{SIA}} = 1.692$ $A_{\text{SSA}} = 4.556$ $U_{\text{ref}} = 100.567$ $(\phi_{\text{min}}, \phi\text{max}, B_{\text{min}}, B\text{max}) = (14.757, 32.077, -166.514, 11.035)$
81	f0100rn014	$\tau_f = 100$ $I_{\text{crit}} = 194.313$ $A_{\text{SIA}} = 4.964$ $A_{\text{SSA}} = 1.599$ $U_{\text{ref}} = 289.022$ $(\phi_{\text{min}}, \phi\text{max}, B_{\text{min}}, B\text{max}) = (18.631, 33.769, -382.980, 333.287)$
82	f0100rn015	$\tau_f = 100$ $I_{\text{crit}} = 335.290$ $A_{\text{SIA}} = 3.170$ $A_{\text{SSA}} = 1.652$ $U_{\text{ref}} = 262.300$ $(\phi_{\text{min}}, \phi\text{max}, B_{\text{min}}, B\text{max}) = (7.943, 38.688, -281.252, 781.542)$
83	f0100rn016	$\tau_f = 100$ $I_{\text{crit}} = 203.298$ $A_{\text{SIA}} = 6.489$ $A_{\text{SSA}} = 0.965$ $U_{\text{ref}} = 51.437$ $(\phi_{\text{min}}, \phi\text{max}, B_{\text{min}}, B\text{max}) = (20.389, 39.244, -390.323, 480.703)$
84	f0100rn017	$\tau_f = 100$ $I_{\text{crit}} = 239.621$ $A_{\text{SIA}} = 4.241$ $A_{\text{SSA}} = 5.628$ $U_{\text{ref}} = 74.416$ $(\phi_{\text{min}}, \phi\text{max}, B_{\text{min}}, B\text{max}) = (5.710, 27.124, -206.006, 634.346)$
85	f0100rn018	$\tau_f = 100$ $I_{\text{crit}} = 203.670$ $A_{\text{SIA}} = 4.161$ $A_{\text{SSA}} = 3.376$ $U_{\text{ref}} = 221.915$ $(\phi_{\text{min}}, \phi\text{max}, B_{\text{min}}, B\text{max}) = (24.973, 34.136, -361.008, 522.233)$
86	f0100rn019	$\tau_f = 100$ $I_{\text{crit}} = 175.306$ $A_{\text{SIA}} = 4.223$ $A_{\text{SSA}} = 3.779$ $U_{\text{ref}} = 154.003$ $(\phi_{\text{min}}, \phi\text{max}, B_{\text{min}}, B\text{max}) = (22.616, 35.260, -117.656, 423.841)$
87	f0100rn020	$\tau_f = 100$ $I_{\text{crit}} = 152.087$ $A_{\text{SIA}} = 1.616$ $A_{\text{SSA}} = 0.774$ $U_{\text{ref}} = 177.468$ $(\phi_{\text{min}}, \phi\text{max}, B_{\text{min}}, B\text{max}) = (7.799, 35.713, -356.247, 207.038)$
88	f0500rn001	$\tau_f = 20$ $I_{\text{crit}} = 345.544$ $A_{\text{SIA}} = 3.970$ $A_{\text{SSA}} = 5.153$ $U_{\text{ref}} = 180.372$ $(\phi_{\text{min}}, \phi\text{max}, B_{\text{min}}, B\text{max}) = (17.503, 40.812, -74.736, 497.574)$
89	f0500rn002	$\tau_f = 20$ $I_{\text{crit}} = 291.643$ $A_{\text{SIA}} = 4.273$ $A_{\text{SSA}} = 3.300$ $U_{\text{ref}} = 243.577$ $(\phi_{\text{min}}, \phi\text{max}, B_{\text{min}}, B\text{max}) = (11.285, 37.667, -367.816, 756.078)$
90	f0500rn003	$\tau_f = 20$ $I_{\text{crit}} = 280.076$ $A_{\text{SIA}} = 6.673$ $A_{\text{SSA}} = 4.279$ $U_{\text{ref}} = 53.014$ $(\phi_{\text{min}}, \phi\text{max}, B_{\text{min}}, B\text{max}) = (12.091, 35.405, -64.119, 59.890)$
91	f0500rn004	$\tau_f = 20$ $I_{\text{crit}} = 194.502$ $A_{\text{SIA}} = 3.381$ $A_{\text{SSA}} = 2.439$ $U_{\text{ref}} = 95.833$ $(\phi_{\text{min}}, \phi\text{max}, B_{\text{min}}, B\text{max}) = (6.143, 30.123, -215.385, 271.029)$

Table 7: Record of all solutions considered, with tags and parameter changes from the SP15 simulation (part 5).

Index	Solution tag	Parameter changes
92	f0500rn005	$\tau_f = 20$ $I_{\text{crit}} = 202.785$ $A_{\text{SIA}} = 4.076$ $A_{\text{SSA}} = 3.692$ $U_{\text{ref}} = 242.301$ $(\phi_{\text{min}}, \phi\text{max}, B_{\text{min}}, B\text{max}) = (22.817, 32.251, -336.609, 113.260)$
93	f0500rn006	$\tau_f = 20$ $I_{\text{crit}} = 279.704$ $A_{\text{SIA}} = 3.730$ $A_{\text{SSA}} = 4.927$ $U_{\text{ref}} = 101.440$ $(\phi_{\text{min}}, \phi\text{max}, B_{\text{min}}, B\text{max}) = (10.406, 38.769, -56.359, 416.858)$
94	f0500rn007	$\tau_f = 20$ $I_{\text{crit}} = 215.139$ $A_{\text{SIA}} = 3.964$ $A_{\text{SSA}} = 1.969$ $U_{\text{ref}} = 237.349$ $(\phi_{\text{min}}, \phi\text{max}, B_{\text{min}}, B\text{max}) = (12.279, 31.583, -314.542, 667.647)$
95	f0500rn008	$\tau_f = 20$ $I_{\text{crit}} = 293.425$ $A_{\text{SIA}} = 3.097$ $A_{\text{SSA}} = 4.083$ $U_{\text{ref}} = 134.859$ $(\phi_{\text{min}}, \phi\text{max}, B_{\text{min}}, B\text{max}) = (22.346, 39.726, -306.199, 646.211)$
96	f0500rn009	$\tau_f = 20$ $I_{\text{crit}} = 181.086$ $A_{\text{SIA}} = 4.313$ $A_{\text{SSA}} = 0.705$ $U_{\text{ref}} = 139.307$ $(\phi_{\text{min}}, \phi\text{max}, B_{\text{min}}, B\text{max}) = (5.501, 34.600, -316.803, 277.816)$
97	f0500rn010	$\tau_f = 20$ $I_{\text{crit}} = 324.450$ $A_{\text{SIA}} = 4.336$ $A_{\text{SSA}} = 5.055$ $U_{\text{ref}} = 95.976$ $(\phi_{\text{min}}, \phi\text{max}, B_{\text{min}}, B\text{max}) = (19.252, 39.156, -175.524, 334.898)$
98	f0500rn011	$\tau_f = 20$ $I_{\text{crit}} = 181.758$ $A_{\text{SIA}} = 6.489$ $A_{\text{SSA}} = 0.951$ $U_{\text{ref}} = 141.640$ $(\phi_{\text{min}}, \phi\text{max}, B_{\text{min}}, B\text{max}) = (24.915, 30.183, -317.530, 84.915)$
99	f0500rn012	$\tau_f = 20$ $I_{\text{crit}} = 185.701$ $A_{\text{SIA}} = 2.594$ $A_{\text{SSA}} = 2.072$ $U_{\text{ref}} = 216.653$ $(\phi_{\text{min}}, \phi\text{max}, B_{\text{min}}, B\text{max}) = (8.544, 41.917, -107.765, 293.515)$
100	f0500rn013	$\tau_f = 20$ $I_{\text{crit}} = 180.317$ $A_{\text{SIA}} = 1.692$ $A_{\text{SSA}} = 4.556$ $U_{\text{ref}} = 100.567$ $(\phi_{\text{min}}, \phi\text{max}, B_{\text{min}}, B\text{max}) = (14.757, 32.077, -166.514, 11.035)$
101	f0500rn014	$\tau_f = 20$ $I_{\text{crit}} = 194.313$ $A_{\text{SIA}} = 4.964$ $A_{\text{SSA}} = 1.599$ $U_{\text{ref}} = 289.022$ $(\phi_{\text{min}}, \phi\text{max}, B_{\text{min}}, B\text{max}) = (18.631, 33.769, -382.980, 333.287)$
102	f0500rn015	$\tau_f = 20$ $I_{\text{crit}} = 335.290$ $A_{\text{SIA}} = 3.170$ $A_{\text{SSA}} = 1.652$ $U_{\text{ref}} = 262.300$ $(\phi_{\text{min}}, \phi\text{max}, B_{\text{min}}, B\text{max}) = (7.943, 38.688, -281.252, 781.542)$
103	f0500rn016	$\tau_f = 20$ $I_{\text{crit}} = 203.298$ $A_{\text{SIA}} = 6.489$ $A_{\text{SSA}} = 0.965$ $U_{\text{ref}} = 51.437$ $(\phi_{\text{min}}, \phi\text{max}, B_{\text{min}}, B\text{max}) = (20.389, 39.244, -390.323, 480.703)$
104	f0500rn017	$\tau_f = 20$ $I_{\text{crit}} = 239.621$ $A_{\text{SIA}} = 4.241$ $A_{\text{SSA}} = 5.628$ $U_{\text{ref}} = 74.416$ $(\phi_{\text{min}}, \phi\text{max}, B_{\text{min}}, B\text{max}) = (5.710, 27.124, -206.006, 634.346)$
105	f0500rn018	$\tau_f = 20$ $I_{\text{crit}} = 203.670$ $A_{\text{SIA}} = 4.161$ $A_{\text{SSA}} = 3.376$ $U_{\text{ref}} = 221.915$ $(\phi_{\text{min}}, \phi\text{max}, B_{\text{min}}, B\text{max}) = (24.973, 34.136, -361.008, 522.233)$
106	f0500rn019	$\tau_f = 20$ $I_{\text{crit}} = 175.306$ $A_{\text{SIA}} = 4.223$ $A_{\text{SSA}} = 3.779$ $U_{\text{ref}} = 154.003$ $(\phi_{\text{min}}, \phi\text{max}, B_{\text{min}}, B\text{max}) = (22.616, 35.260, -117.656, 423.841)$
107	f0500rn020	$\tau_f = 20$ $I_{\text{crit}} = 152.087$ $A_{\text{SIA}} = 1.616$ $A_{\text{SSA}} = 0.774$ $U_{\text{ref}} = 177.468$ $(\phi_{\text{min}}, \phi\text{max}, B_{\text{min}}, B\text{max}) = (7.799, 35.713, -356.247, 207.038)$

Table 8: Record of all solutions considered, with tags and parameter changes from the SP15 simulation (part 6).

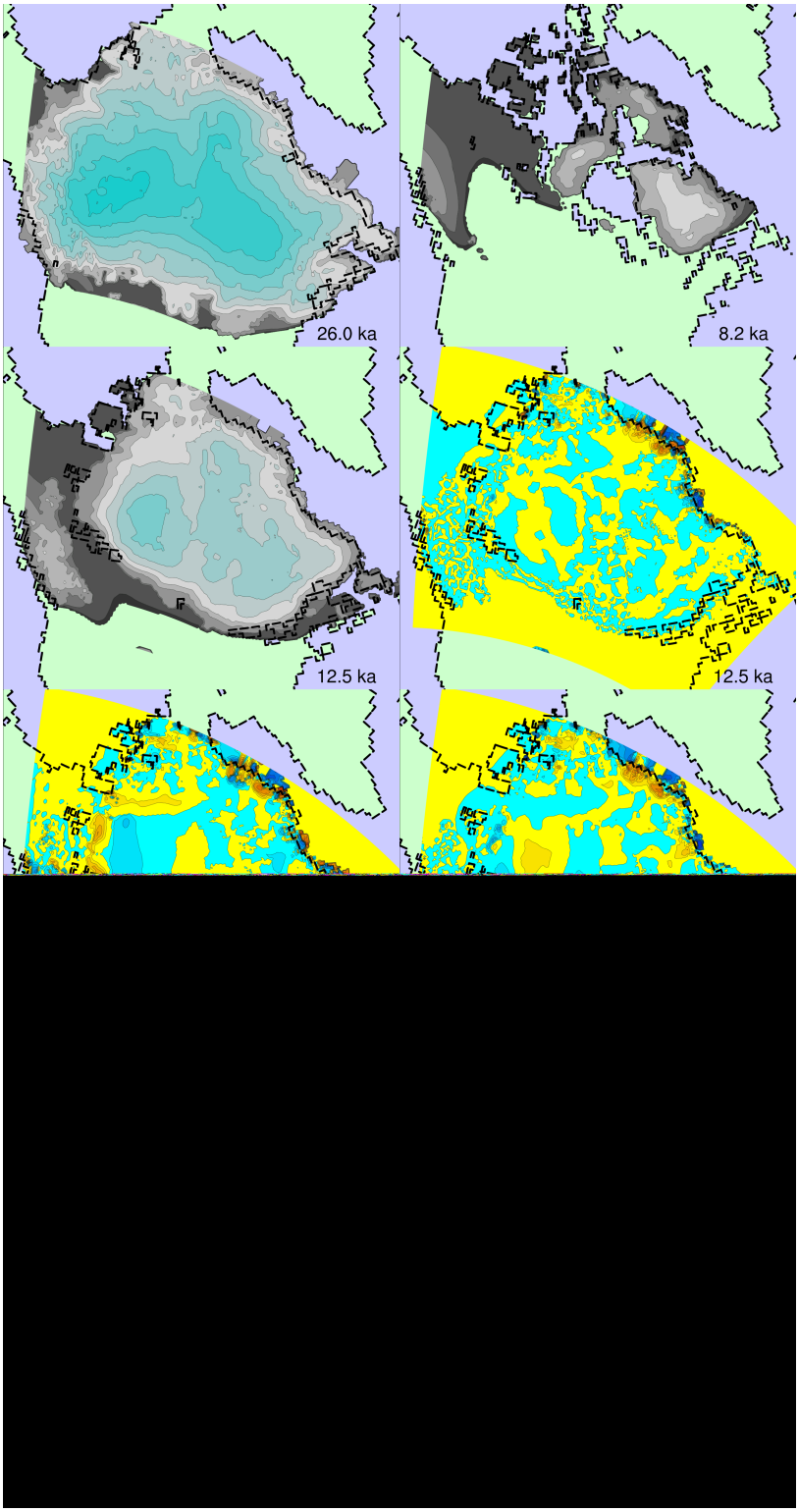

Figure 5: Plots of ice thickness at LGM (upper left), 8.2 kyr BP (upper right), and 12.5 kyr BP (second row left), followed (in continuing left-right, top-bottom sequence) by variability plots with respect to A_{SSA} (f0100c0ssax), ϕ_{min} and ϕ_{max} (f0100c0ttpx), A_{SIA} (f0100c0siax), random parameters (f0100rnxxx), and a subset of the random parameters (f0100rn01x) at 12.5 kyr BP.

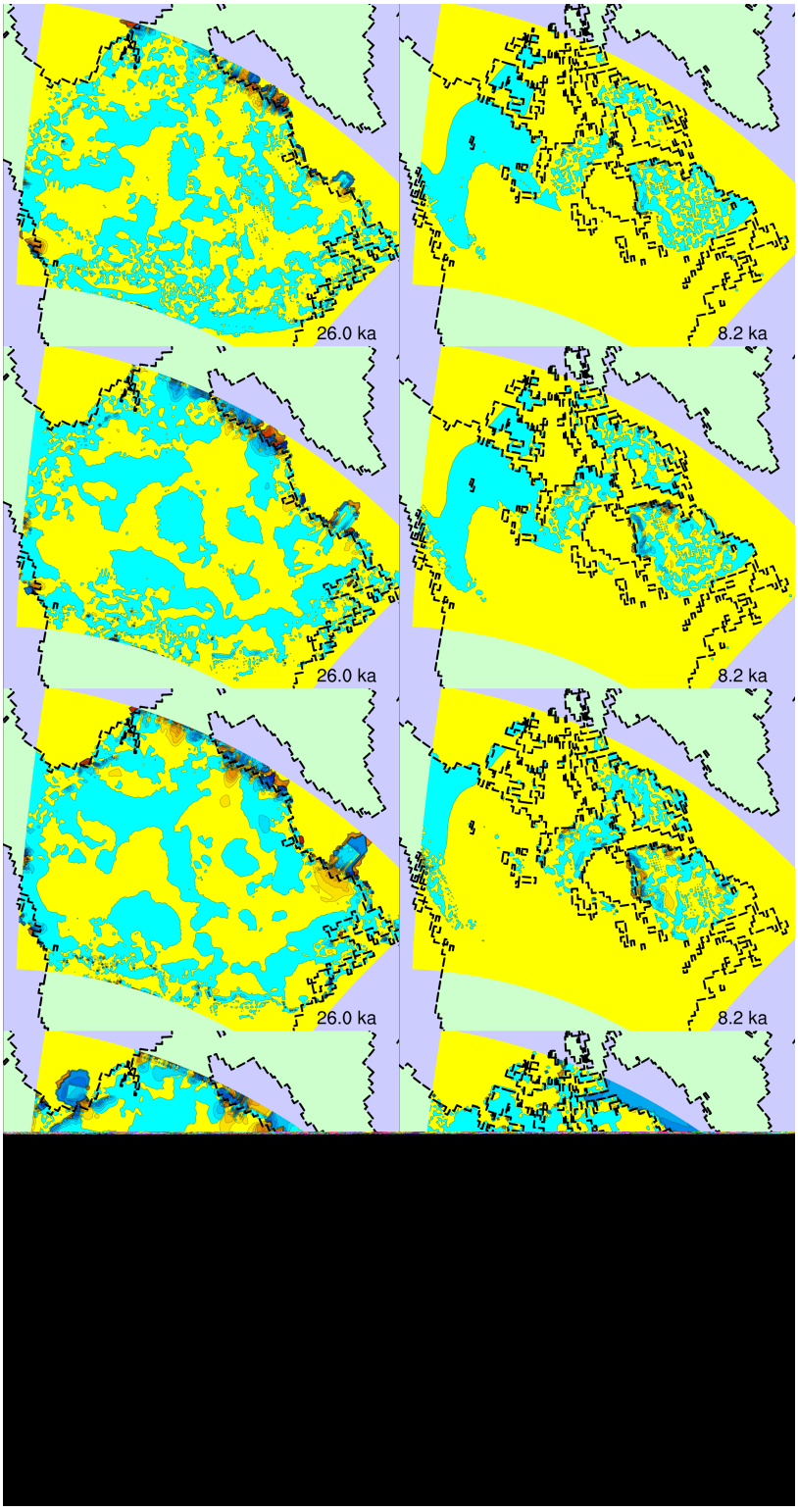

Figure 6: Variability of ice thickness with respect to A_{SSA} (f0500c0ssax, f0100c0ssax, f0050c0ssax, and f0010c0ssax) at LGM (left) and 12.5 kyr BP (right) for τ_f increasing top to bottom.

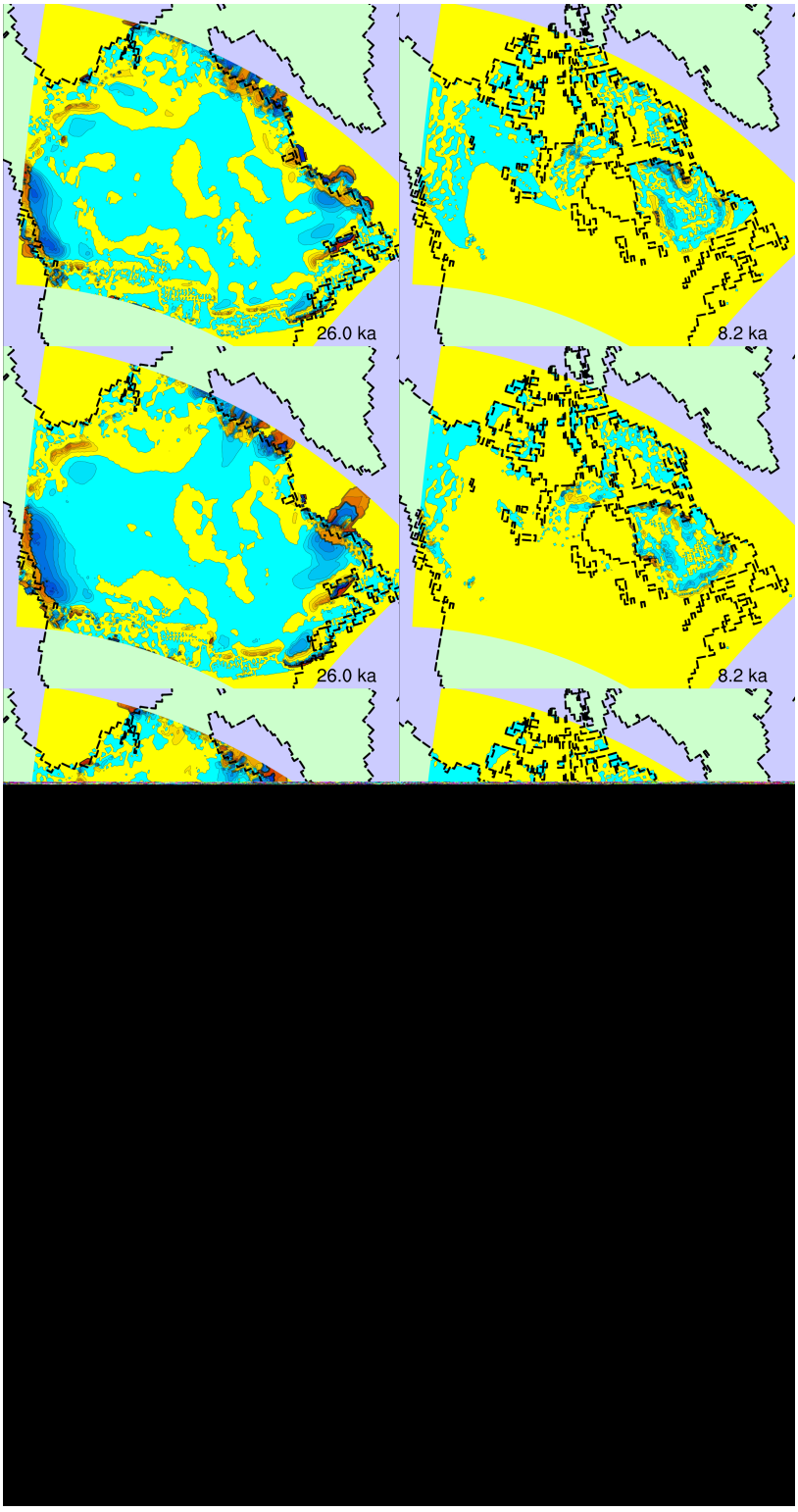

Figure 7: Variability of ice thickness with respect to ϕ_{min} and ϕ_{max} (f0500c0ttpx, f0100c0ttpx, f0050c0ttpx, and f0010c0ttpx) at LGM (left) and 12.5 kyr BP (right) for τ_{f} increasing top to bottom.

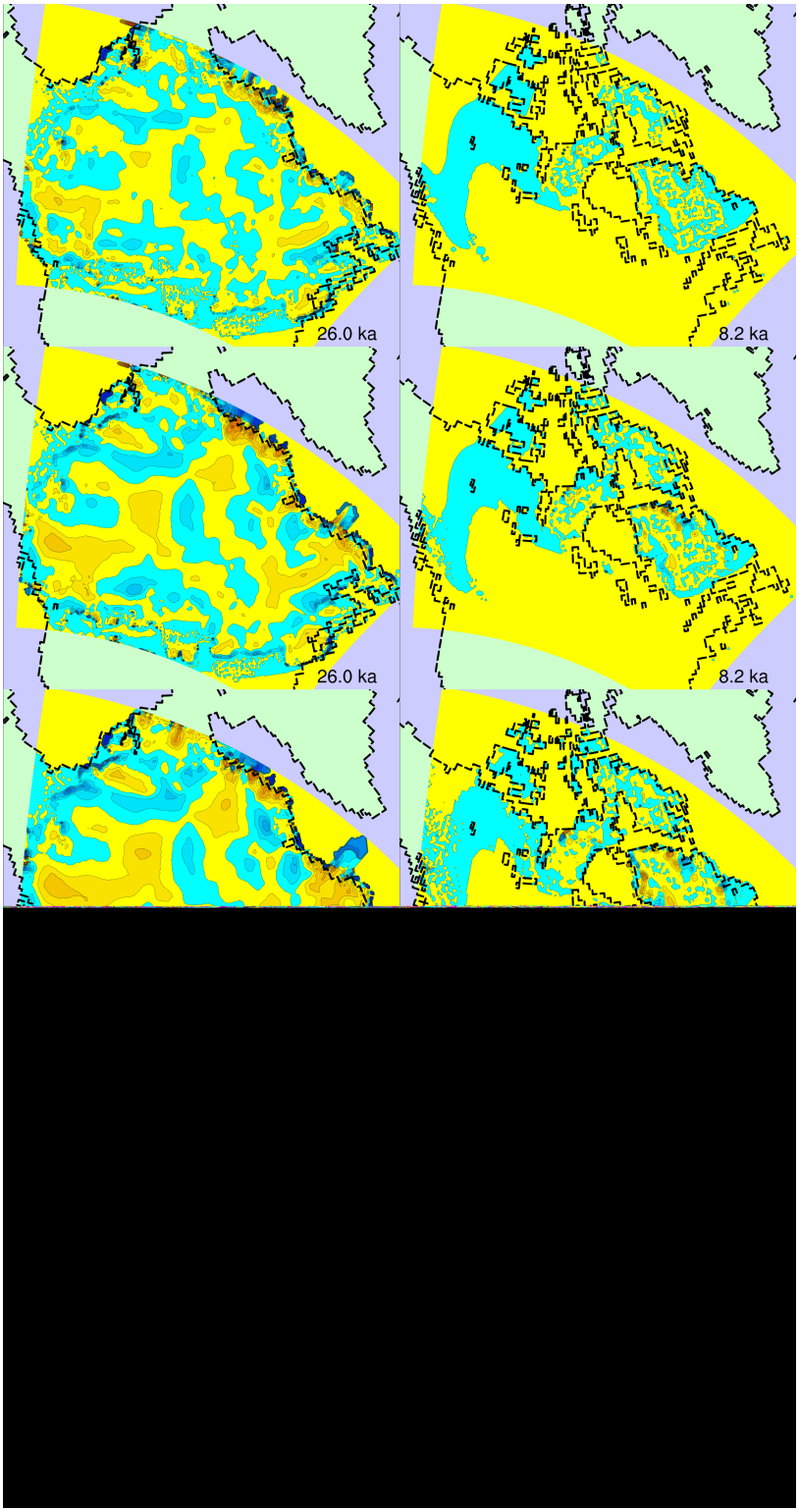

Figure 8: Variability of ice thickness with respect to A_{SIA} (f0500c0siax, f0100c0siax, f0050c0siax, and f0010c0siax) at LGM (left) and 12.5 kyr BP (right) for τ_f increasing top to bottom.

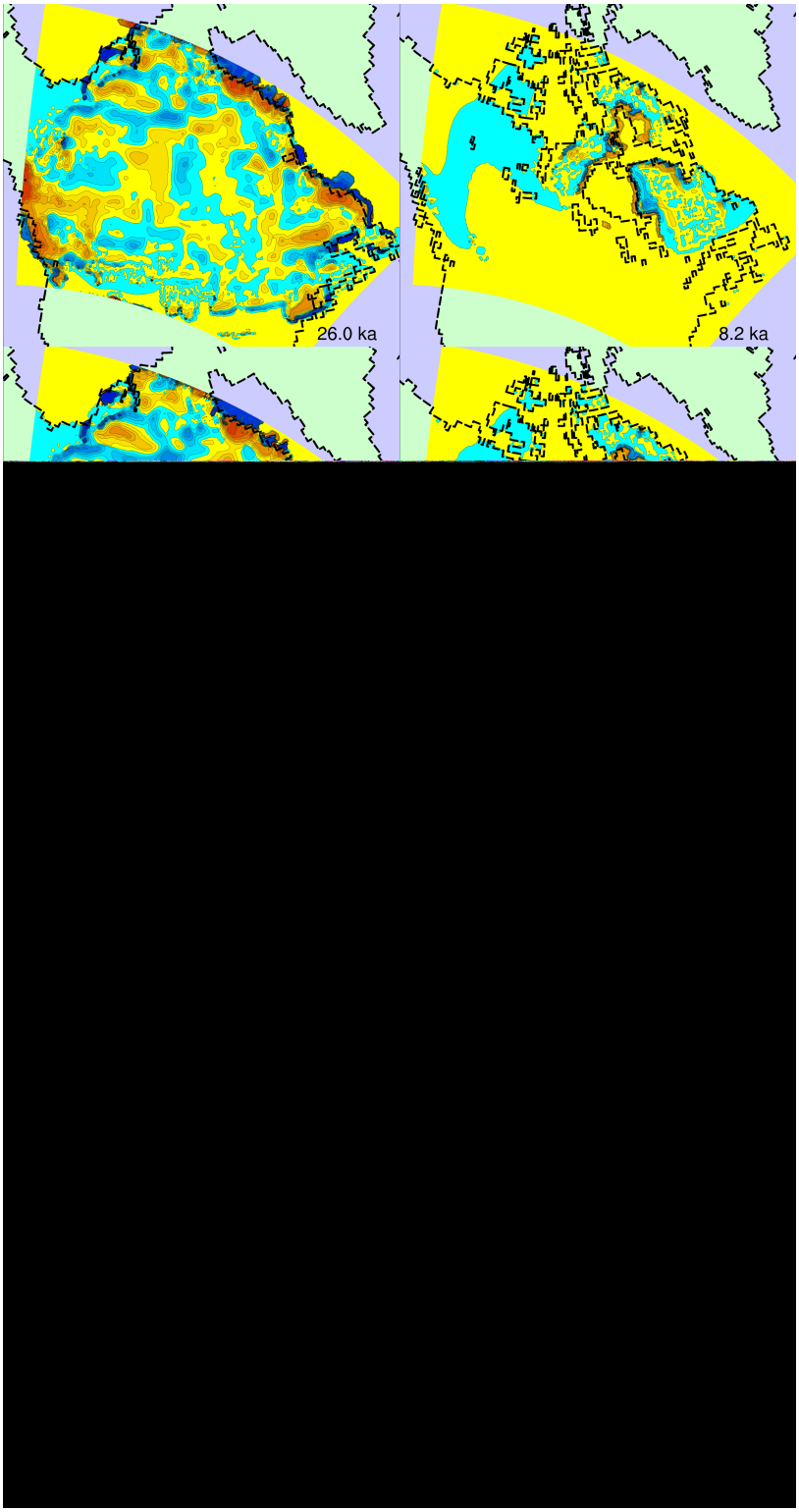

Figure 9: Variability of ice thickness with respect to random parameters (f0500rnxxx, f0100rnxxx, f0050rnxxx, and f0010rnxxx) at LGM (left) and 12.5 kyr BP (right) for τ_f increasing top to bottom.

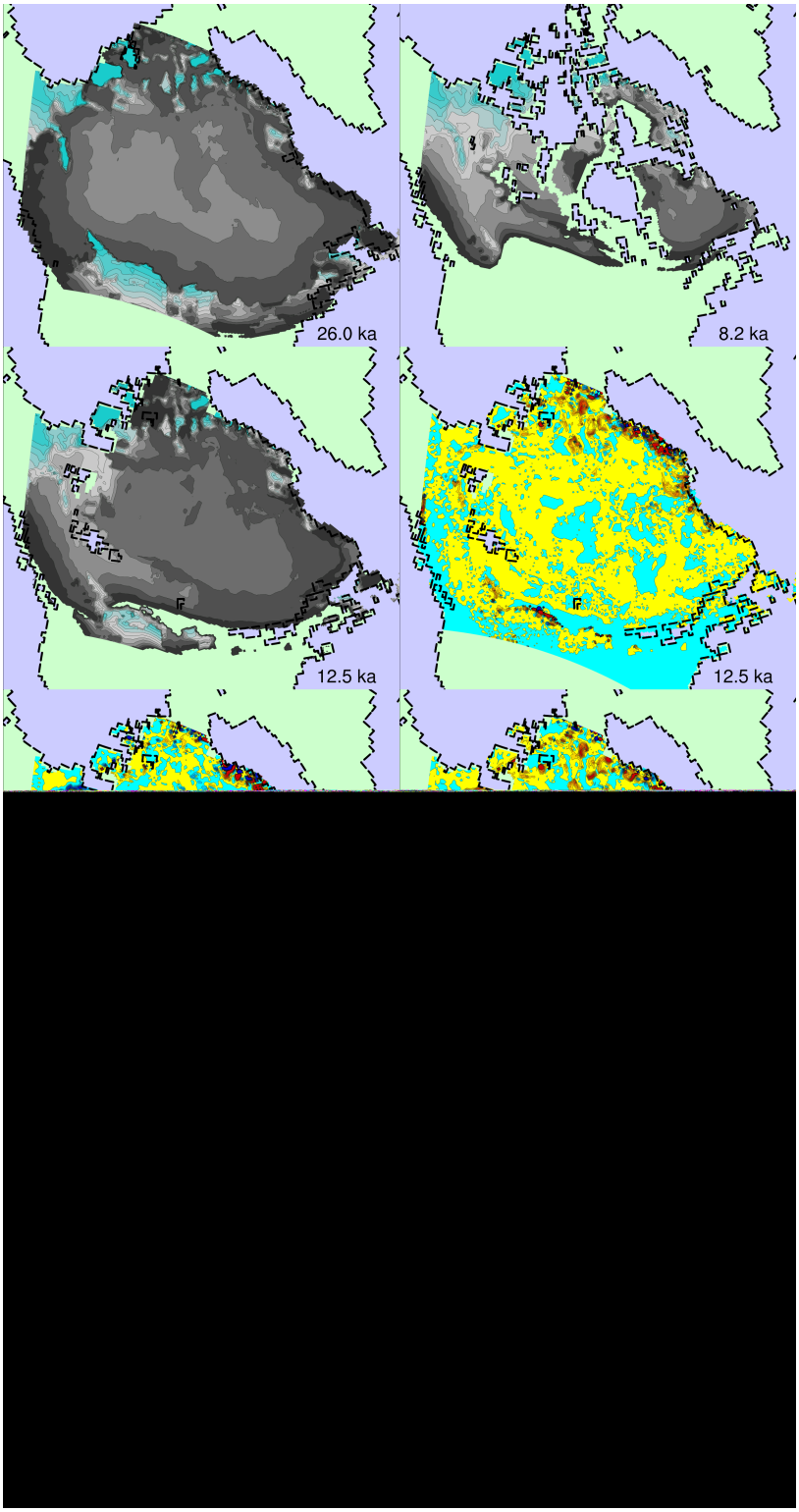

Figure 10: Plots of permafrost thickness at LGM (upper left), 8.2 kyr BP (upper right), and 12.5 kyr BP (second row left), followed (in continuing left-right, top-bottom sequence) by variability plots with respect to A_{SSA} (f0100c0ssax), ϕ_{min} and ϕ_{max} (f0100c0ttpx), A_{SIA} (f0100c0siax), random parameters (f0100rnxxx), and a subset of the random parameters (f0100rn01x) at 12.5 kyr BP.

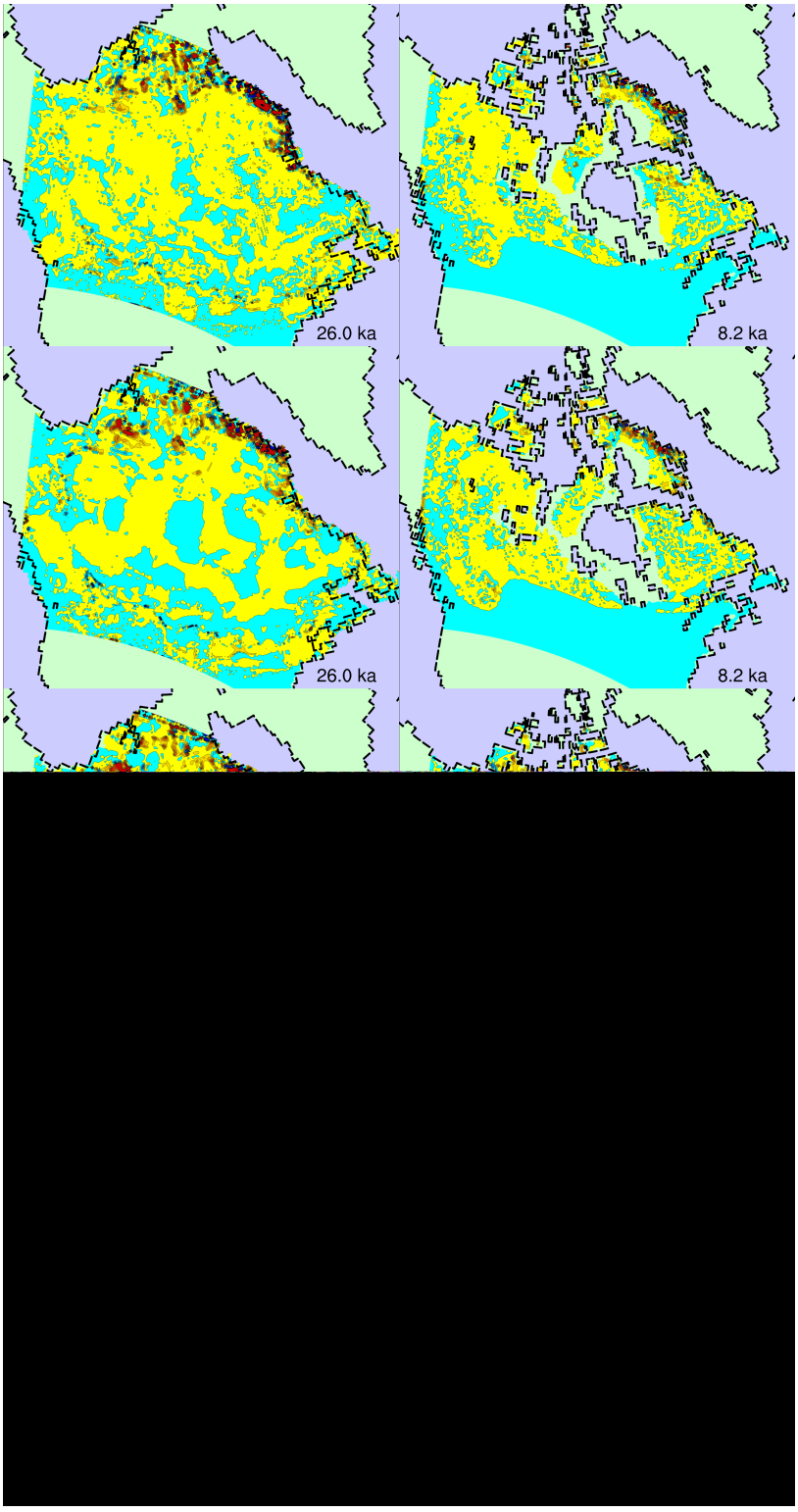

Figure 11: Variability of permafrost thickness with respect to A_{SSA} (f0500c0ssax, f0100c0ssax, f0050c0ssax, and f0010c0ssax) at LGM (left) and 12.5 kyr BP (right) for τ_f increasing top to bottom.

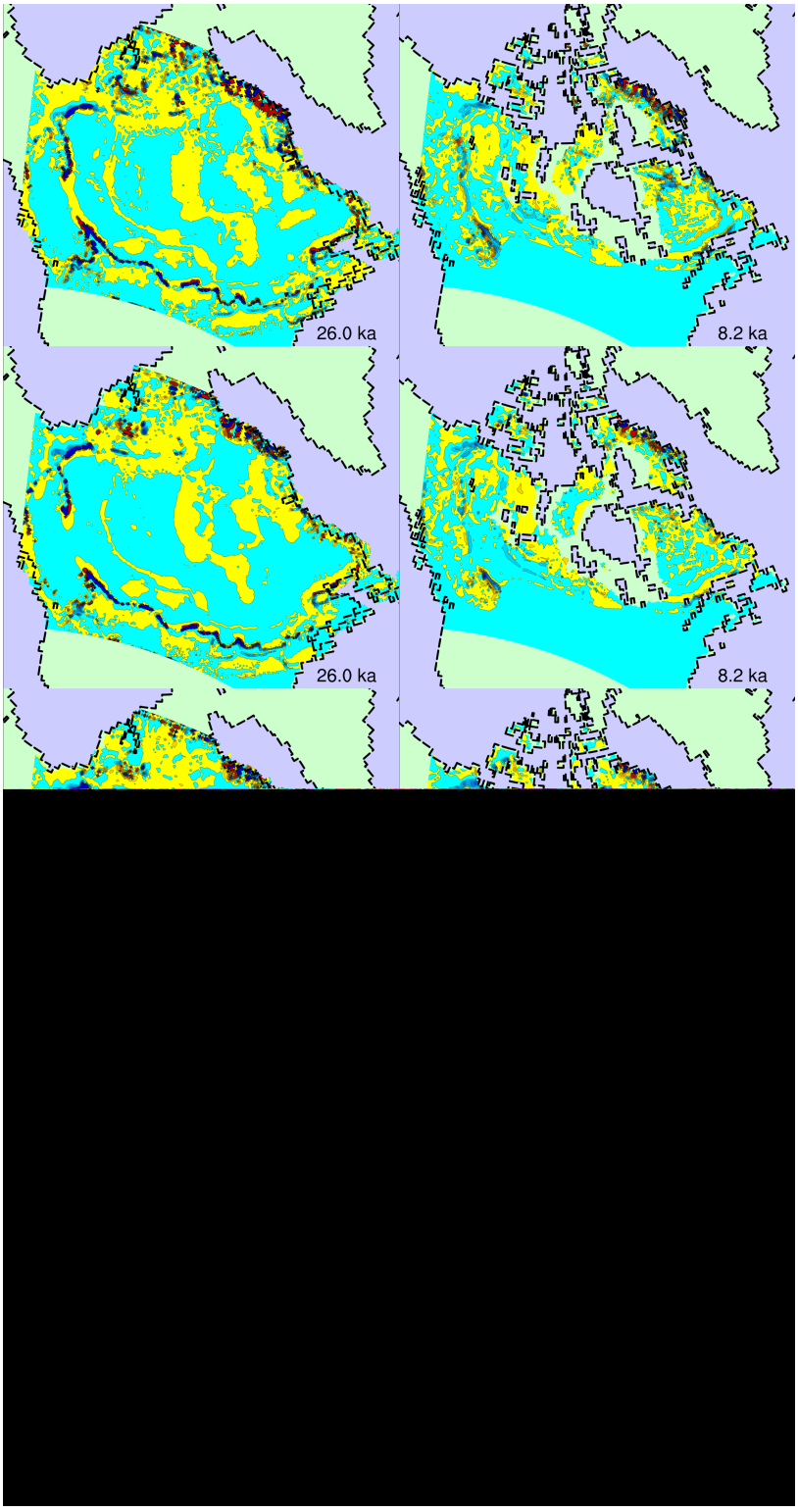

Figure 12: Variability of permafrost thickness with respect to ϕ_{min} and ϕ_{max} (f0500c0ttpx, f0100c0ttpx, f0050c0ttpx, and f0010c0ttpx) at LGM (left) and 12.5 kyr BP (right) for τ_{f} increasing top to bottom.

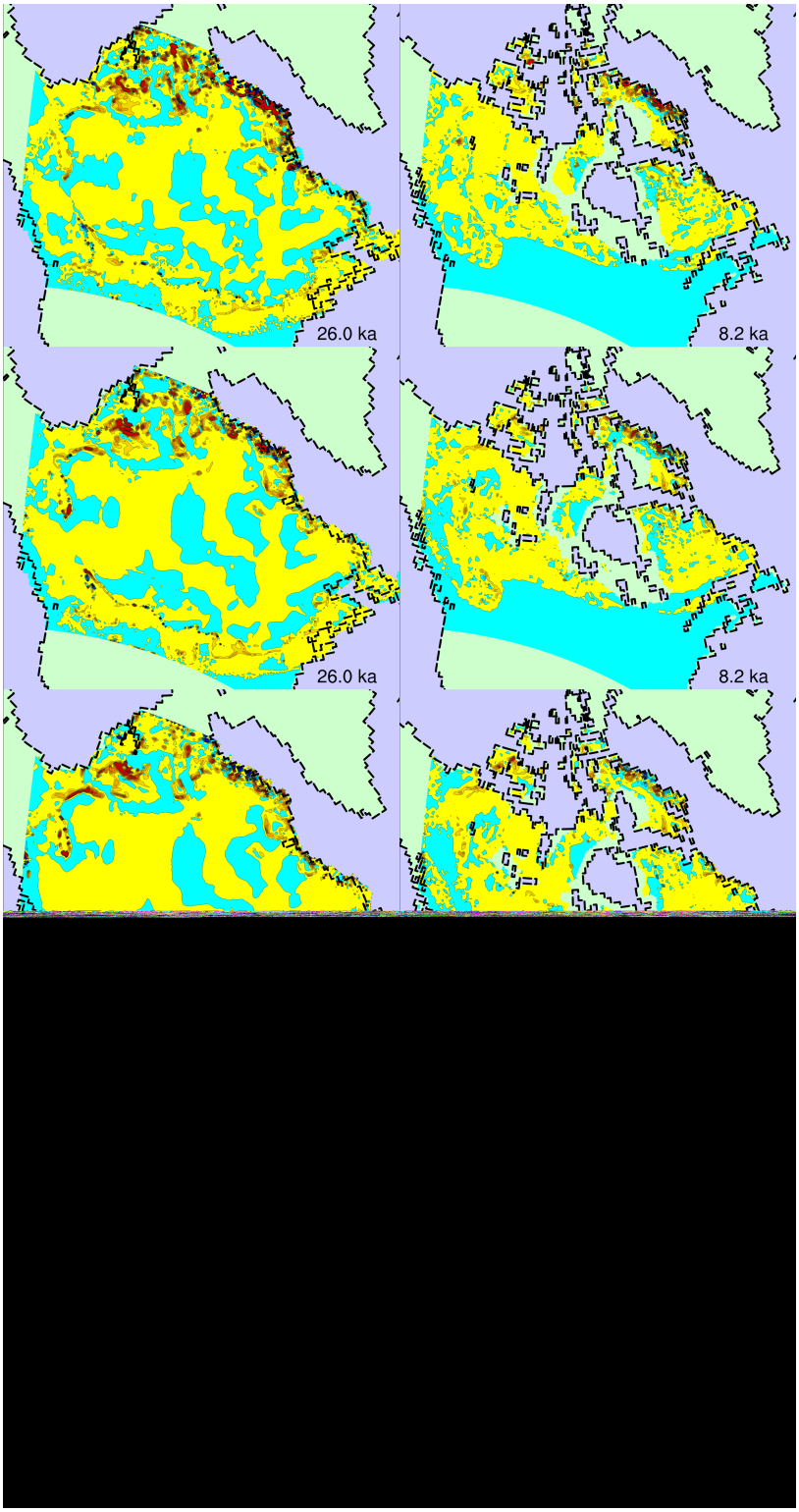

Figure 13: Variability of permafrost thickness with respect to A_{SIA} (f0500c0siax, f0100c0siax, f0050c0siax, and f0010c0siax) at LGM (left) and 12.5 kyr BP (right) for τ_f increasing top to bottom.

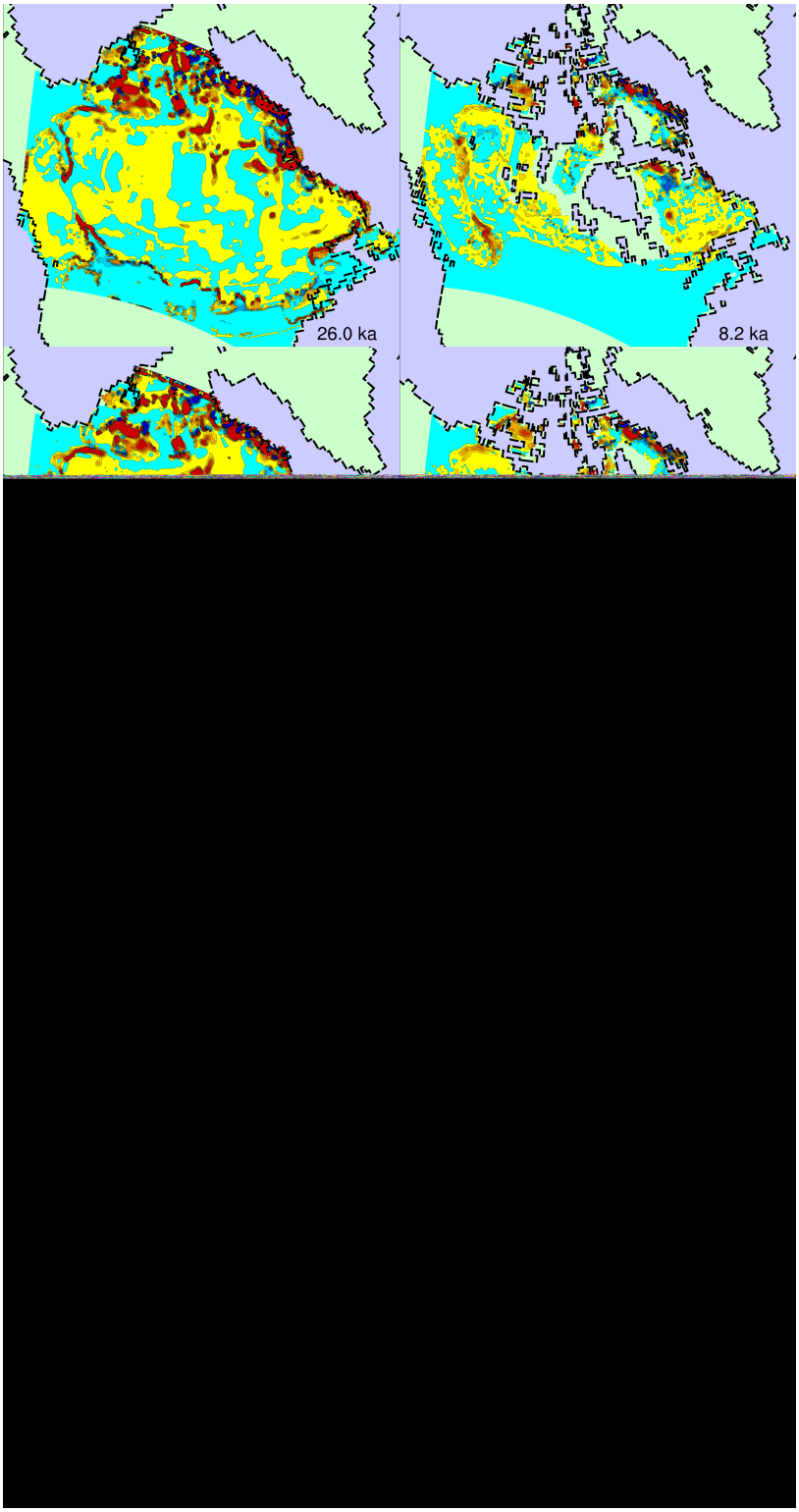

Figure 14: Variability of permafrost thickness with respect to random parameters (f0500rnxxx, f0100rnxxx, f0050rnxxx, and f0010rnxxx) at LGM (left) and 12.5 kyr BP (right) for τ_f increasing top to bottom.

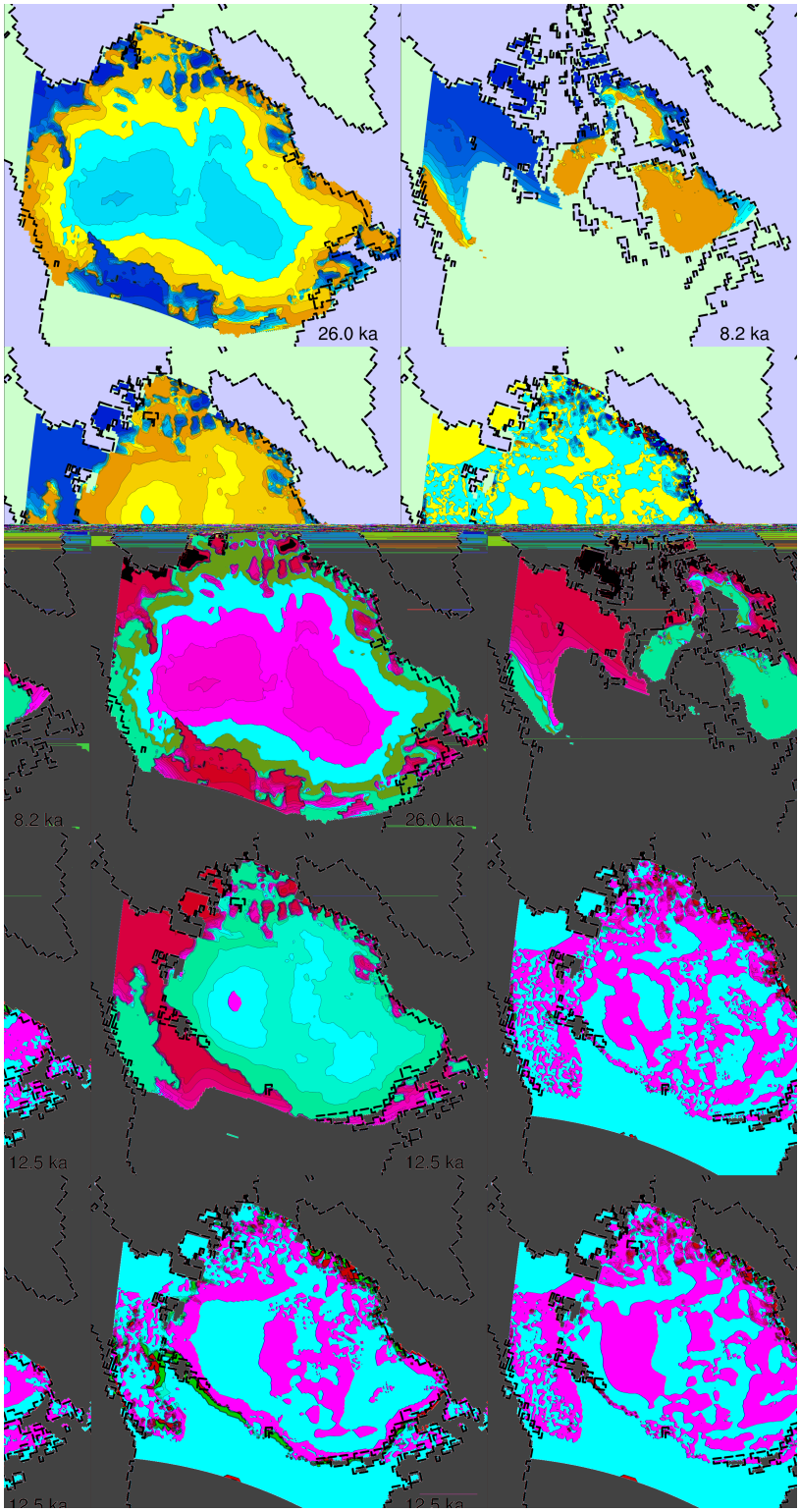

Figure 15: Plots of basal temperature at LGM (upper left), 8.2 kyr BP (upper right), and 12.5 kyr BP (second row left), followed (in continuing left-right, top-bottom sequence) by variability plots with respect to A_{SSA} (f0100c0ssax), ϕ_{min} and ϕ_{max} (f0100c0ttpx), A_{SIA} (f0100c0siax), random parameters (f0100rnxxx), and a subset of the random parameters (f0100rn01x) at 12.5 kyr BP.

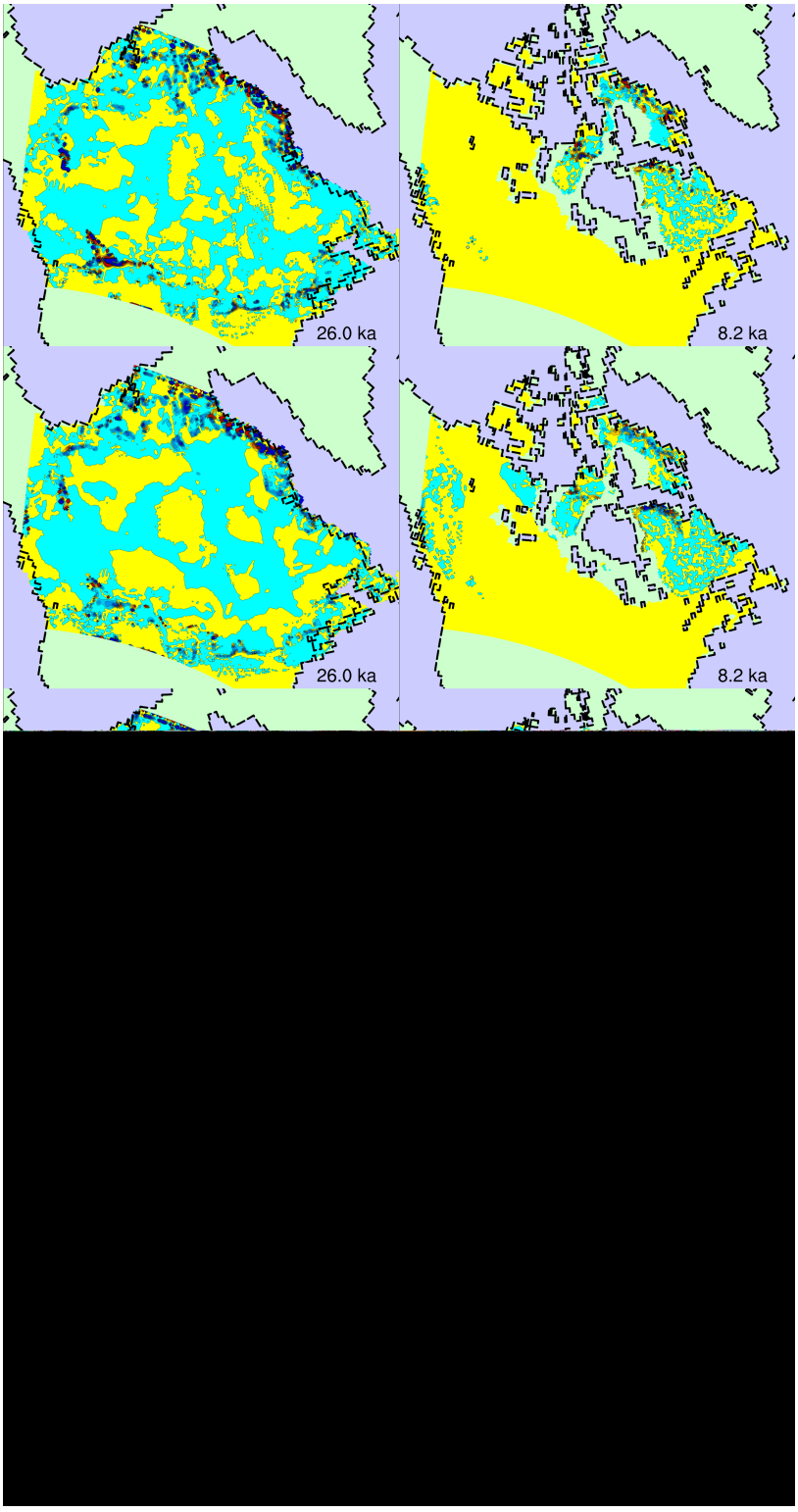

Figure 16: Variability of basal temperature with respect to A_{SSA} (f0500c0ssax, f0100c0ssax, f0050c0ssax, and f0010c0ssax) at LGM (left) and 12.5 kyr BP (right) for τ_f increasing top to bottom.

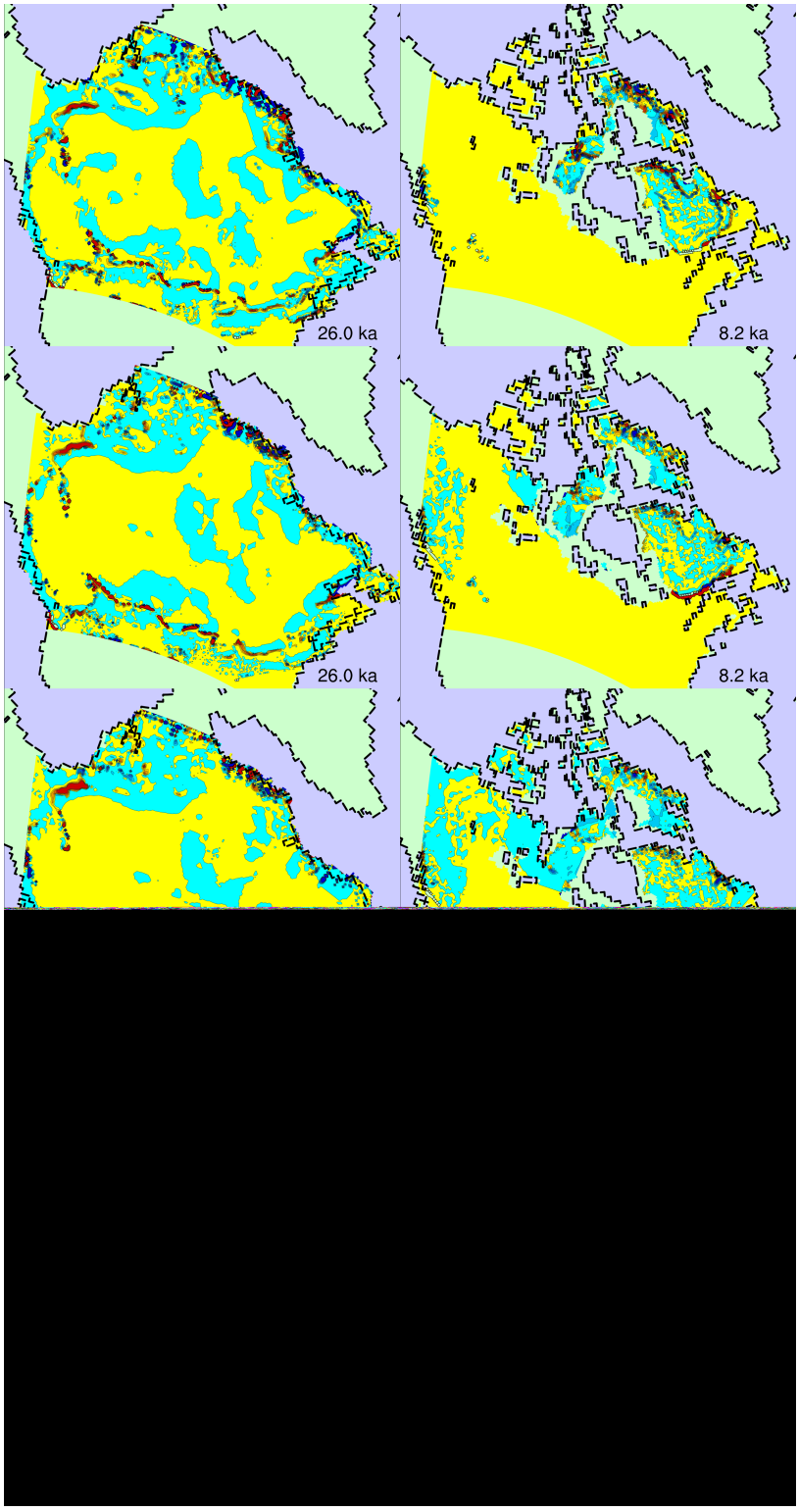

Figure 17: Variability of basal temperature with respect to $\phi_{\mathbf{min}}$ and $\phi_{\mathbf{max}}$ (f0500c0ttpx, f0100c0ttpx, f0050c0ttpx, and f0010c0ttpx) at LGM (left) and 12.5 kyr BP (right) for τ_{f} increasing top to bottom.

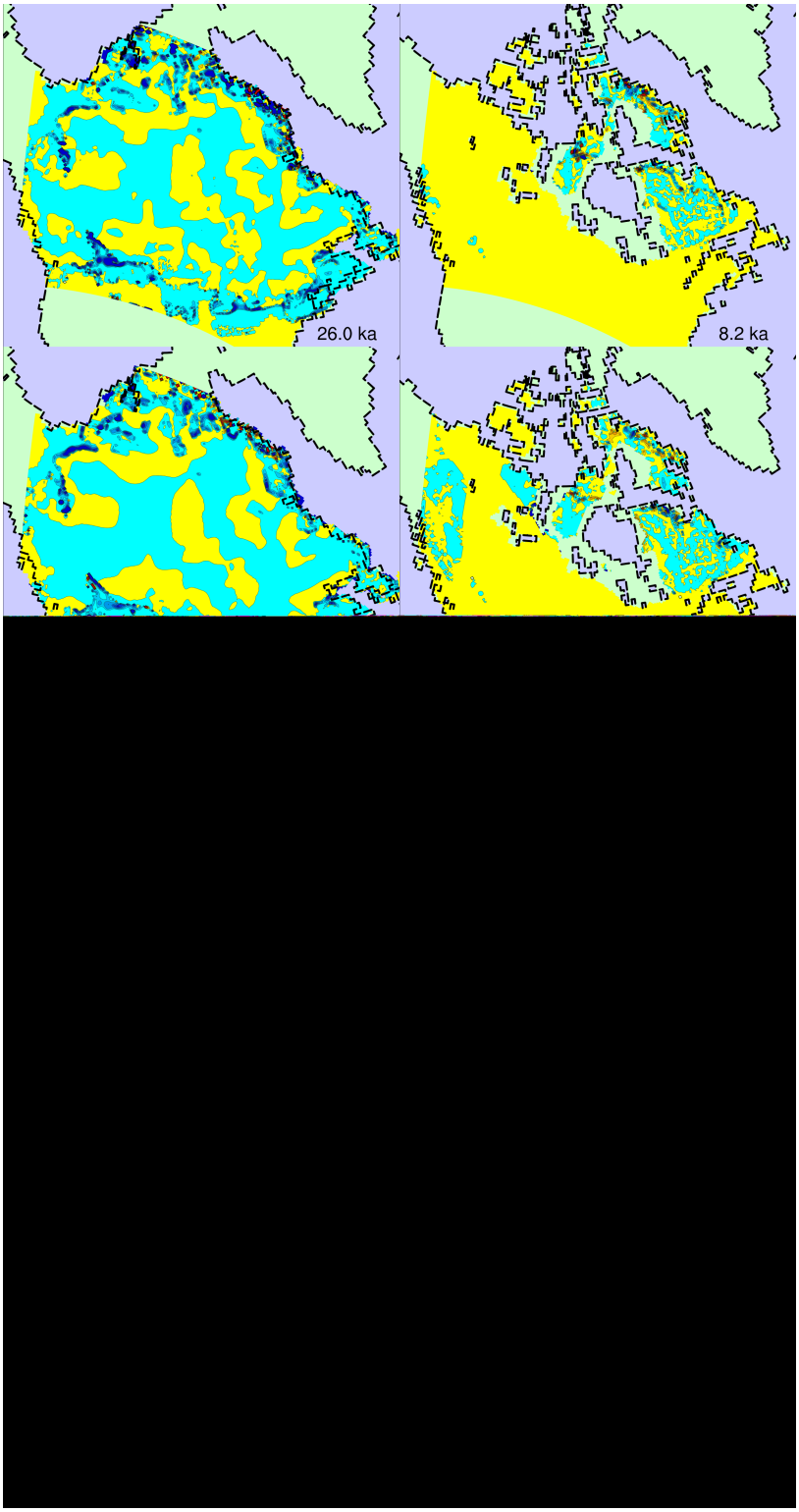

Figure 18: Variability of basal temperature with respect to A_{SIA} (f0500c0siax, f0100c0siax, f0050c0siax, and f0010c0siax) at LGM (left) and 12.5 kyr BP (right) for τ_f increasing top to bottom.

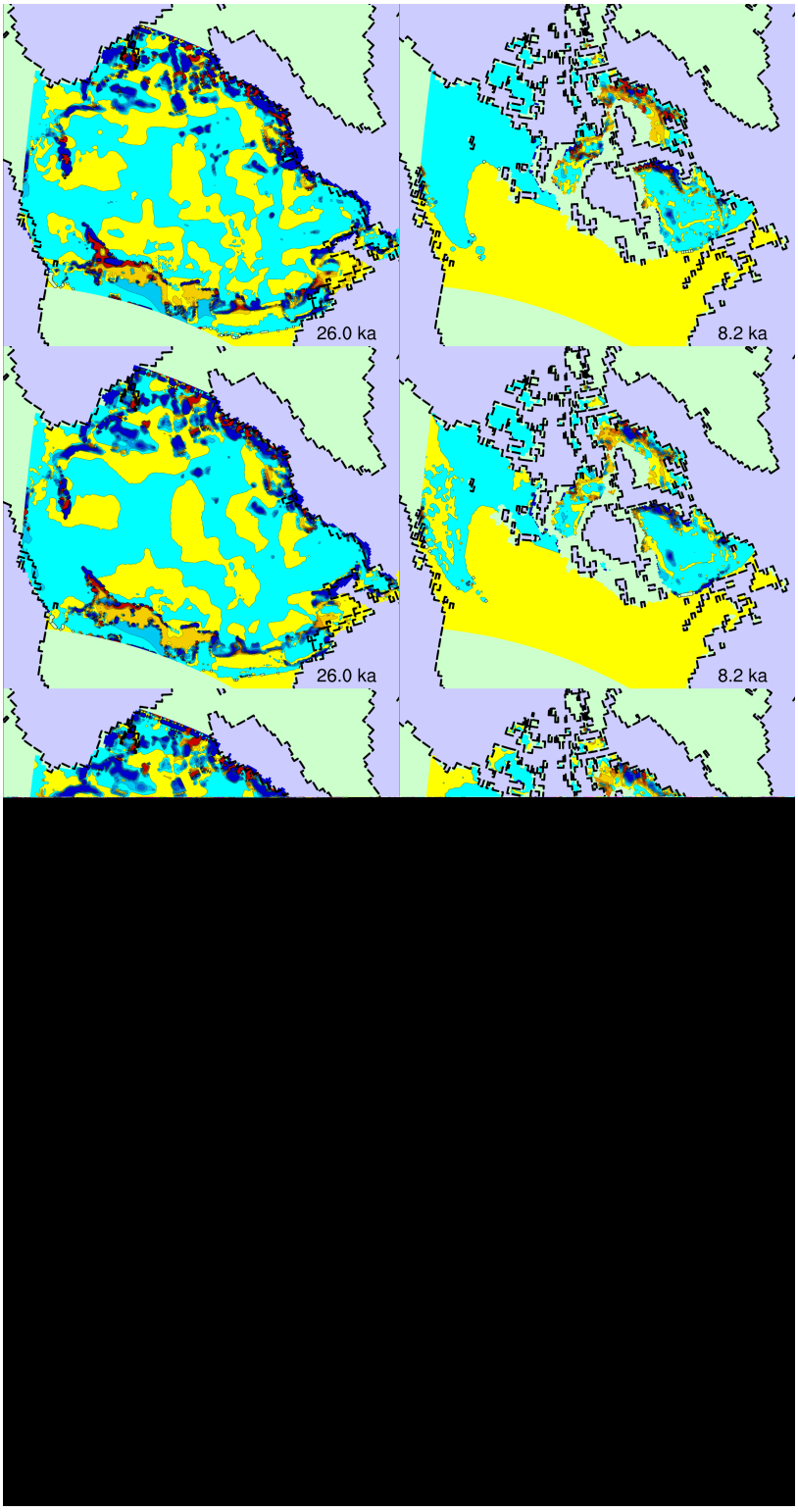

Figure 19: Variability of basal temperature with respect to random parameters (f0500rnxxx, f0100rnxxx, f0050rnxxx, and f0010rnxxx) at LGM (left) and 12.5 kyr BP (right) for τ_f increasing top to bottom.

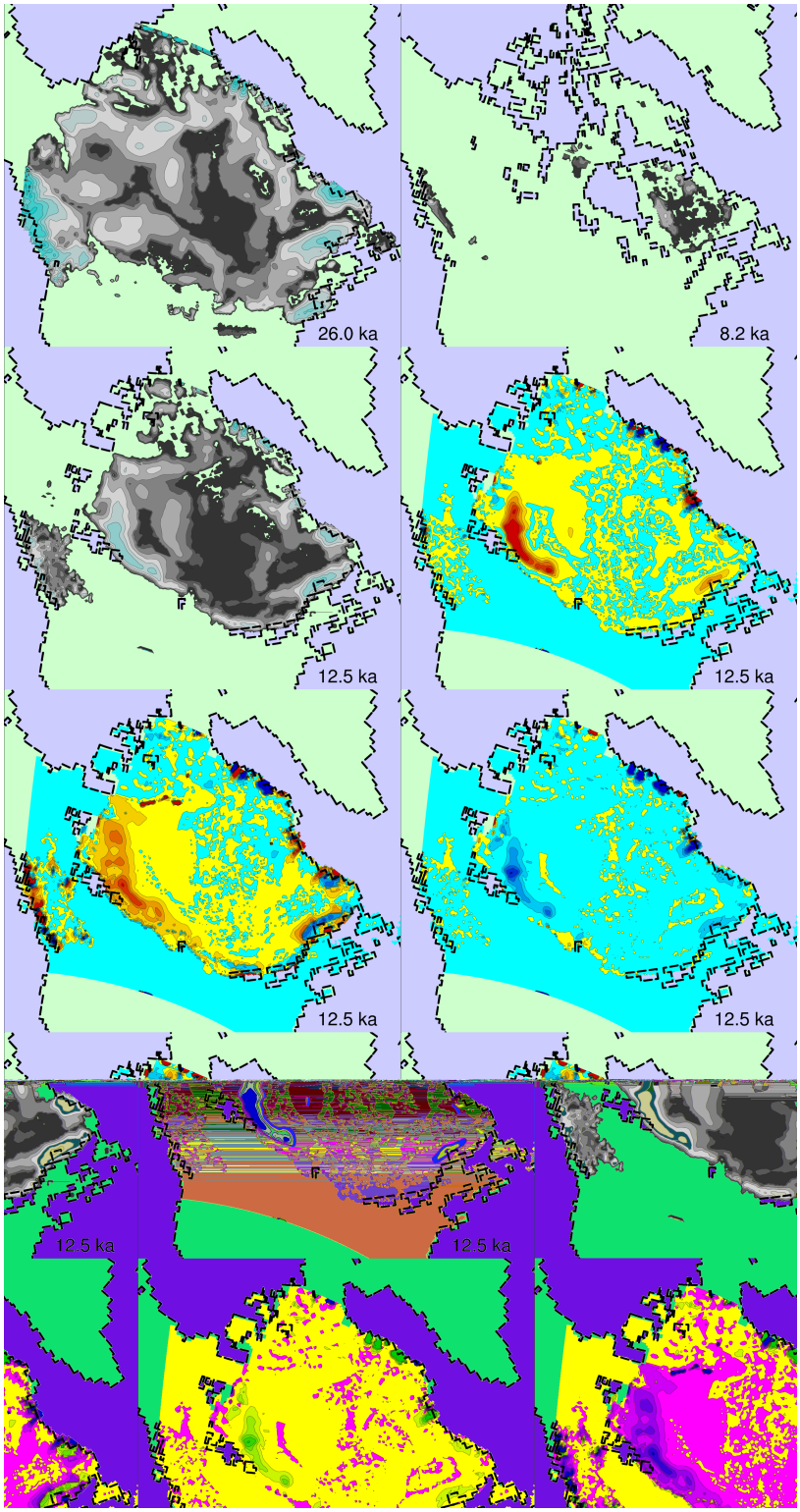

Figure 20: Plots of basal meltwater production at LGM (upper left), 8.2 kyr BP (upper right), and 12.5 kyr BP (second row left), followed (in continuing left-right, top-bottom sequence) by variability plots with respect to A_{SSA} (f0100c0ssax), ϕ_{min} and ϕ_{max} (f0100c0ttpx), A_{SIA} (f0100c0siax), random parameters (f0100rnxxx), and a subset of the random parameters (f0100rn01x) at 12.5 kyr BP.

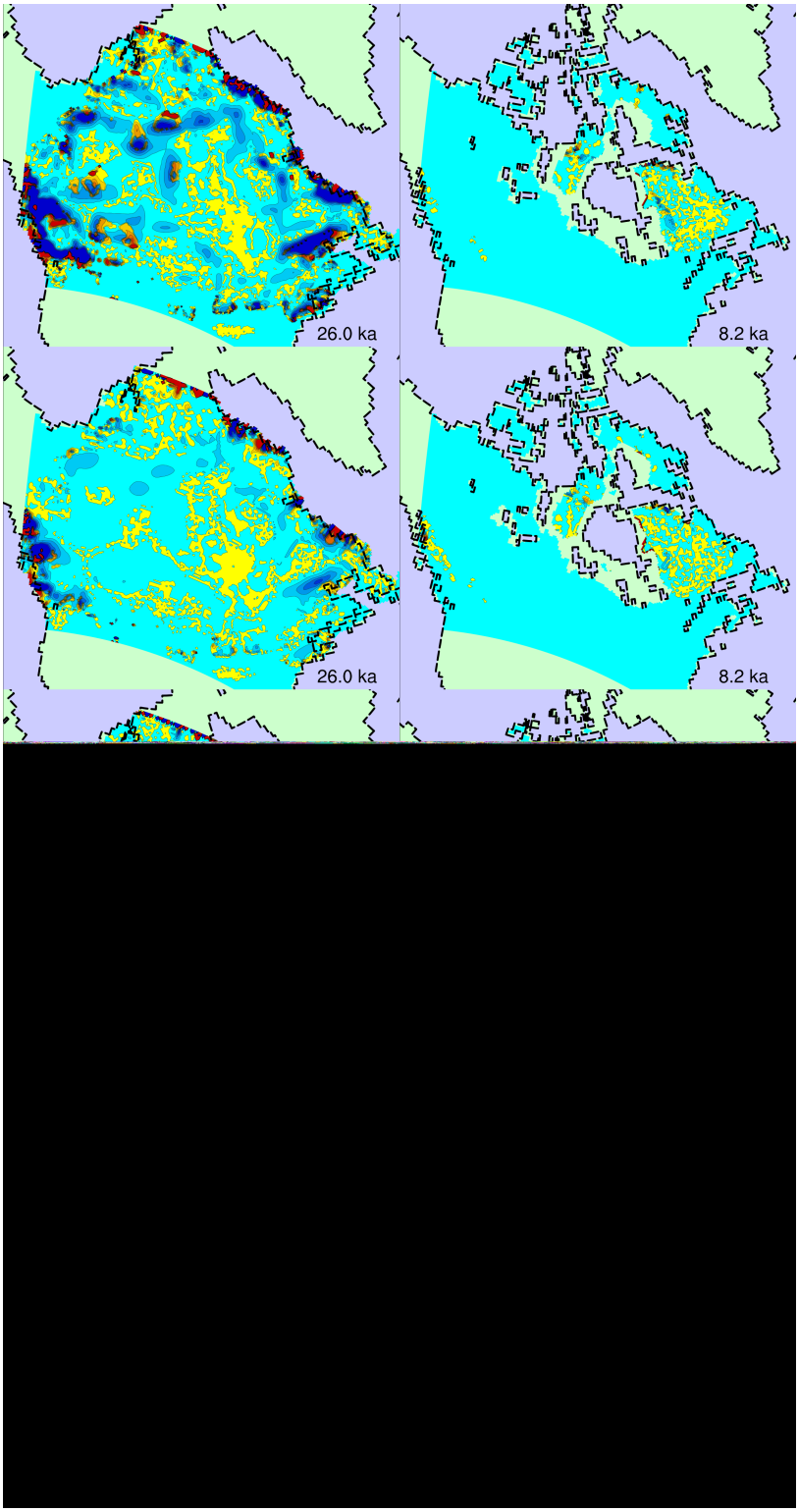

Figure 21: Variability of basal meltwater production with respect to A_{SSA} (f0500c0ssax, f0100c0ssax, f0050c0ssax, and f0010c0ssax) at LGM (left) and 12.5 kyr BP (right) for τ_f increasing top to bottom.

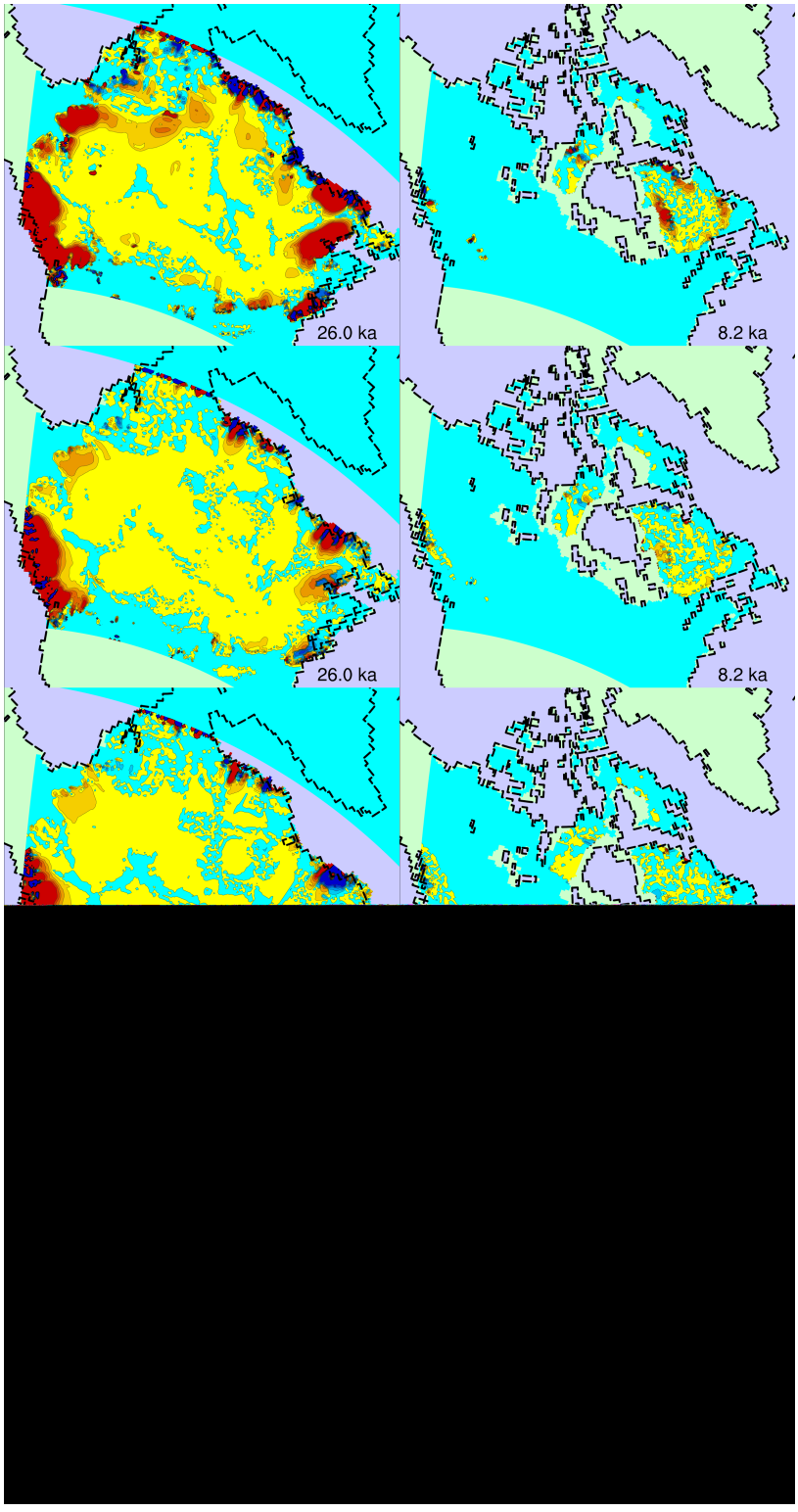

Figure 22: Variability of basal meltwater production with respect to ϕ_{min} and ϕ_{max} (f0500c0ttpx, f0100c0ttpx, f0050c0ttpx, and f0010c0ttpx) at LGM (left) and 12.5 kyr BP (right) for τ_f increasing top to bottom.

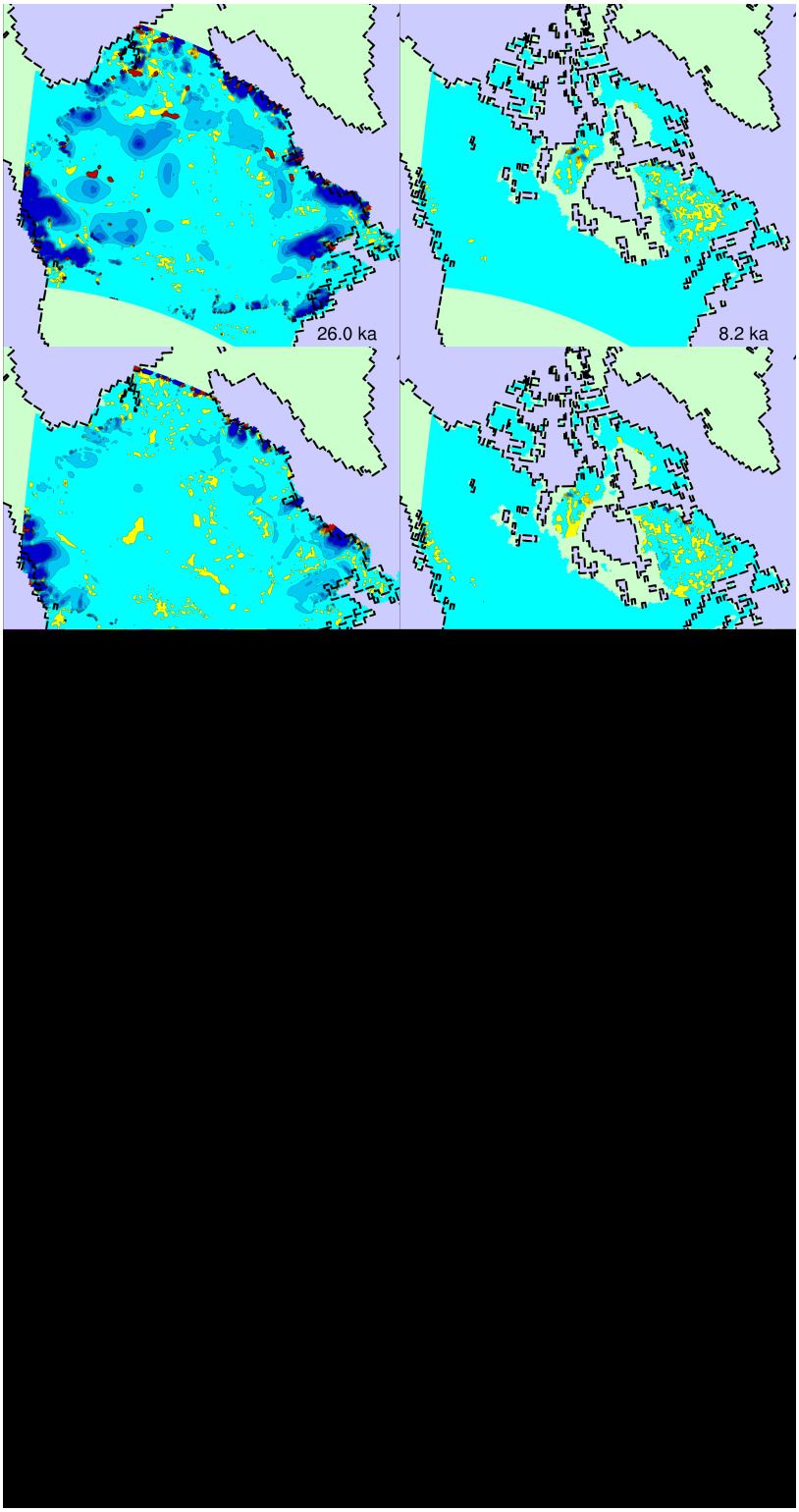

Figure 23: Variability of basal meltwater production with respect to A_{SIA} (f0500c0siax, f0100c0siax, f0050c0siax, and f0010c0siax) at LGM (left) and 12.5 kyr BP (right) for τ_f increasing top to bottom.

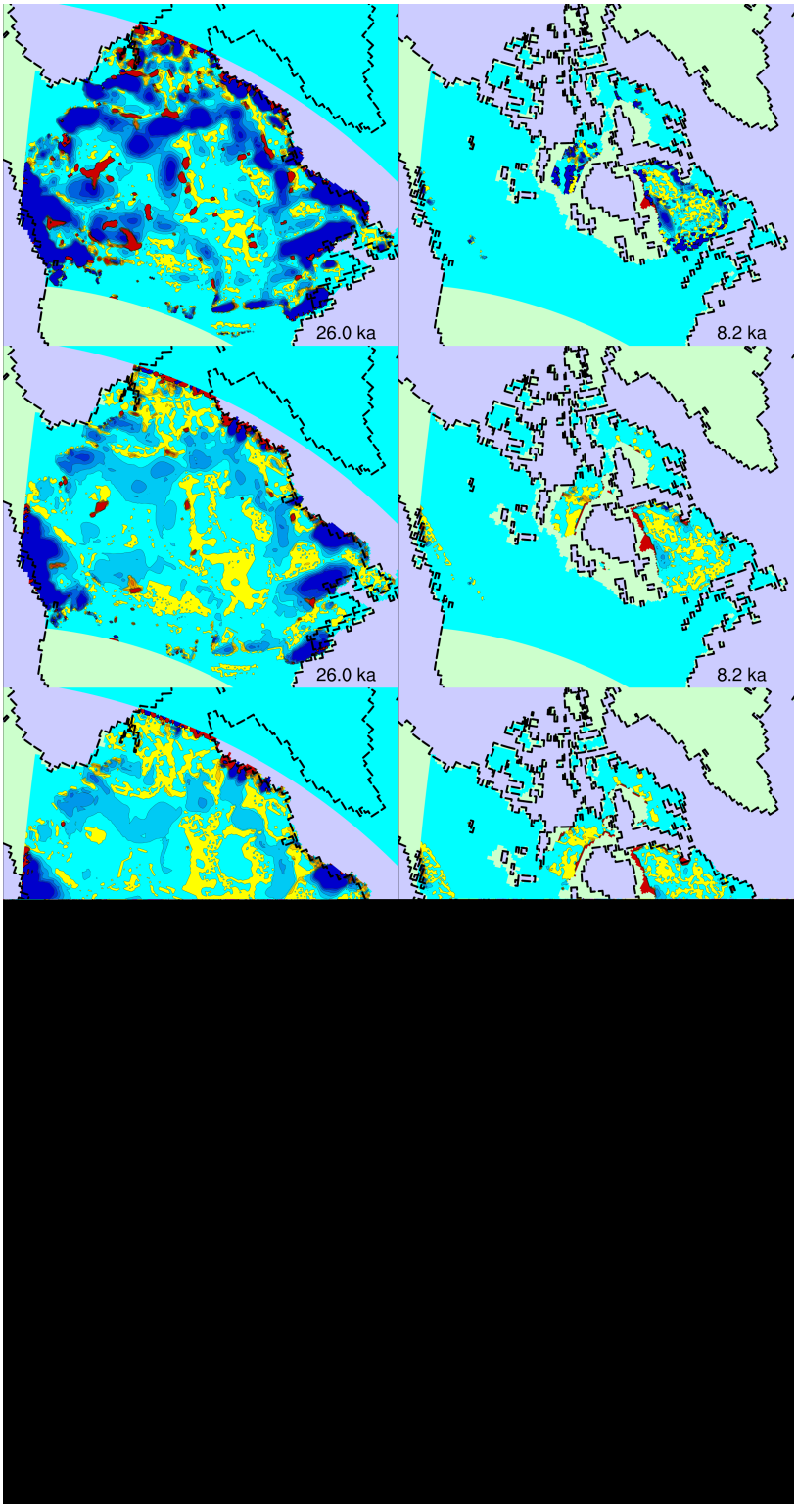

Figure 24: Variability of basal meltwater production with respect to random parameters (f0500rnxxx, f0100rnxxx, f0050rnxxx, and f0010rnxxx) at LGM (left) and 12.5 kyr BP (right) for τ_f increasing top to bottom.

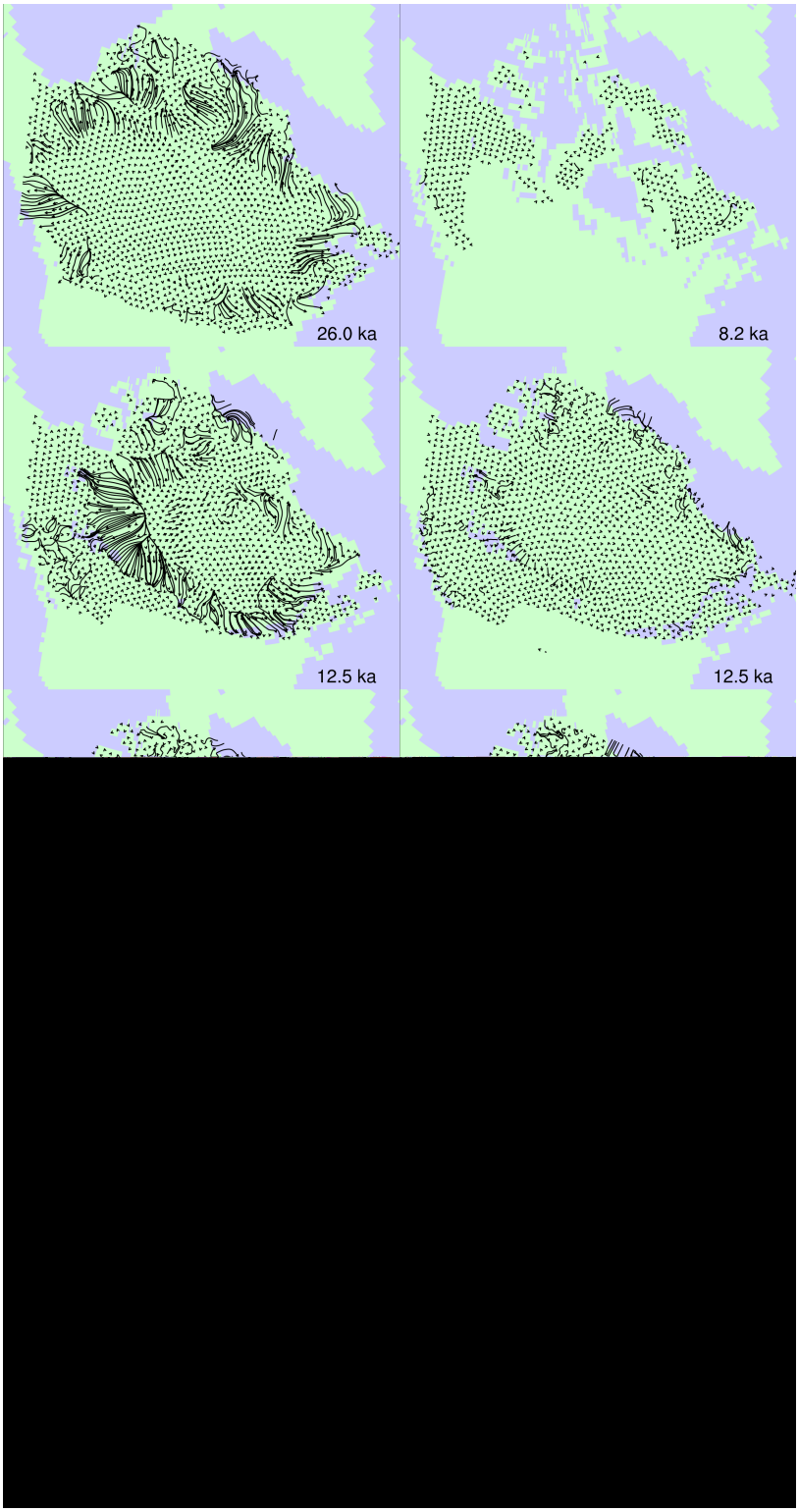

Figure 25: Plots of basal velocity at LGM (upper left), 8.2 kyr BP (upper right), and 12.5 kyr BP (second row left), followed (in continuing left-right, top-bottom sequence) by variability plots with respect to A_{SSA} (f0100c0ssax), ϕ_{min} and ϕ_{max} (f0100c0ttpx), A_{SIA} (f0100c0siax), random parameters (f0100rnxxx), and a subset of the random parameters (f0100rn01x) at 12.5 kyr BP.

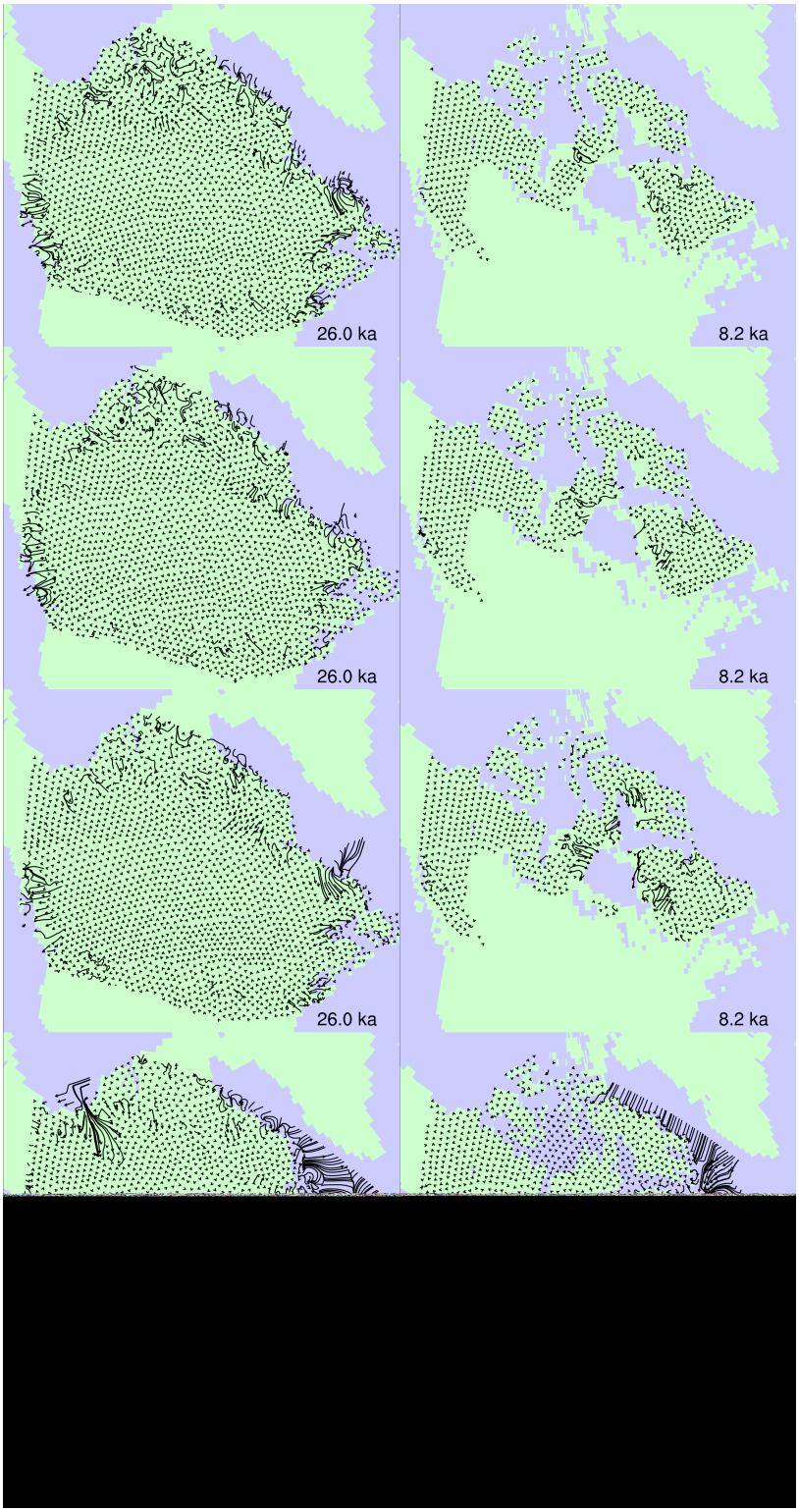

Figure 26: Variability of basal velocity with respect to A_{SSA} (f0500c0ssax, f0100c0ssax, f0050c0ssax, and f0010c0ssax) at LGM (left) and 12.5 kyr BP (right) for τ_f increasing top to bottom.

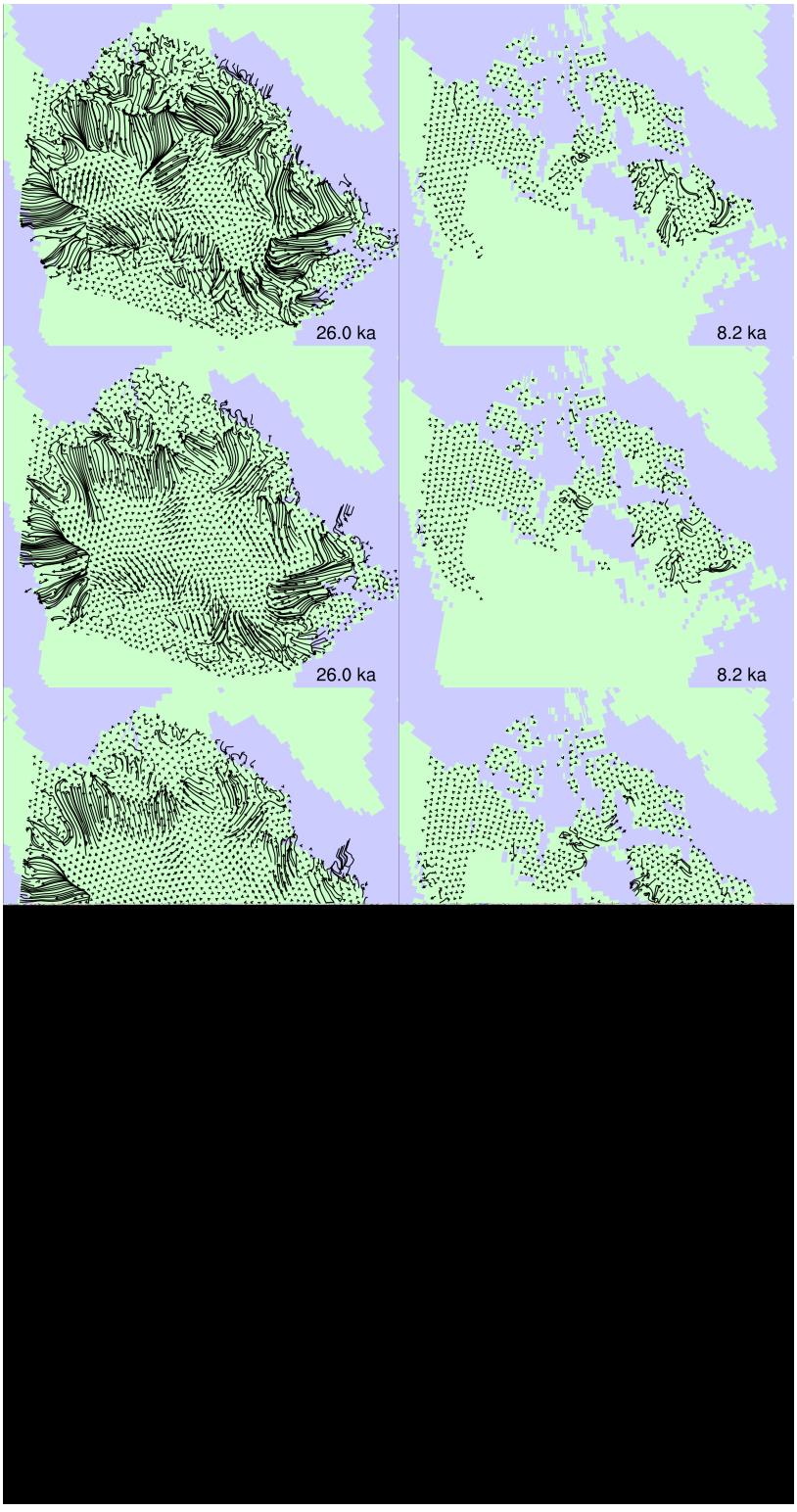

Figure 27: Variability of basal velocity with respect to $\phi_{\mathbf{min}}$ and $\phi_{\mathbf{max}}$ (f0500c0ttpx, f0100c0ttpx, f0050c0ttpx, and f0010c0ttpx) at LGM (left) and 12.5 kyr BP (right) for τ_{f} increasing top to bottom.

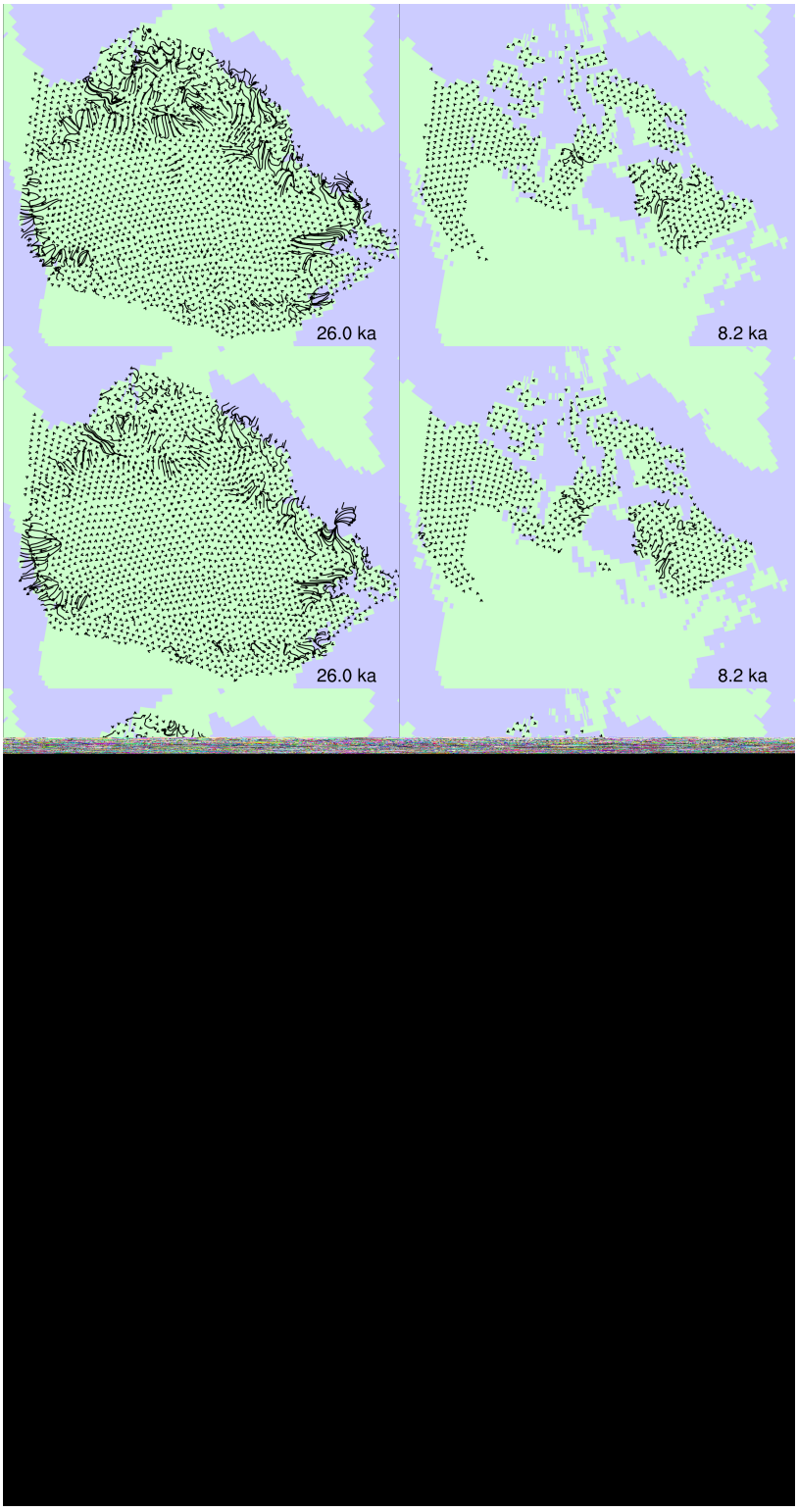

Figure 28: Variability of basal velocity with respect to A_{SIA} (f0500c0siax, f0100c0siax, f0050c0siax, and f0010c0siax) at LGM (left) and 12.5 kyr BP (right) for τ_f increasing top to bottom.

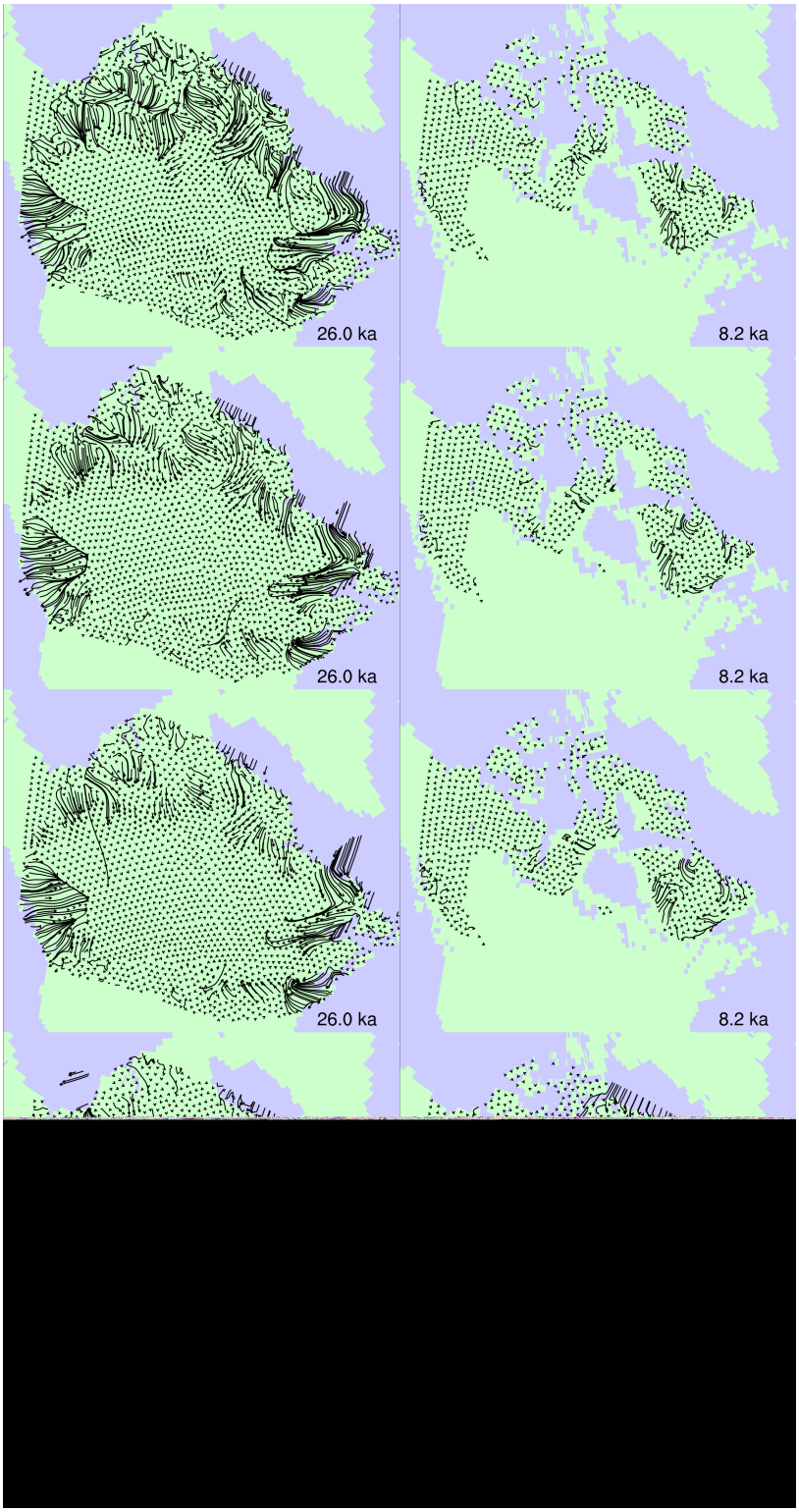

Figure 29: Variability of basal velocity with respect to random parameters (f0500rnxxx, f0100rnxxx, f0050rnxxx, and f0010rnxxx) at LGM (left) and 12.5 kyr BP (right) for τ_f increasing top to bottom.

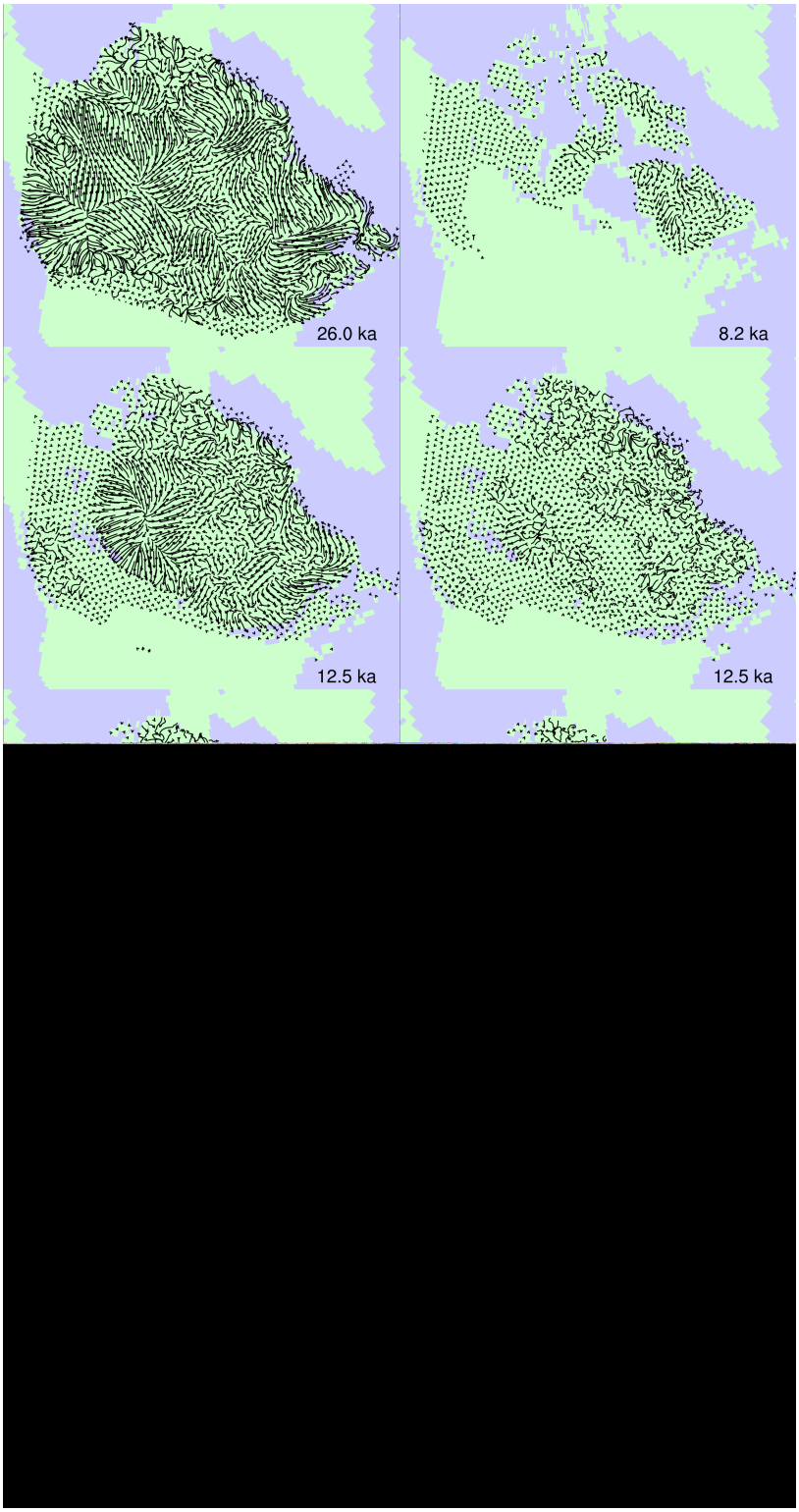

Figure 30: Plots of basal shear stress at LGM (upper left), 8.2 kyr BP (upper right), and 12.5 kyr BP (second row left), followed (in continuing left-right, top-bottom sequence) by variability plots with respect to A_{SSA} (f0100c0ssax), ϕ_{min} and ϕ_{max} (f0100c0ttpx), A_{SIA} (f0100c0siax), random parameters (f0100rnxxx), and a subset of the random parameters (f0100rn01x) at 12.5 kyr BP.

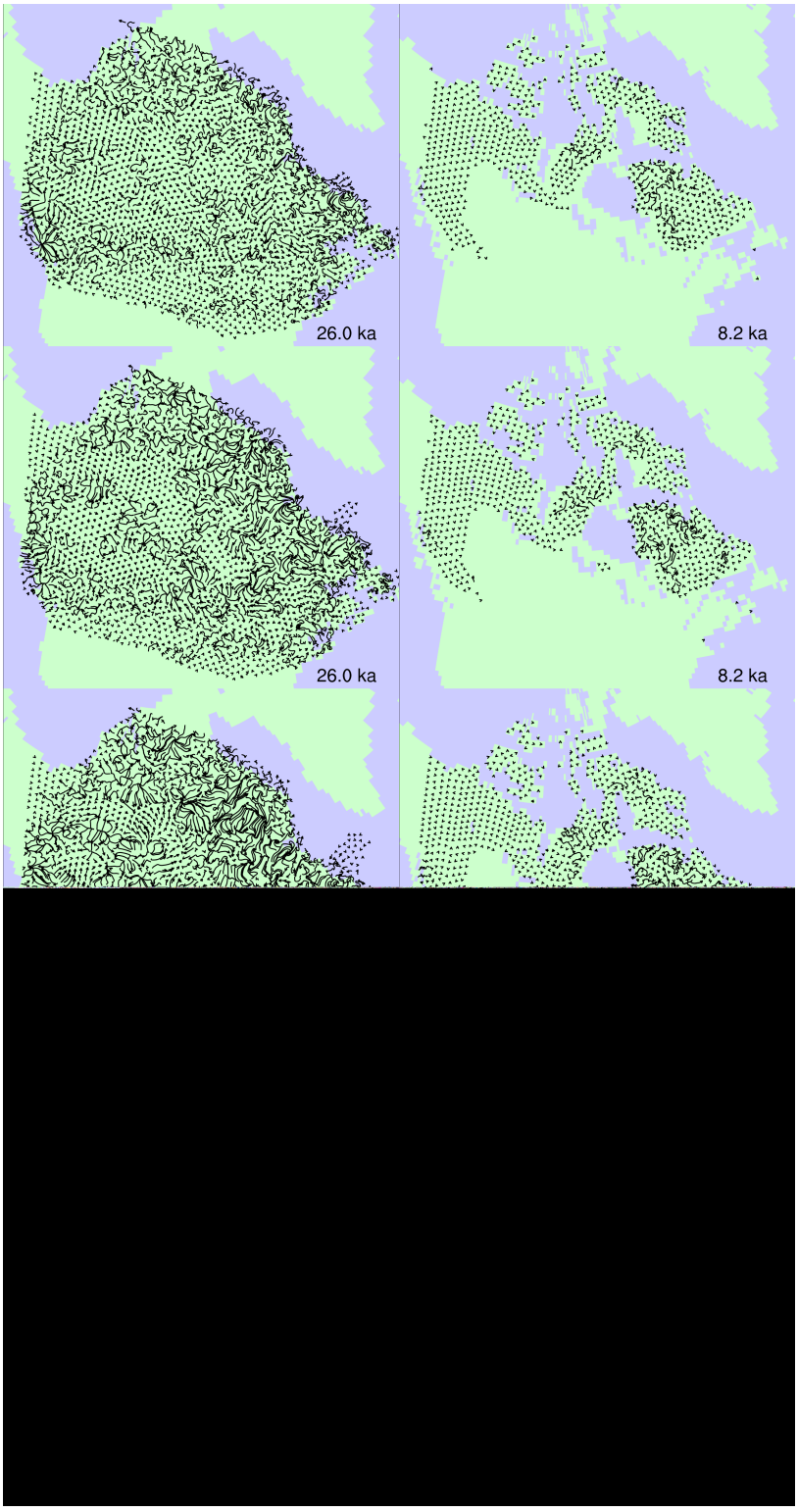

Figure 31: Variability of basal shear stress with respect to A_{SSA} (f0500c0ssax, f0100c0ssax, f0050c0ssax, and f0010c0ssax) at LGM (left) and 12.5 kyr BP (right) for τ_f increasing top to bottom.

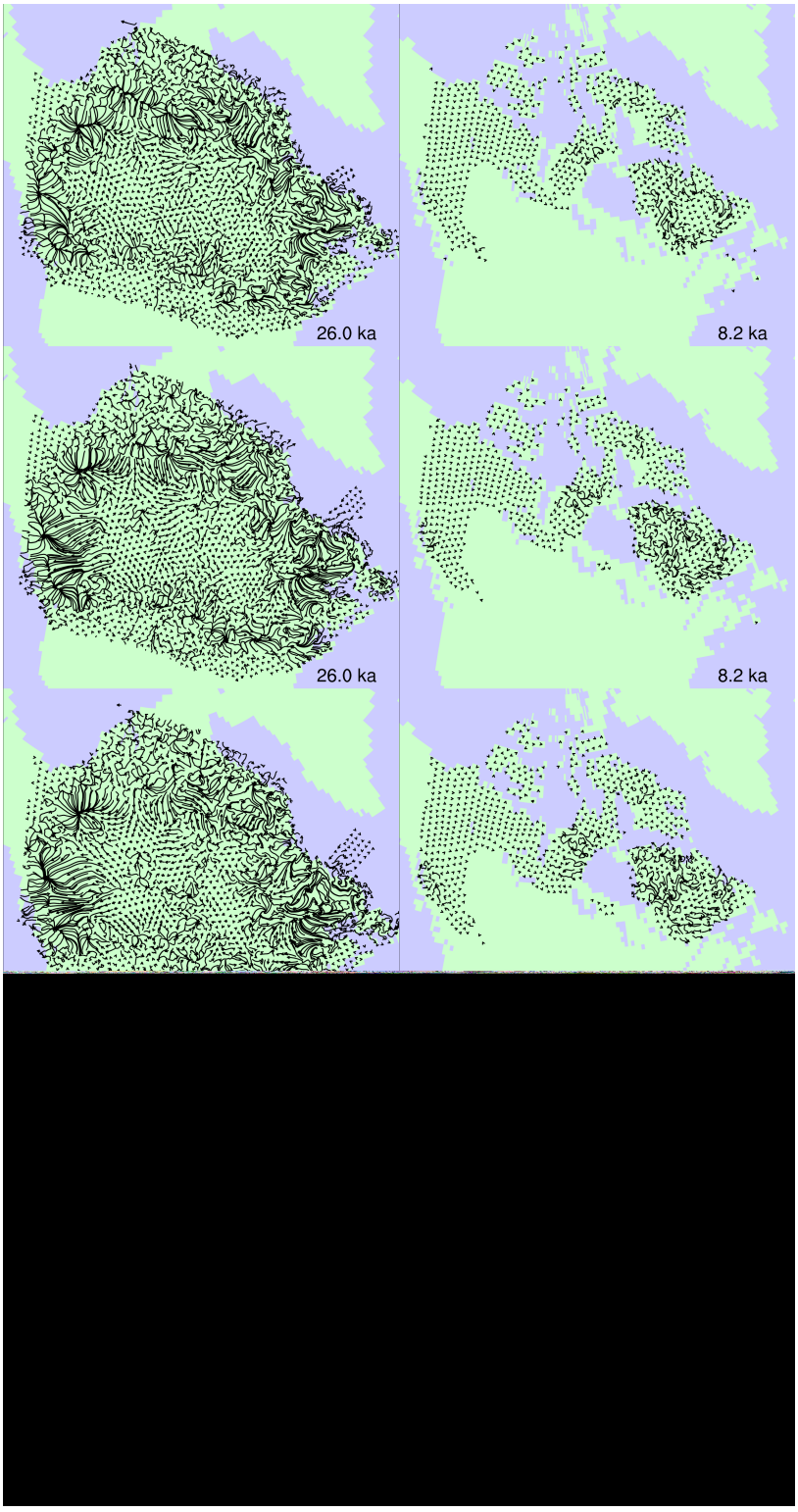

Figure 32: Variability of basal shear stress with respect to ϕ_{min} and ϕ_{max} (f0500c0ttpx, f0100c0ttpx, f0050c0ttpx, and f0010c0ttpx) at LGM (left) and 12.5 kyr BP (right) for τ_f increasing top to bottom.

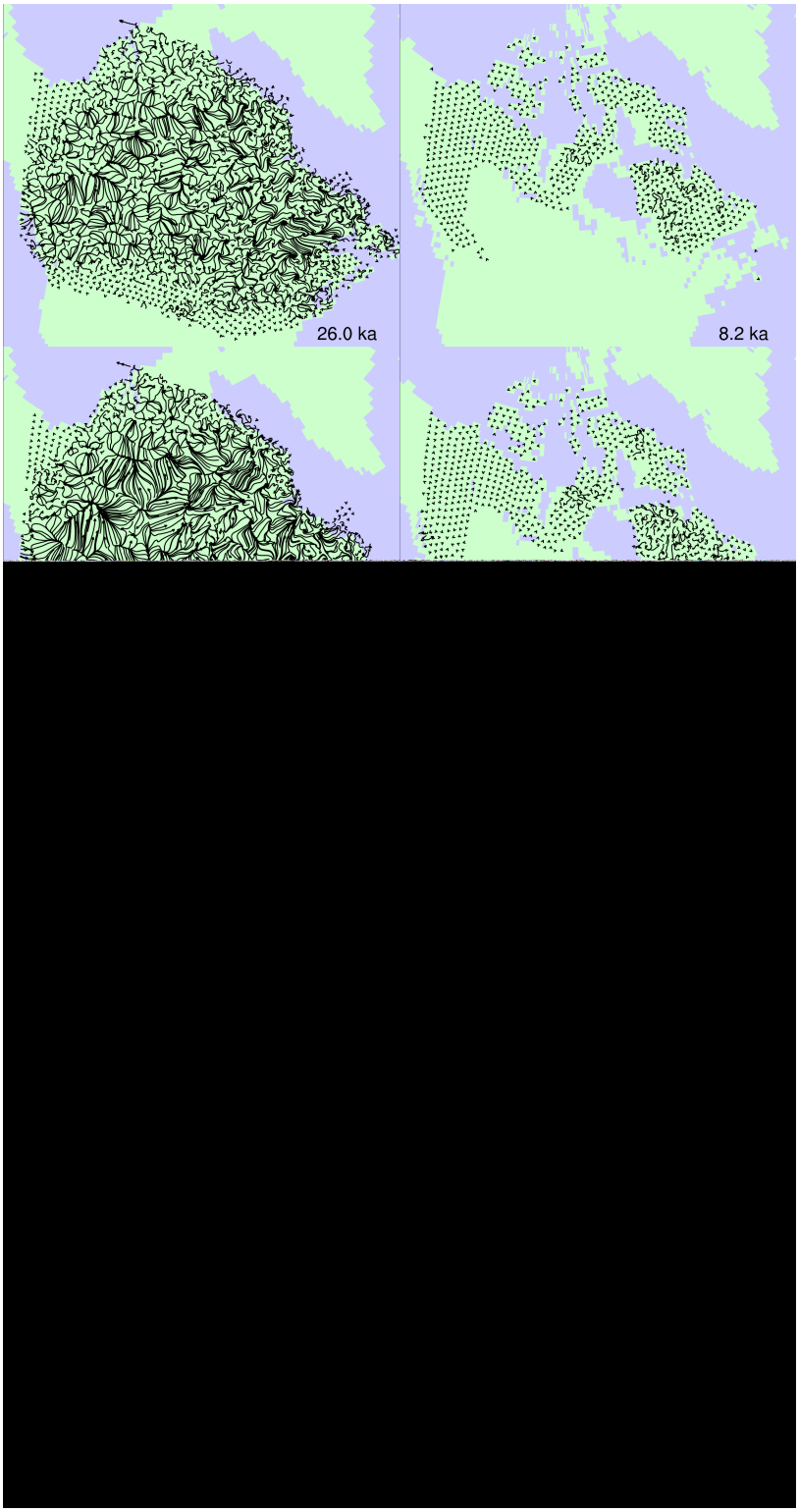

Figure 33: Variability of basal shear stress with respect to A_{SIA} (f0500c0siax, f0100c0siax, f0050c0siax, and f0010c0siax) at LGM (left) and 12.5 kyr BP (right) for τ_f increasing top to bottom.

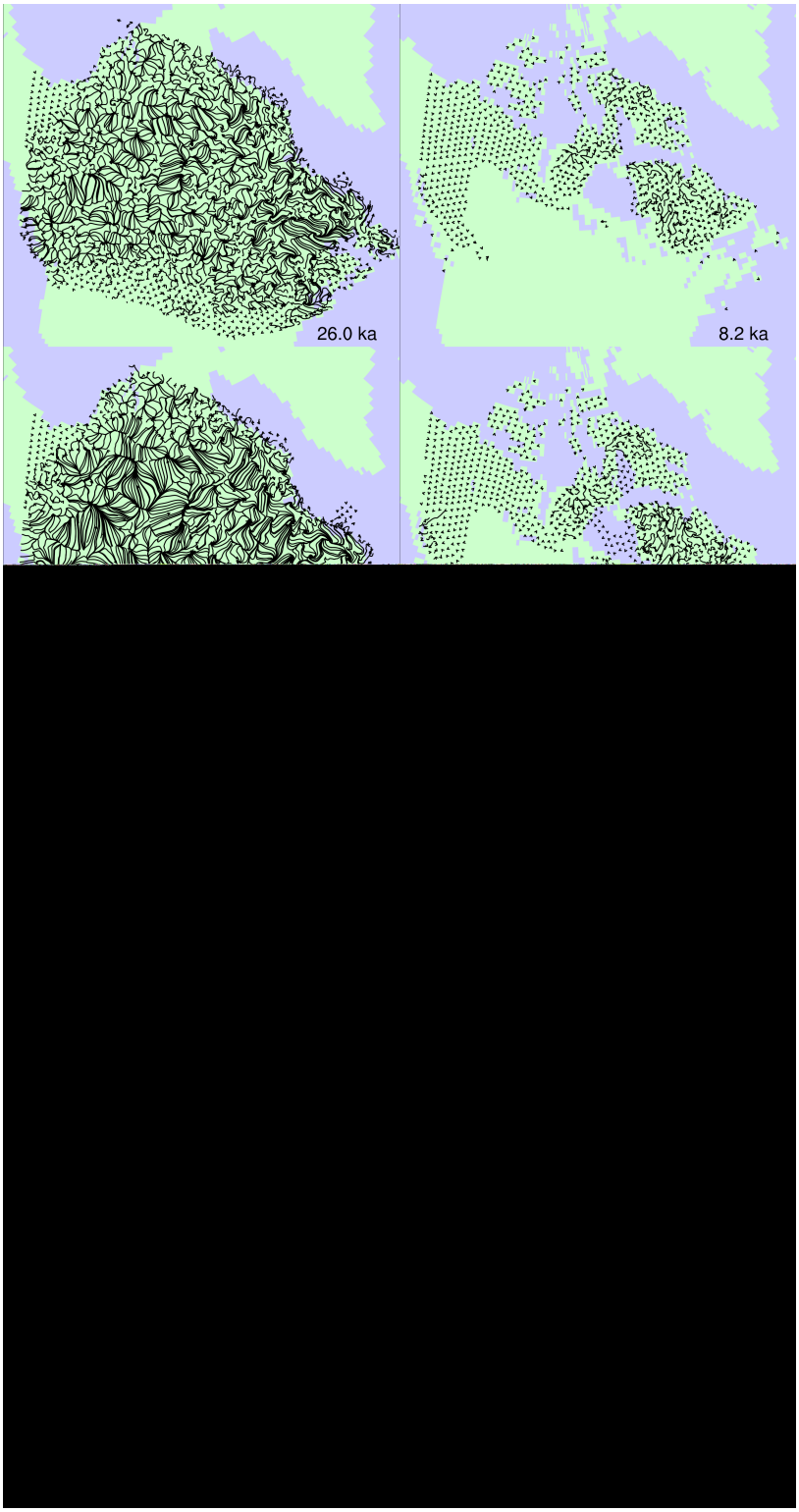

Figure 34: Variability of basal shear stress with respect to random parameters (f0500rnxxx, f0100rnxxx, f0050rnxxx, and f0010rnxxx) at LGM (left) and 12.5 kyr BP (right) for τ_f increasing top to bottom.

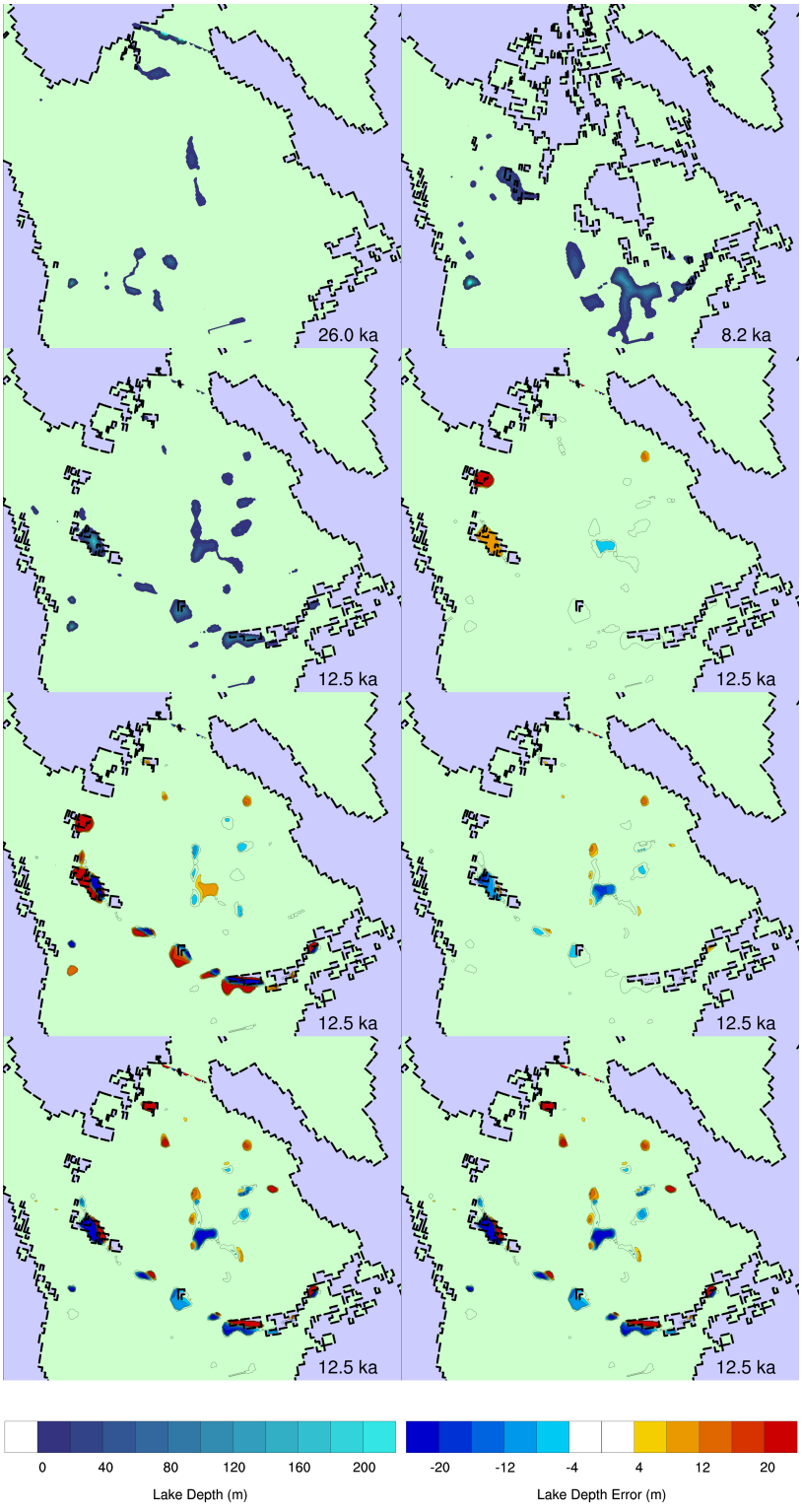

Figure 35: Plots of lake depth at LGM (upper left), 8.2 kyr BP (upper right), and 12.5 kyr BP (second row left), followed (in continuing left-right, top-bottom sequence) by variability plots with respect to A_{SSA} (f0100c0ssax), ϕ_{min} and ϕ_{max} (f0100c0ttpx), A_{SIA} (f0100c0siax), random parameters (f0100rnxxx), and a subset of the random parameters (f0100rn01x) at 12.5 kyr BP.

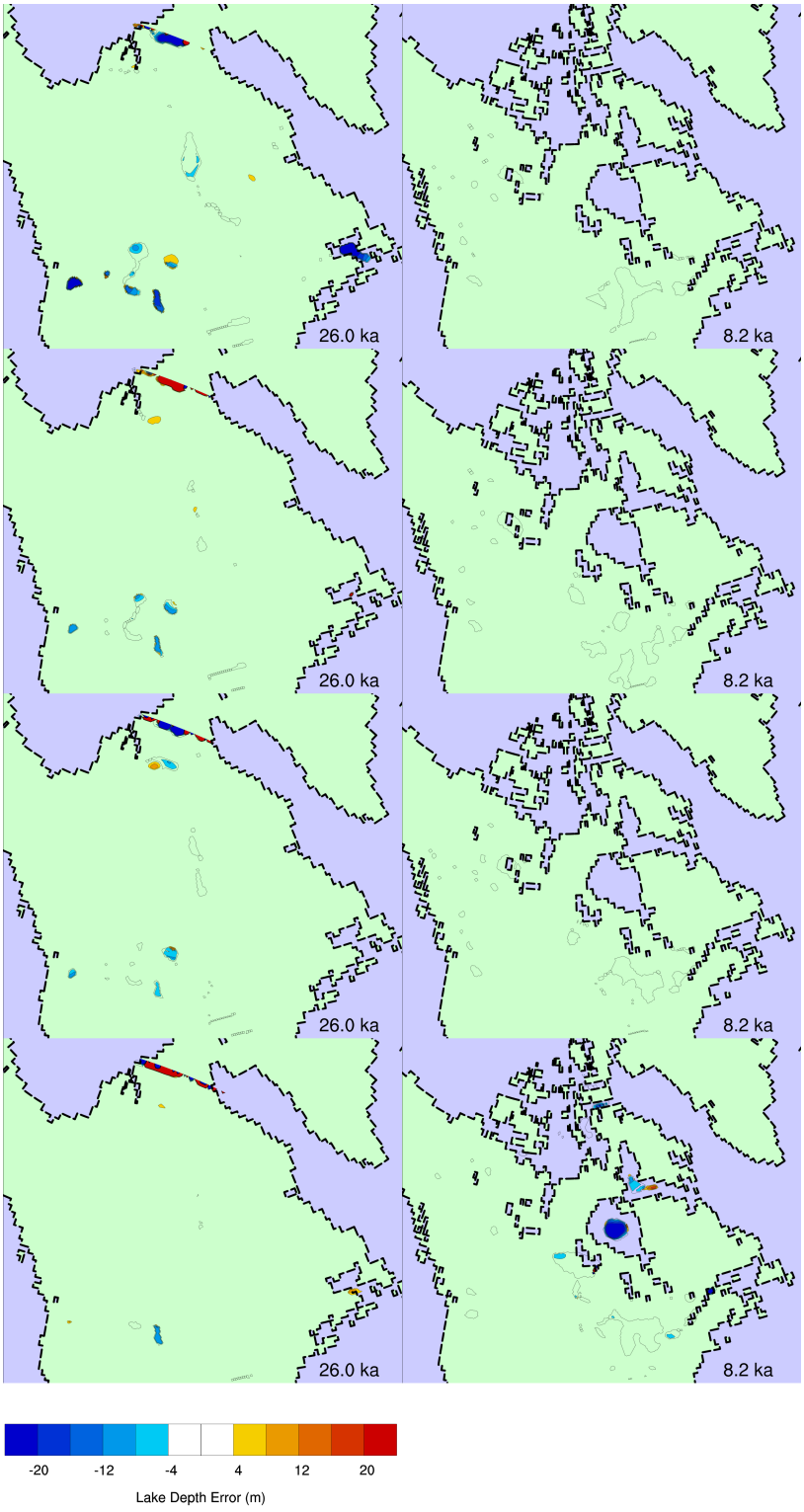

Figure 36: Variability of lake depth with respect to A_{SSA} (f0500c0ssax, f0100c0ssax, f0050c0ssax, and f0010c0ssax) at LGM (left) and 12.5 kyr BP (right) for τ_f increasing top to bottom.

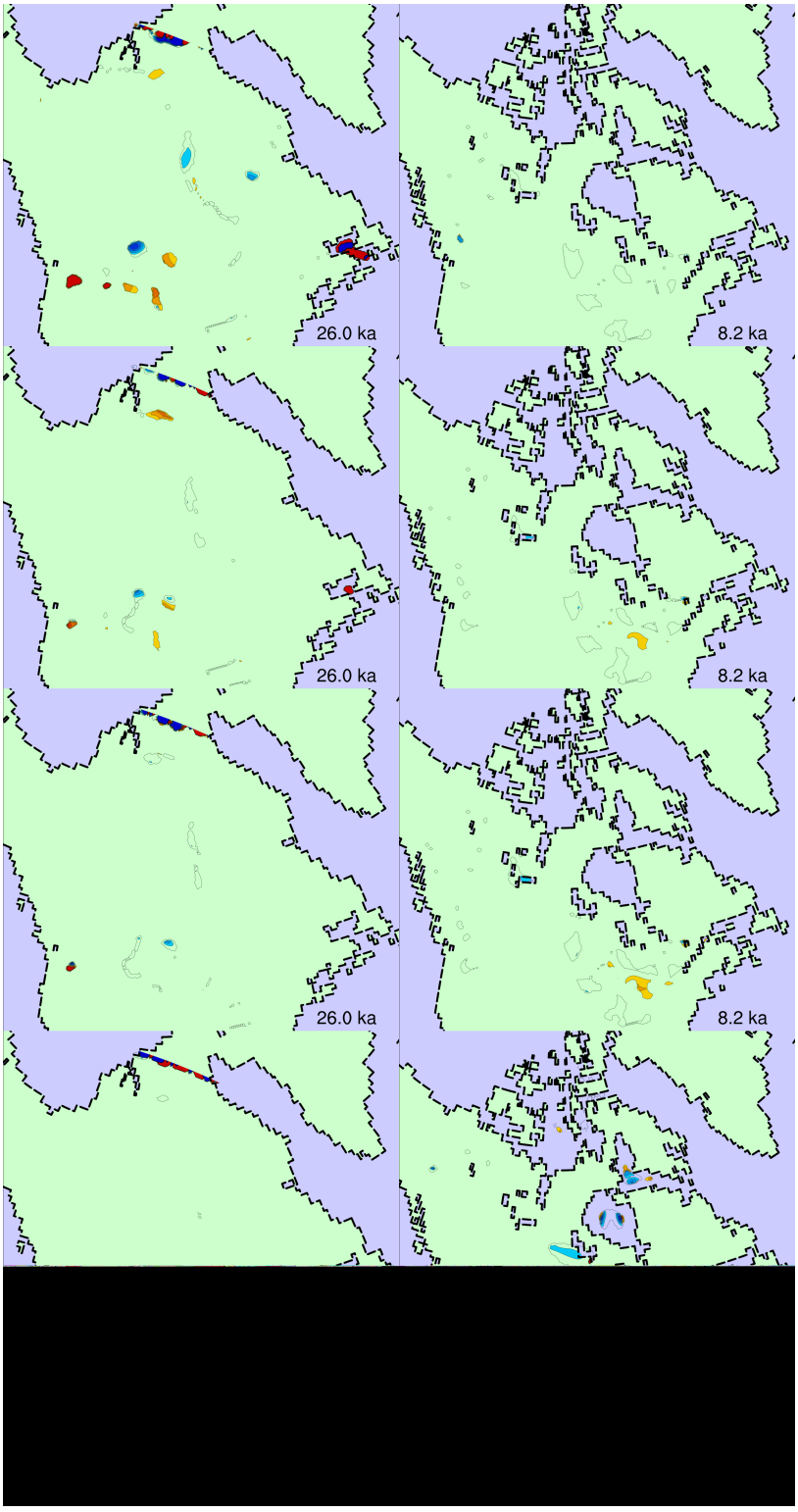

Figure 37: Variability of lake depth with respect to ϕ_{min} and ϕ_{max} (f0500c0ttpx, f0100c0ttpx, f0050c0ttpx, and f0010c0ttpx) at LGM (left) and 12.5 kyr BP (right) for τ_f increasing top to bottom.

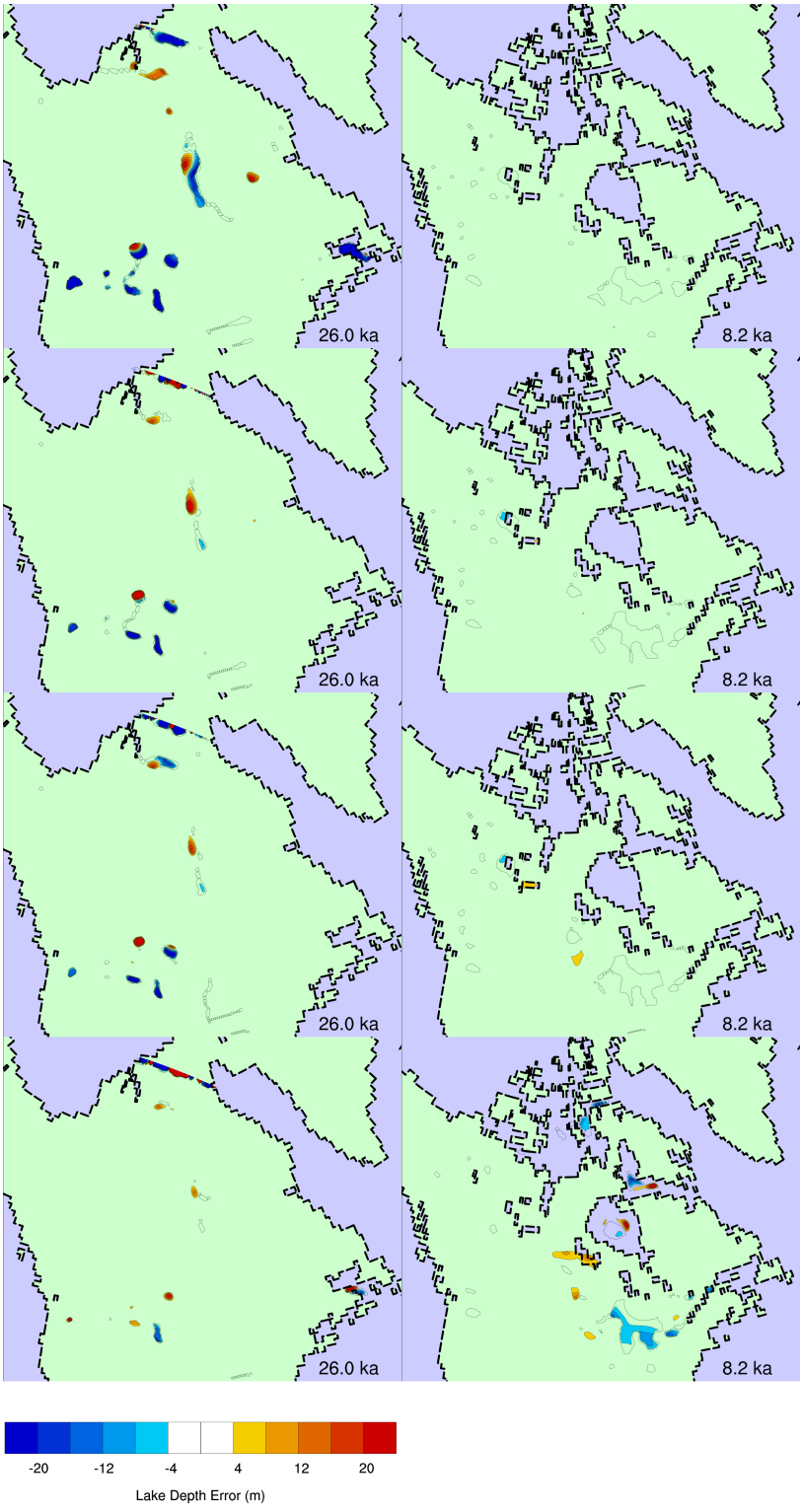

Figure 38: Variability of lake depth with respect to A_{SIA} (f0500c0siax, f0100c0siax, f0050c0siax, and f0010c0siax) at LGM (left) and 12.5 kyr BP (right) for τ_f increasing top to bottom.

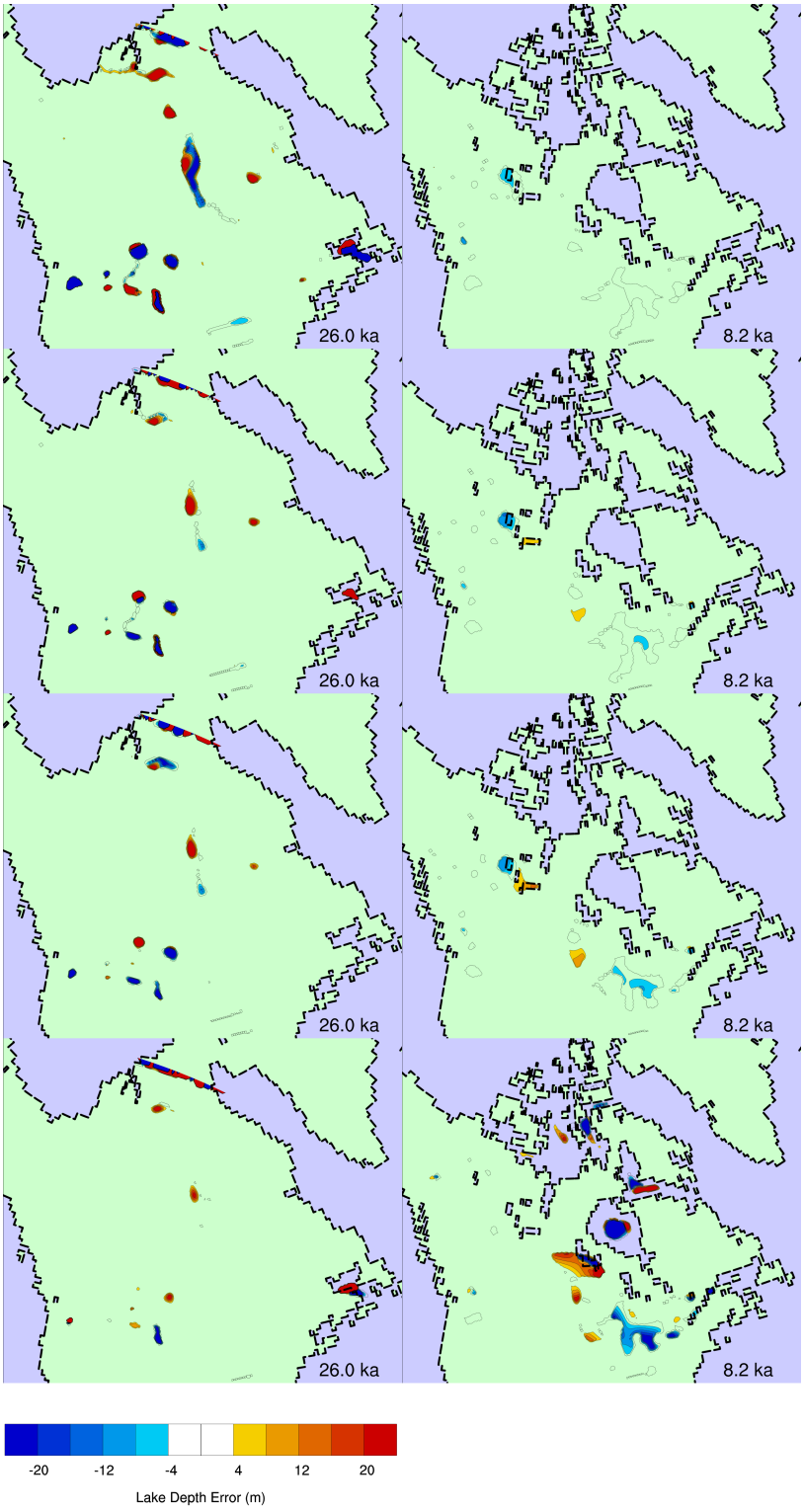

Figure 39: Variability of lake depth with respect to random parameters (f0500rnxxx, f0100rnxxx, f0050rnxxx, and f0010rnxxx) at LGM (left) and 12.5 kyr BP (right) for τ_f increasing top to bottom.